FORCED CONVECTION BOILING FROM A CYLINDER NORMAL TO THE FLOW

By

HUGH RICHARD MCKEE

Bachelor of Science
Tri-State College
Angola, Indiana
1956

Master of Science
University of Tulsa
Tulsa, Oklahoma
1959

Submitted to the faculty of the Graduate College
of the Oklahoma State University
in partial fulfillment of the requirements
for the degree of
DOCTOR OF PHILOSOPHY
July, 1967

FORCED CONVECTION BOILING FROM A

CYLINDER NORMAL TO THE FLOW

Thesis Approved:

Kenneth J. Bell

Thesis Adviser

Gerald D. Parker

John B. West

Robert L. Robinson, Jr.

N. N. Durham

Dean of the Graduate College

PREFACE

The author wishes to express his indebtedness to Dr. Kenneth J. Bell for his valuable guidance and inspiration supplied during this study. Appreciation is also expressed to both the School of Chemical Engineering of Oklahoma State University and the University of Tulsa for financial assistance received while this research was being conducted.

Particular gratitude is due my wife, Irene, whose patience and encouragement made this undertaking feasible.

TABLE OF CONTENTS

LIST OF TABLES

LIST OF FIGURES

CHAPTER I

INTRODUCTION

Prior to the middle of the twentieth century, the attention devoted to boiling heat transfer was sporadic and without a specific goal or application. Credit for the first scientific study of boiling goes to Nukiyama (1) for his determination of the basic boiling curve from pool boiling studied in 1934. The basic boiling curve is shown as 3-4-5 in Figure 1.

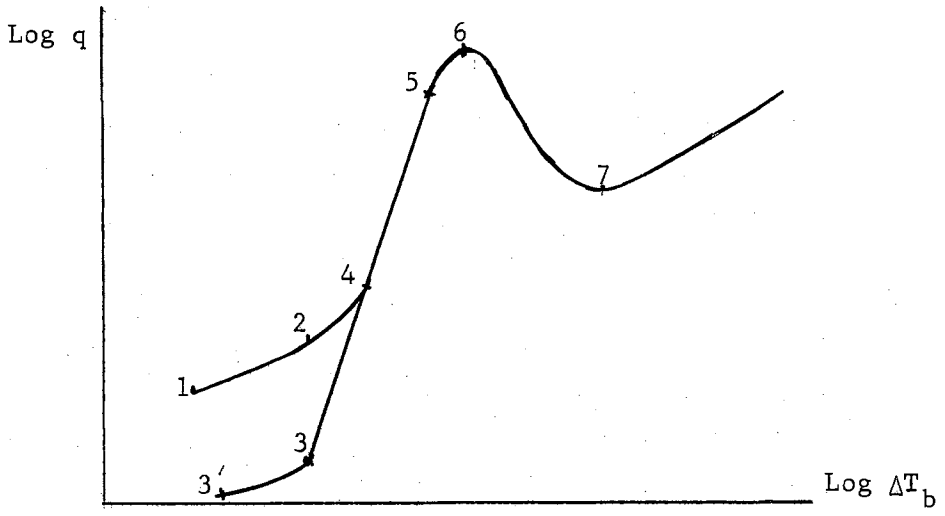

Figure 1. Basic Boiling Curve.

The portion of the curve labeled 1-2 represents nonboiling forced convection heat transfer. Point 2 represents incipient or local boiling and between 4 and 5 nucleate boiling exists. The curve 3-4-5 is a pool boiling curve and heat transfer between 3′ and 3 would be due to

nonboiling free convection. Point 5 represents the departure from nucleate boiling (often termed DNB). Point 6 is the critical flux or first boiling crisis, and 6-7 represents the transition boiling region. Point 7 is the Leidenfrost point or second boiling crisis, beyond which fully established film boiling exists.

Quantitative understanding of the basic boiling mechanisms became important with the introduction of equipment containing components exposed to high heat fluxes, such as rocket engines and nuclear reactors. Nucleate boiling offered a means of removing large quantities of heat at relatively low temperature differences. The coolant system of early nuclear reactors avoided the phase change by resorting to elevated coolant pressures. Boiling water reactors have evolved as a result of research in this area.

The interest in boiling having been aroused and research initiated, it became apparent that a detailed knowledge of the mechanism of boiling was necessary. Included in a complete understanding of the boiling mechanism are such individual problems as bubble nucleation and growth, phase stability, viscous and turbulent flow effects, bubble vibrations and collisions, and the influence of surface conditions. The latter point is of paramount importance to boiling studies, yet the characteristics of a surface remain to be described, methods of testing the surface devised, and finally, the role of each characteristic in boiling determined. The individual mechanisms have not yet been completely separated, so that much remains to be done before these completed theories can be described. Therefore the combination of all the separate theories into a common understanding is still to be accomplished.

In view of the aforementioned inadequacies, research has been directed into areas which will provide practical solutions to specific problems, or into highly specialized new areas which will hopefully provide insight into voids in the existing understanding of the boiling process, or both. Recent studies have been undertaken either with the heat-removing fluid surrounding the hot surface (e.g., pool boiling) or with convection occurring inside a conduit (e.g., forced convection inside tubes).

A significant amount of vapor production is necessary to study the entire nucleate boiling region. This means either a fluid with a relatively low latent heat of vaporization, or a system with the capacity of producing the high heat generation rates required by a fluid such as water. A convenient, controllable, and measurable means of producing high heat fluxes is through electrical resistance heating. Similarly, an expedient method of heat removal is to force a liquid to flow parallel to the longitudinal axis of a cylinder, either inside the heating element, or outside through an annulus. Considerable data exist today for these two flow geometries. The terminal point of an experimental study is the maximum heat flux which a material will withstand, under a given set of conditions, above which complete destruction is inevitable. This destructive flux will be termed the burnout point. Burnout occurs when the temperature increases and exceeds the melting point of the surface material, due to local vapor blanketing.

The exploration of the film boiling region, where a continuous vapor film exists, requires a high melting point surface material, or a coolant of low latent heat of vaporization. The vapor film produces a characteristically low heat transfer coefficient, and the surface

material must be capable of sustaining high temperatures. Burnout in the nucleate boiling region occurs when a local area enters the film boiling region by maintaining a vapor space above itself long enough for surface destruction to occur. Electrically heated systems develop local areas of current concentration when the resistance of an adjoining area increases due to a temperature increase. The production of stable film boiling areas with electrical heating is limited, and not commonly attempted.

Boiling studies with the liquid outside the solid have been performed with wires, small tubes, and flat strips in pool boiling, and around very small diameter wires under forced convection. The latter wires were placed with their longitudinal axis normal to the moving stream. It was decided that a fruitful area of research would be to use tubes of a more practical diameter, say up to 1/2 or 3/4 inch. The larger diameters would allow wall temperatures to be measured at several points around the tube in an effort to describe the interactions of forced convection and boiling.

Diameters above 1/4 inch should be of interest as a possible geometry for nuclear reactor fuel elements, and the electrical heating mode provides a heat source similar to that encountered in reactors, in that flux is controlled rather than surface temperature.

This, then, is a study of forced convection nucleate boiling heat transfer with flow normal to cylinders between 0.25 and 0.71 inches outside diameter.

CHAPTER II

LITERATURE SURVEY

Literature and Correlation Reviews

Heat transfer which occurs in the presence of boiling from a surface can be described in terms of the liquid temperature, (saturated or subcooled); the boiling mechanism, which is indicative of the surface temperature, (nucleate, transition, or film); and the fluid circulation method, (pool boiling, thermosiphon, or forced convection). Bonilla (2) has classified these combinations and discussed both the important physical effects and the available correlations under each type of boiling. Emmerson (3) and Roberts and Bowring (4) authored over-all reviews of boiling, and summarized nucleate boiling and burnout correlations. Lottes, et al. (5) presented summaries of the more widely published correlations for boiling heat transfer including the burnout phenomenon.

Gambill (6) presented a broad survey of boiling burnout in subcooled flowing systems and classified 103 references within this survey. This same author has periodically published a survey of developments in the boiling burnout literature (7).

Kepple and Tung (8) have abstracted the 1950-1962 literature on heat transfer and hydraulics for two phase systems which includes sections devoted to boiling, bubble dynamics, nuclear reactor heat removal, and two-phase flow.

Eckert, et al. (9-13) have presented a continuing heat transfer literature review with such pertinent categories as flow with separated regions, and change of phase. This same general group of authors has also published a heat transfer bibliography containing sections concerning phase changes and separated flow (14-33).

Luikov (34-40) has prepared bibliographies of the heat transfer publications in the U. S. S. R. Similarly, Sato (41-46) has edited bibliographies of Japanese heat transfer publications. Both series have sections devoted to heat transfer with phase changes.

Correlation reviews for burnout in tubular geometries and bundles with flow parallel to the longitudinal axis have been written for the American (47-48) and Russian (49) literature.

Pool Boiling

Bubble dynamics, pool boiling, and forced convection boiling inside tubes have been summarized by Rohsenow (50). Included in this summary are the effects of non-uniform heat flux, cross-sectional shape, tube size, and system instabilities on the burnout point. The author considers design recommendations based on available correlations in relation to their various effects.

Correlations of nucleate pool boiling generally originate with a physical model of a single bubble, with a column of single bubbles above it, leaving a nucleation site. An expression for the heat removal rate at the site is written in terms of bubble diameter, and bubble departure frequency. These variables are combined with the physical properties of the liquid and vapor, and the bubble contact angle to yield bubble Reynolds and Nusselt numbers. Some combination of Prandtl

number and the bubble Nusselt and Reynolds numbers is sought by comparison to forced convection heat transfer, e.g.

$$Nu_B = \xi\ (Re_B,\ Pr) \qquad 2\text{-}1$$

or by dimensional analysis. Rohsenow (50, 51) and Forster and Zuber (52) have used this approach in correlating pool boiling data. Zuber and Tribus (53) note that this approach omits surface roughness and thus will not predict nucleate boiling curves for all systems. They also mention that due to ignoring bubble interaction in the model, the surmised relationships will not predict the peak or critical flux between nucleate and transition boiling. The maximum nucleate boiling flux is a major area of interest to designers, since above this point burnout occurs or the less efficient film boiling begins.

Madejski (54) proposes that the bubble flux expression be divided into three terms: the first due to the motion of the column of bubbles; the second due to molecular transport in the liquid; the third due to eddy convection. The proposed model is capable of indicating one criterion of burnout, together with a method of examining surface influences.

The mechanism of heat transfer in terms of bubble initiation, growth, and departure above a gas-filled surface cavity has been studied by Han and Griffith (55). Their model consists of a transient thermal layer on the surface which is periodically disturbed by the departure of a bubble. The time delay between bubble initiations is theoretically a function of the bulk fluid and wall temperatures. By finding the thermal layer thickness as a function of time, a growth rate was established, and the effect of growth velocity on departure

volume was found to be due to contact angle changes. The authors (56) later demonstrated that this model would predict the boiling performance of a surface if the surface nucleation properties, contact angle, and the fluid properties are known. The authors admit that their procedure does not provide a general method of solving boiling heat transfer problems, but they feel they have illuminated the physics of nucleate boiling.

These pool boiling models are based on the formation of a vapor bubble on a favorable site on the heater surface. The energy path in boiling heat transfer is from the heater surface to the liquid and thus to the vapor bubble. Conduction from the metal directly to the vapor is significant only during the initiation stage. This is the basis for using the equation for conduction within the liquid. The appreciable contribution to the increased heat flux by the formation of vapor bubbles arises from the agitation of the liquid layer as the bubble leaves the surface or collapses on it. A volume of cold liquid equal to the bubble volume is brought to the hot surface in either case. The Reynolds number in 2-1 is then a measure of the amount of agitation provided by the bubble.

The critical heat flux region, (Fig. 1, points 5-6), was photographically studied by Cole (57) who concluded that the primary forces on a bubble leaving the surface are drag and buoyancy forces. A dimensionless relationship between bubble diameter, velocity, and contact angle was developed.

Another photographic study by Gaertner (58) resulted in his dividing the nucleate regime into at least three regions depending upon the mode of vapor generation. These modes were found to be discrete

bubbles, vapor columns, and finally vapor mushrooms as the surface temperature increased in saturated pool boiling. The author concluded that serious error must exist in any model which is based on a single mechanism such as individual bubbles.

The peripheral variation of the boiling coefficient on horizontal tubes was investigated by Lance and Myers (59). They found a cardioid configuration when boiling methanol with the maximum coefficient at the bottom, and an ellipitic configuration with n-hexane, the maximum coefficient occurring at the horizontal.

Taylor and Helmholtz instabilities are considered in the derivation of an expression to predict the burnout point by Zuber, Tribus, and Westwater (60). The Helmholtz instability states that the relative tangential velocity between two phases at their interface is always a destabilizing influence. The Taylor instability states that acceleration from the denser fluid towards the lighter fluid exerts a stabilizing influence on the two phase interface, and acceleration from the lighter fluid towards the denser fluid is destabilizing. Surface tension is a stabilizing force at the interface. Zuber, et al. (60) discussed the similarity of the conditions at the critical flux and the phenomenon known as "flooding". Instability theories are used to predict the nucleate to transition region change where burnout often occurs. Temperature increases in the nucleate region are accompanied by an increase in the number of active sites. A condition is reached where the vapor bubbles interfere with each other and an unstable, irregular vapor film is formed as a result of bubble coalescence. This vapor film is in violent motion and exists throughout the transition region. Surface temperature increases in this region tend to stabilize

the film, and finally the stable film condition is reached where an increase in surface temperature again causes an increase in the heat flux. Instability theories are hydrodynamic in origin and do not predict any effect of surface condition on the burnout heat flux.

A series of tests designed to demonstrate the inherent uncertainty in the pool boiling burnout flux have been reported by Gambill (61). A burnout detector circuit was used to preserve the test element and avoid surface variations due to different test specimens. The critical flux varied between 201,000 and 596,000 Btu/hr.sq.ft. for these saturated boiling tests on a 0.234 inch O.D. nickel tube. A general conclusion was reached that the surface condition has an important effect on the burnout point. The critical heat flux was increased by the presence of a thin deposit of copper or copper oxide on the nickel surface. The author decided a non-hydrodynamic factor related to the wettability of the coolant was responsible for the increase.

Vliet and Leppert (68) noted that aged surfaces subjected to boiling periods of 1 1/2 to 2 hours gave higher critical heat fluxes than unaged surfaces. Owens (86) obtained a significant variation in the critical heat flux from stainless steel cylinders in pool boiling by varying the surface cleaning method. Cleaning agents were carbon tetrachloride, ether, and acetone. The largest flux, 521,000 Btu/hr.sq.ft., occurred with tap water on a slightly contaminated surface.

Additional references and reviews on pool boiling are to be found in (62) in the section by Leppert and Pitts.

Forced Convection Boiling Inside Tubes

The boiling heat transfer literature has numerous publications on forced convection boiling inside tubes. Most of the papers on burnout with forced convection inside tubes have been reviewed by Gambill (63) and a statistical approach to the burnout prediction problem has been studied by Longo (64).

Forced Convection Boiling Outside Tubes

The section by Leppert and Pitts (62) contains a review of the external boiling literature.

The case of non-boiling forced convection heat transfer from a cylinder normal to the flow has been recently investigated by Perkins and Leppert (65, 66) for liquids at Reynolds numbers and temperature differences greater than formerly available in the literature. The authors (65) used an area correction factor and a velocity profile correction to accommodate the effects of cylinder blockage in the test section. The results are presented in graphical form and are utilized in the calculation of the channel Reynolds number. The final correlation for a Reynolds number range of 40 to 100,000, a Prandtl number range of 1 to 300, and a viscosity ratio range of 0.25 to 0.95 is:

$$(Nu)\left(\frac{\mu_w}{\mu_b}\right)^{0.25}(Pr)^{-0.40} = 0.30\,(Re)^{0.50} + 0.10\,(Re)^{0.67} \qquad 2\text{-}2$$

The general form of this equation was proposed by Richardson (67) who argues that the first term on the right-hand side of the equation represents the forward portion of the cylinder, and the second term the separated flow portion of the cylinder. Heat transfer studies in

the separated flow region of cylinders and flat plates in air have found the 2/3 exponent of Reynolds number to be adequate in describing experimental results.

Equation 2-2 was later modified by its authors (66) to the extent of replacing the Reynolds number coefficients of 0.30 and 0.10 by 0.31 and 0.11, respectively. Included in this work is an analysis of heat transfer in the laminar layer. A fourth order velocity profile expression and a third order temperature profile expression were used in the integral momentum boundary layer and thermal boundary layer equations respectively. For potential flow they arrive at the following expression for the laminar layer:

$$Nu = \frac{3}{a} \left(\frac{\cos \theta}{\lambda}\right)^{0.5} (Pr)^{b} (Re)^{0.5} \qquad 2\text{-}3$$

where: a = cylinder radius

θ = angle measured from the front stagnation point

λ = pressure gradient parameter

Equation 2-3 shows the origin of the 0.5 exponent on Reynolds number in equation 2-2. Channel blockage effects, local heat transfer coefficients, and turbulence levels are also examined and compared with other sources. This work was the predecessor of the forced convection boiling study of Vliet and Leppert (68).

These authors used water with a small amount of sub-cooling ($4^{o}F$) and forced it normal to wires and tubes of 0.01 to 0.189 inches O.D. at flow velocities of 1.2 to 9.5 fps. A model is presented in terms of the peak heat flux in the wake of the cylinder. The growing bubbles on the surface are assumed spherical with a contact angle of 45^{o} with the surface. The boundary layer thickness is assumed to be 1.707 times the

average bubble radius. Considering the boundary layer, it is assumed that the velocity distribution is linear in the layer. Outside the layer potential flow is assumed to describe the liquid velocity distribution and finally the bubble velocity in the layer is assumed to be one-half of the potential liquid velocity. Expressions for the vapor and liquid flow rates around the cylinder are written in terms of bulk velocity, angular position, and bubble radius; these expressions are combined with the original flux expression and simplified. An expression for the bubble radius is obtained from the work of Forster and Zuber (87), and substituted into the original expression to produce for the peak heat flux:

$$\phi_c = \frac{1.083\ k\ \Delta T_s}{\bar{F}\ \sqrt{\alpha}} \sqrt{\frac{U}{D}} \qquad 2\text{-}4$$

where k and α are the thermal conductivity and diffusivity of the coolant and $\bar{F}$ is the angle averaged fraction of the flux transferred from the heater surface directly to the bubble vapor and is determined experimentally.

The effect of wall thickness on burnout flux was next explored on 1/8 inch cylinders and rods; little effect was found for thicknesses varying from 0.006 inches to a solid rod.

The burnout flux as a function of velocity at a constant cylinder diameter of 1/8 inch was found to be:

$$\phi_c = 178\ U^{0.5} \qquad 2\text{-}5$$

The burnout flux as a function of diameter was:

$$\phi_c \cong D^{-0.15} \qquad 2\text{-}6$$

The expression determined for $\overline{F}$ was:

$$\overline{F} = 0.2\ U^{0.25} \qquad 2\text{-}7$$

For subcoolings less than $10^{o}F$ it was proposed:

$$\phi_c = 90\ \frac{U^{0.5}}{D^{0.15}} \qquad 2\text{-}8$$

A burnout flux correlation based on the superposition of convective and boiling contributions to the final flux has been proposed by Gambill (63). The procedure of superposition was proposed by Rohsenow (50) for the prediction of the forced convection boiling curve, Fig. 1, points 1-2-3-4-5. Provided reliable information for pool boiling and single phase forced convection for the flow geometry of interest is available, the boiling curve can be constructed. The procedure of combining contributions was utilized by Gambill (63) in the development of a burnout correlation. The final flux is determined by a contribution from each mode of heat transfer. Since burnout is concerned with a single point, Gambill's superposition method can be used directly to obtain a predicted burnout value. The author (63) has applied the correlation to all types of flow geometries for subcooled liquids, at wide ranges of velocity and pressure.

An example of burnout in annular flow has been presented by Becker (69) and the forced flow film boiling regime has been investigated by Bromley, et al. (70).

CHAPTER III

THEORETICAL CONSIDERATIONS

The theoretical analysis for single phase forced convection around a cylinder has been studied by Perkins and Leppert (66). The momentum equation is:

$$U^2 \frac{d\theta'}{dx} + 2(\theta' + \delta^*)\, U \frac{dU}{dx} = \frac{w}{\rho} \qquad 3\text{-}1$$

The velocity profile was assumed to be fourth order:

$$U = a_o + a_1 y + a_2 y^2 + a_3 y^3 + a_4 y^4 \qquad 3\text{-}2$$

A shape parameter was introduced:

$$\lambda = \frac{\delta^2}{\upsilon} \frac{dU}{dx} \qquad 3\text{-}3$$

The Holstein - Bohlen (71) method was used on a digital computer to find the variation of λ with angle for various velocity distributions.

The integral energy equation

$$\frac{d}{dx} \int_o^{\Delta} (T_1 - T)\, U dy = \alpha \left(\frac{T_1}{y}\right)_w = - \frac{q'}{\rho c_p} \qquad 3\text{-}4$$

was combined with a third order temperature profile

$$T = b_o + b_1 y + b_2 y^2 + b_3 y^3 \qquad 3\text{-}5$$

and a functional dependency of the Nusselt number of Prandtl and

Reynolds numbers was deduced. The agreement was noted between this basically theoretical approach and earlier experimentally determined correlations.

The equation governing the growth of a vapor bubble in the absence of forced convection, i.e., pool boiling, is the transient conduction equation which, when combined with expressions for the thermal layer thickness and bubble radius as functions of time, can be used to estimate values for the frequency cycle.

$$\frac{\partial T}{\partial t} = \alpha \frac{\partial^2 T}{\partial y^2} \qquad 3\text{-}6$$

This procedure has been followed by Han and Griffith (55) for the case of a linear temperature profile at the wall. The authors (56) also show agreement of their bulk convection model with experimental data. Considering one active site, any steady-state temperature profile above the cavity will be periodically disturbed by the departing bubble, see Fig. 2 (a) and (b). If the linear profile is assumed

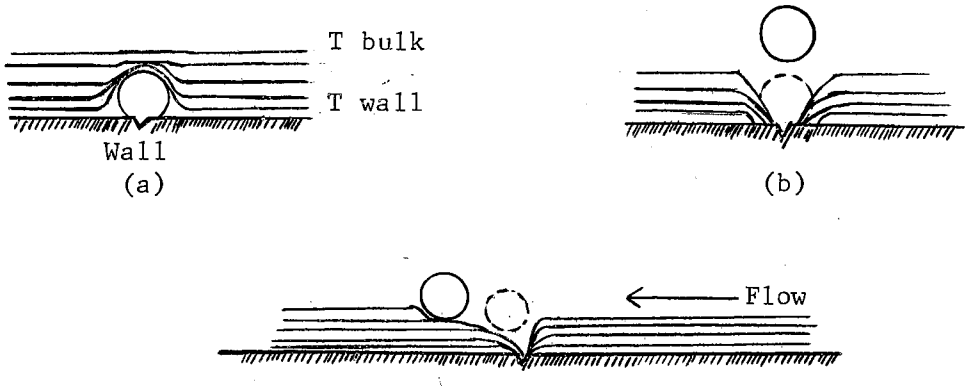

Figure 2. Schematic Diagram for Detaching Vapor Bubble

valid at the time the cold fluid reaches the wall, the addition of forced convection will decrease the period in which the linear profile exists.

The frequency of bubble emission has been divided into two parts: the waiting period and the growing period. The waiting period begins as soon as a bubble departs, and continues until growth initiates. This delay period is the result of cold liquid being forced to the wall in the wake of the departing bubble. The growth period starts when the thermal layer around the active nucleus has a mean temperature equal to the saturation temperature.

The sequence of events for the bubble cycle may be summarized as: (a) the bubble departs from the nucleation site, (b) the departure motion brings cold liquid to the hot surface, (the disturbed region surrounding the site is about twice the bubble departure diameter in a non-flowing medium), (c) the transient thermal layer grows by conduction away from the active site, (d) the steady-state convection thermal layer approaches the site, (e) the saturation temperature is reached and slightly exceeded on the nucleus surface starting growth, (f) the growing bubble influences the laminar velocity profile and the convection-transient temperature profile by both its physical presence and by microlayer vaporization, (g) bubble growth is terminated at the site by bubble departure when the restraining forces are overcome by the removing forces, (h) the bubble departs along some path in the vicinity of the surface. Consideration of each of these events will illustrate the problems involved in formulating an analytical model for forced convection boiling.

Steps (a) and (b) represent part of the accepted mechanism of heat transfer with boiling. Forster and Grief (72) have shown that a mechanism based on micro-convection in a sublayer cannot adequately account for the observed heat transfer rates. Micro-convection in the sublayer is a result of the radial velocity of the growing bubble. The induced liquid velocity components determine the temperature distribution near the heating surface. The micro-convection mechanism predicts that the flux will be directly proportional to the temperature difference between the wall and the liquid. This dependency has not been found to be experimentally consistent, and the micro-convection mechanism cannot be used to explain the major portion of the nucleate boiling heat flux.

Step (b) is concerned with the radius of influence of a departing bubble and remains open to investigation for both flowing and non-flowing systems. The case of pool boiling has been approximated by Han and Griffith (56) who observed the vortex ring in the wake of a ball pulled from the chalk-covered bottom of a tank of water. The departing sphere left a disturbed region whose radius was approximately twice the radius of the sphere. A bubble departing into a moving stream will have an area of influence which varies from the upstream to the downstream portions. The scavenging effect in the upstream direction will be less than that for the pool boiling case, due to the moving laminar boundary layer. The thermal layer downstream from the site will be furrowed for a distance by the moving bubble. The total influence of the bubble on heat transfer then does not end at the start of another frequency cycle with the flowing system as it does for the non-flowing system. Photographic observations in this work show some

liquid between the moving vapor bubble and the surface, but extensive work must be done to determine the relationship between liquid velocity, heat flux, point of origin, and bubble trajectory.

The disturbed thermal layer at the site may be considered as made up of a transient component and a steady-state component, steps (c) and (d). The transient component is due to conduction from the solid surface into the active nucleus, and the steady-state component is due to the forced convection of the liquid across the site. The time required to re-establish the temperature profile will be some function of the bubble diameter at departure divided by the average boundary layer velocity. This time represents the period required for the profile to cross the void previously occupied by the bubble, plus any additional area disturbed at departure. The net effect of the convection thermal layer will be to decrease the delay period by bringing hot fluid to the cavity nucleus more rapidly than in the non-flowing system. The actual time dependent temperature profile at the site is a necessary part of an analytical model. Thus the role of the area of influence of the departing bubble can be seen to be critical.

Step (e), during which the bubble nucleus surface reaches saturation temperature, requires a description of the path of heat flow, the surface temperature variation within the bubble cycle, and the dimensions of the active site. This latter point requires the correct description of an active site, its characteristics, and the effects of the liquid and solid, in determining what points will be active sites.

The growing process, step (f), is still subject to research to determine the actual mechanism of heat flow into the vapor void. The model of Forster and Greif (72) and the model of Han and Griffith (55)

both require that the growing bubble receive heat from the surrounding liquid. The microlayer model, however, states that heat flows from the surface into a microlayer which vaporizes, diffuses to the top of the vapor void, whereupon a portion of the heat is released to the liquid by condensation, and a portion remains as an increase in vapor volume. Moore and Mesler (88) have assigned the major portion of the boiling heat flux to microlayer vaporization. In either case, the growing bubble is affecting the transient temperature profile which can be considered as approaching some steady-state condition depending upon the flux level and velocity profile. At high heat fluxes or high frequencies, the bubble stream will approach a column and will be more important than the velocity profile effects in determining the temperature profile. The velocity profile description around a growing sphere on a flat plate will be three dimensional which will contribute to the complexity of the expressions involved.

The bubble finally reaches a point, step (g), at which the forces holding it to the surface are less than the removing forces, and it departs. The components acting on the bubble arise from dynamic forces, inertia forces, buoyant forces, and surface tension. Components normal to the bubble surface consist of inertia forces and forces arising from the movement of the flowing liquid around the sphere. Components due to buoyant forces will be a function of surface orientation. Tangential components come from flowing (dynamic) forces, surface tension, and a buoyant component. By assuming thermodynamic and hydrodynamic equilibrium as the bubble approaches its maximum surface size, a force balance will yield the departure diameter. These forces have been reviewed by Chang (73) where it is noted that a constant arises as each

force is resolved into its components. These constants have not yet been determined by research.

The departure trajectory, step (h), has its greatest influence on the shape of the area which is disturbed as the bubble departs. The bubble also contributes to the agitation of the fluid stream along the heater surface, since it is traveling at a velocity greater than the average boundary velocity, and possibly greater than the bulk velocity due to buoyant effects. An adequate velocity profile expression at bubble departure and movement into the fluid stream would be required to find the distance downstream from the active site at which the bubble influence ceases.

The unknowns in the foregoing discussion which remain subject to research are: cavity radius, force coefficients on the growing bubble, temperature and velocity profiles as functions of time, and the bubble departure diameter with the accompanying disturbed area.

Finally, the number of active sites as a function of temperature has not been investigated to the point of reliable prediction even for non-flowing systems. The number of active sites emitting vapor bubbles into the fluid stream varies greatly from the upstream portion of the cylinder to the wake region. Only when each of the foregoing has been thoroughly investigated, can an analytical model be formulated.

CHAPTER IV

EXPERIMENTAL APPARATUS

Pool Boiling

The pool investigations were conducted in a cylindrical ceramic vessel, 11 inches inside diameter and 12 inches deep (Fig. 3). A steam coil, 10 inch diameter, consisting of three turns of 1/4 inch copper tubing was installed in the bottom of the bath near the walls to preheat and maintain the boiling temperature of the distilled water. A plate glass cover served to retard evaporation.

The cylinder to be tested was mounted horizontally between two vertical solid copper rods, each one inch in diameter by one foot long. The copper rods were suspended (Fig. 3), from a rubber-coated phenolic block which rested, during operation, on the rim of the vessel. A second, smaller, rubber-coated phenolic resin block between the rods at their lower end served to strengthen the arrangement.

Temperatures inside the cylinder were measured by four thermocouples placed at 90° intervals around the circumference, starting at the lowermost point on the circumference. The thermocouples were as close to the midpoint of the cylinder between the electrodes as possible. The cylinder thermocouple lead wires passed through the longitudinal axis of one electrode (Fig. 3b), and the bulk water temperature thermocouple was located at the same level as the cylinder centerline.

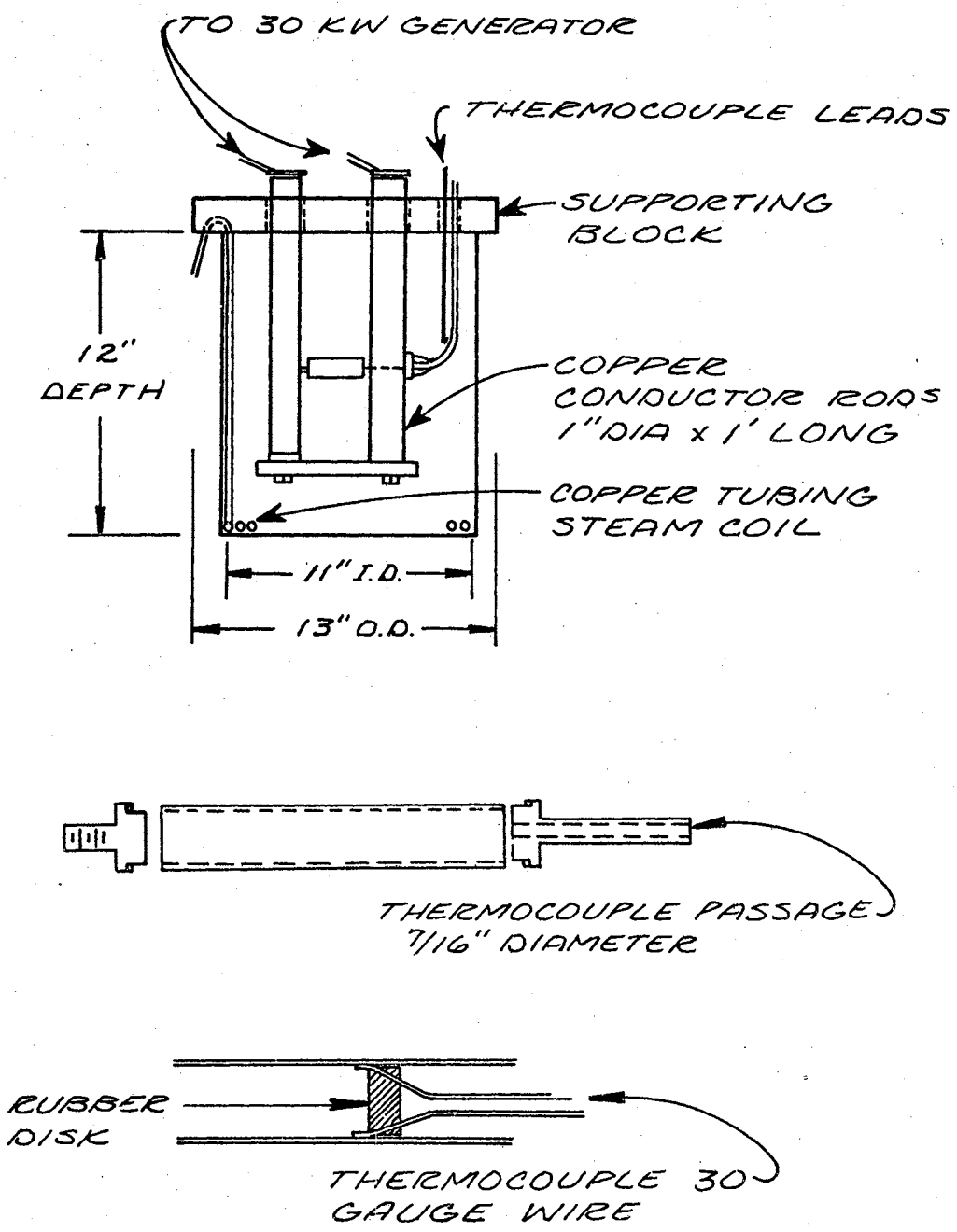

Figure 3. Pool Boiling Equipment

Thermocouple readings were made on a Leeds and Northrup model 8686 millivolt potentiometer.

The power source was a 30 kw Lincolnweld SA-750 motor generator. An external water-cooled resistor was included in the electrical circuit to allow control of the current flow. A remote control switch was installed in the generator field as suggested by the manufacturer to allow the power source to be turned on and off while observing the power meters and the cylinder itself. The remote control switch was used in an attempt to preserve the internal thermocouples by terminating the power as soon as burnout had occurred.

The power input to the cylinder was measured by a 0-5 volt voltmeter with leads connected to the ends of the cylinder, and a 1000 amp, 50 mv, shunt and ammeter. The voltmeter was calibrated with a volt potentiometer and the shunt, ammeter and leads were calibrated by the manufacturer.

The cylinders themselves were prepared by machining stainless steel (type 304) tubing until approximately half the wall thickness was removed. The variation in the outside diameter was held to less than 0.001" along the length of the cylinder. Since the cylinder stock was commercial seamless tubing, lengthwise variation of the inside diameter by 0.001" is to be expected. The wall thickness was measured at each end with a micrometer at 45° intervals. The resulting wall thickness variation was less than 0.0008 inches. Cylinders with larger variations were not used. The cylinders were polished with crocus cloth before using.

Thermocouples

The iron-constantan thermocouples were purchased pre-assembled from Omega Engineering Inc., Springdale, Connecticut. They were made from 30 gauge (0.010 inch diameter) wire. The thermocouples were prepared for use by covering the junction and at least three inches of each lead wire with 0.0034 inch thick Teflon film coating. The film was held in place by epoxy resin which was diluted and applied to the film and wire. The film was folded over the wire and the resin allowed to harden before trimming the excess film. This arrangement allowed eight wires to be passed through the 7/64 inch hole in the center of the electrode. Beyond the Teflon coating, the remaining iron lead wires were covered with a liquid porcelain paint for identification, insulation, and surface preservation.

Inside the cylinder, the thermocouples were supported against the cylinder wall by a silicone rubber disk, (Fig. 3). The disk was prepared in a mold first, then notched at 90^{o} intervals to accommodate the thermocouples. Each thermocouple was carefully mounted individually around the disk with its junction extending slightly out from and beyond any of the disk's surfaces. This insured mechanical contact with the cylinder wall without allowing unnecessary material to thermally insulate the contact point.

Forced Convection Boiling

This equipment consisted of a flow loop (Fig. 4), a test section, (Fig. 5), the same power source as the pool boiling studies, and the additional instrumentation required for measuring flow rates and higher power inputs.

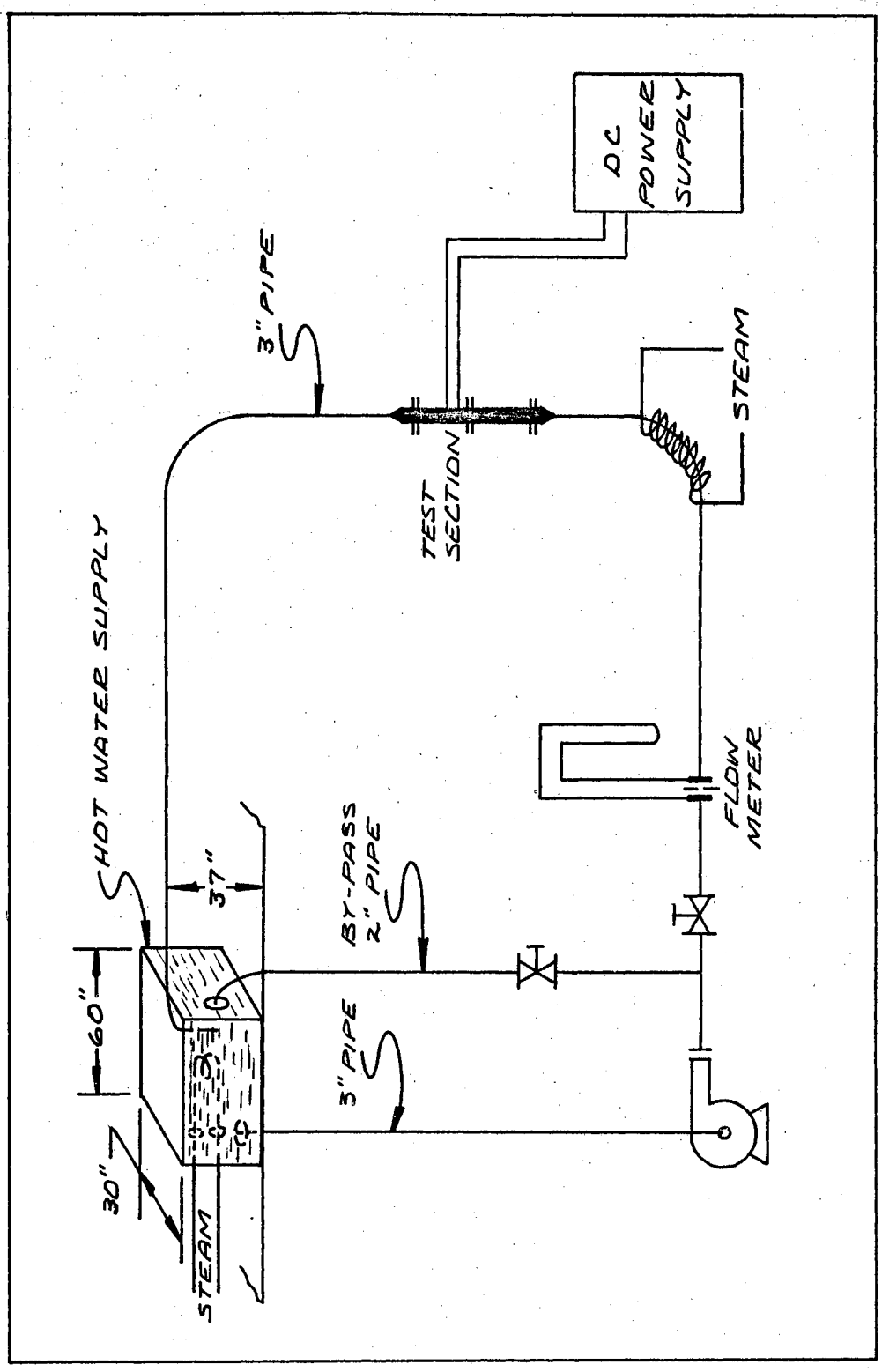

Figure 4. Schematic Diagram of the Flow Loop

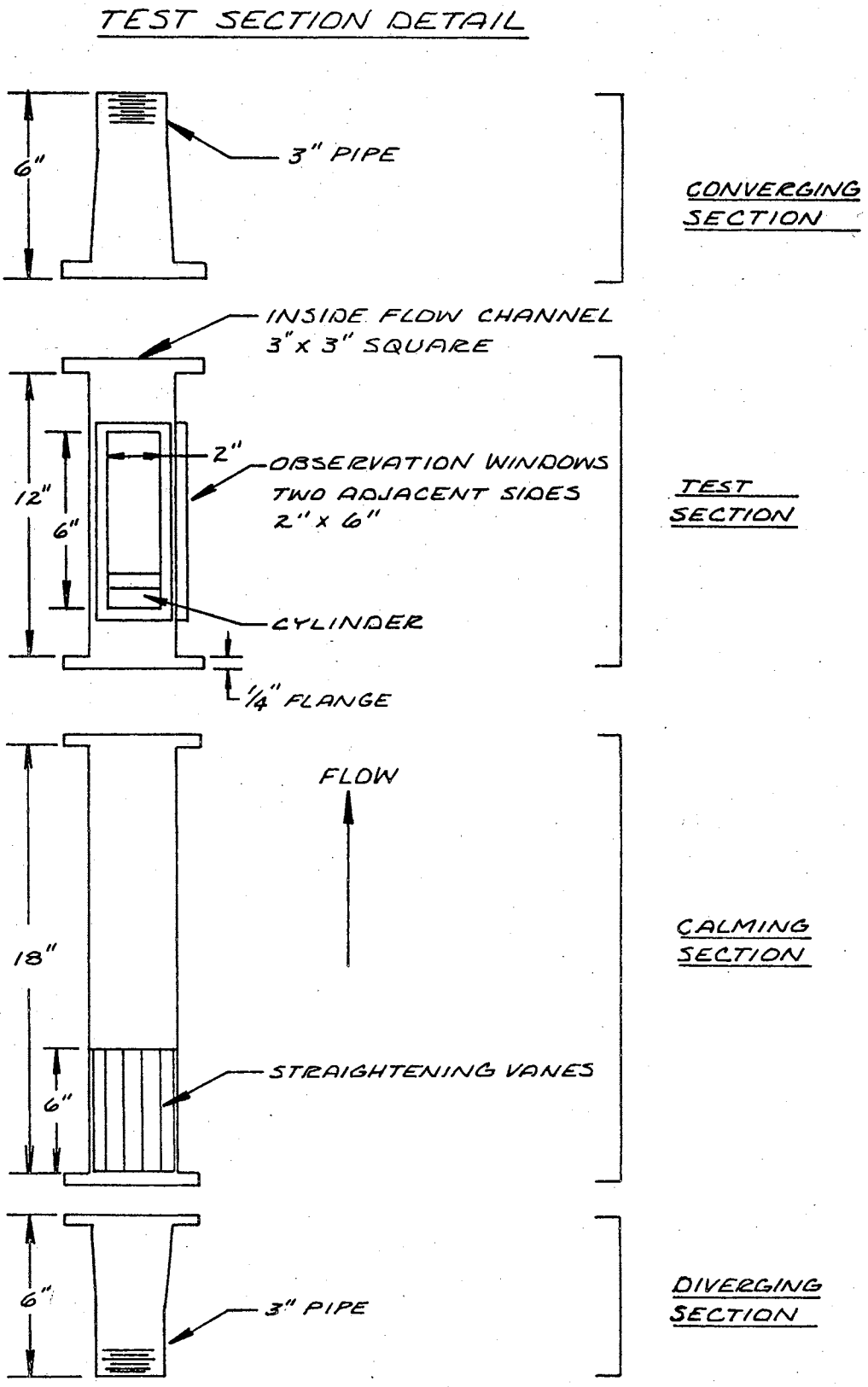

Figure 5. Test Section Arrangement

The test section (Fig. 6), has an inside cross section of 3 x 3 inches, a wall thickness of 3/16 inch, and a length of one foot. The test section was windowed on two adjacent sides providing two 2 x 6 inch viewing ports. The mounted specimen was supported by two copper electrodes, (Fig. 4), one entering the flow channel directly along the longitudinal axis of the cylinder, the other entering perpendicular to the longitudinal axis, passing in front of one window. The windows provided a complete lengthwise view of the cylinder and an end view of the cylinder which included both stagnation points for cylinders above 0.25 inches in diameter. Entrance ports were included in the test section wall to accommodate a pitot tube for traverses parallel and perpendicular to the longitudinal cylinder axis.

Located upstream from the test section was a 6 inch long diverging section, and a flanged 18 inch long calming section containing straightening vanes. The outlet end of the test section was flanged to a 6 inch long converging section.

The flow loop reservoir was constructed from a 275 gallon tank, which was insulated, enclosed, and equipped with a heating - cooling coil. A second, open, 275 gallon tank was used for orifice calibration purposes. The transfer line was 3 inch galvanized pipe, insulated, and steam traced with copper tubing along a 4 foot section prior to the test section. Circulation was supplied by a Goulds 4 x 4.7 centrifugal pump driven by a 5 Hp. electric motor, with a capacity of 300 gpm at 40 feet of head.

Water flow rates were measured by a 1.60 inch diameter orifice plate connected to a mercury manometer.

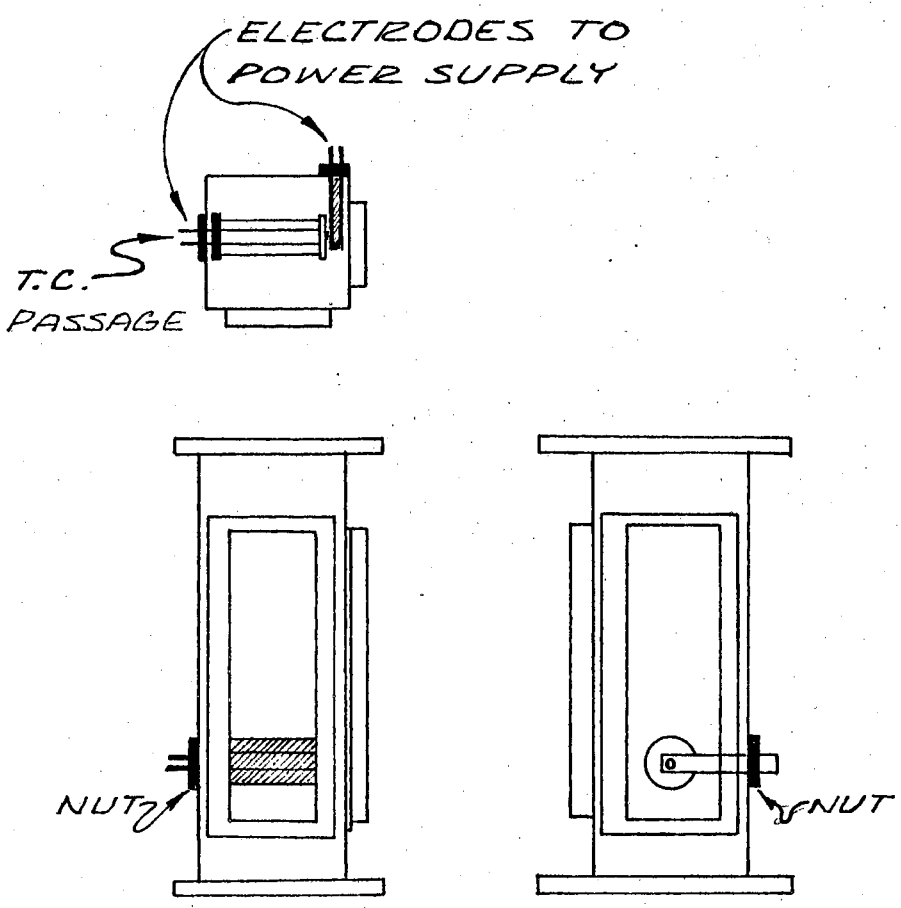

Figure 6. Test Section Detail

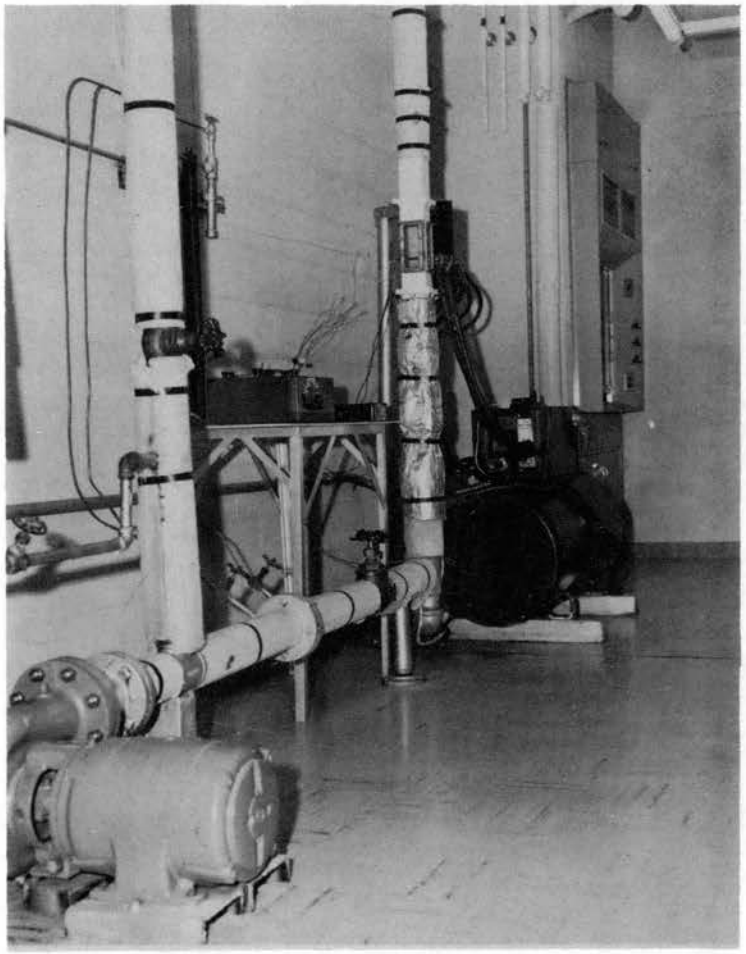

(a) Flow Loop

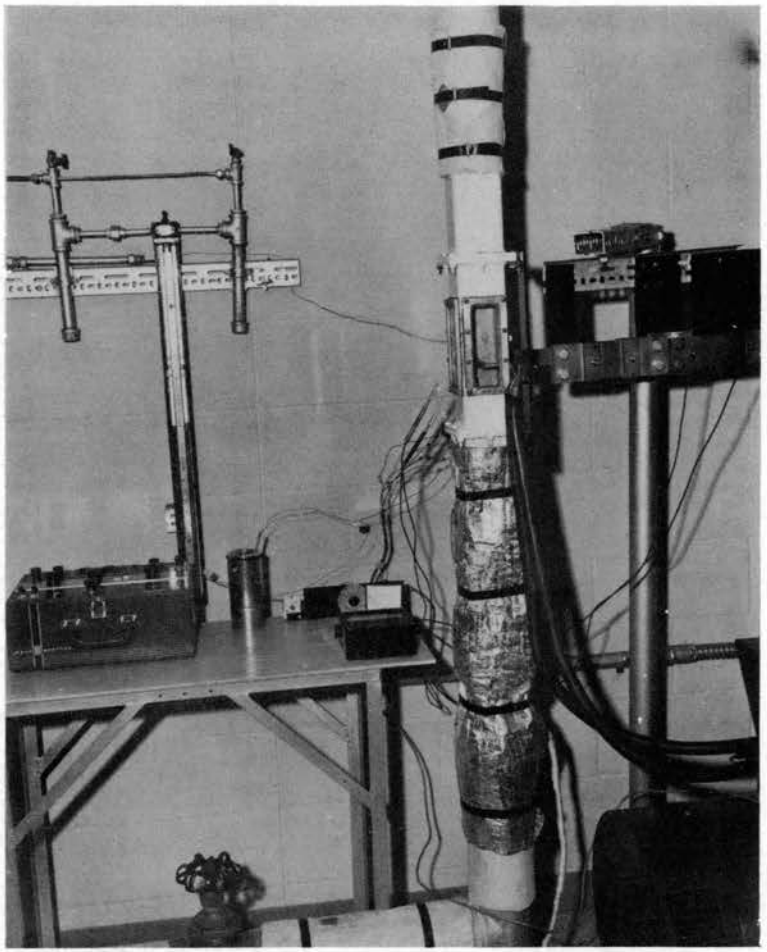

(b) Instrumentation

Figure 7. Forced Convection Boiling Equipment

The same thermocouple arrangement, power source, voltmeter, ammeter and potentiometer as used in the pool boiling studies, were employed for the forced convection boiling work. Inside cylinder temperatures included the forward and rear stagnation points and the two horizontal points. A reservoir thermocouple was used for heating control purposes.

Two shunts were connected in series for the forced convection boiling work. A 1500 ampere, 50 mv. shunt was used when the current exceeded the 1000 ampere range of the calibrated shunt and ammeter. The 1500 ampere shunt was used with a 0 - 750 ampere, 50 mv. ammeter, and the voltage drop across the 1500 ampere shunt was also measured by a second potentiometer. Readings below 1000 amperes were taken for both shunts where it was anticipated that currents greater than 1000 amperes would be required to cause burnout. In actuality, this occurred only once at 1060 amperes for the 0.707" O.D. cylinder with a flow of 3.42 fps.

CHAPTER V

EXPERIMENTAL PROCEDURE

Pitot Tube Studies

The flow pattern inside the test section was investigated to determine the presence of any large channelling effects. Pitot tube traverses were performed at various flow rates across the empty channel in two perpendicular directions. A 1/2 inch O.D. cylinder was installed in the test section and pitot tube traverses were made perpendicular to the cylinder in a plane which included the wake region of the cylinder. A traverse was also performed in the wake region parallel to the longitudinal axis of the cylinder. No gross channelling could be detected and the results of these studies are presented as Appendix B.

Thermocouples

Two sets of thermocouples were calibrated against a National Bureau of Standards resistance thermometer. The commercially prepared thermocouples showed variations of less than $0.2^{\circ}F$ between each other, the variation remaining essentially constant over the 200 to $300^{\circ}F$ temperature range. In this temperature range, the thermocouples indicated the actual temperature within $1^{\circ}F$. Since a temperature difference was of primary interest, one thermocouple was set up as a standard

and the bulk water thermocouple compared to the standard thermocouple. The remaining thermocouples used inside the cylinder were then checked against the bulk water thermocouple before each run with the circulating water at operating temperature and the correction factors established.

Pool Boiling

The copper electrodes which held the cylinder in place were coated with a thin film of solder, and then a heavier layer of soft lead. The lead was next machined to a flat even surface which acted as a gasket between the electrode and the cylinder. The electrodes and the inside contact area of the cylinder were polished with crocus cloth until the correct fit between the cylinder and electrode had been obtained. The voltmeter leads were soldered to the surface of the cylinder as close to the ends of the cylinder as possible.

The thermocouples were installed in the cylinder, the thermocouple leads extending through one electrode. The electrodes and cylinder were secured between the copper rods and the lower phenolic block tightened to discourage any movement. The thermocouple leads were sealed to the electrode with silicone rubber to prevent water from entering the cylinder. The submerged portion of the iron wires were also sealed to prevent corrosion.

The equipment was next placed in the distilled water bath, and the necessary power and instrument connections made. The steam to the heating coil was turned on, and remained on during operation to assure continuous boiling. When steady boiling of the bath had been

reached, an initial set of thermocouple readings was taken prior to turning on the power source.

The power was turned on, and a period of 10 to 20 minutes allowed for degassing and temperature stabilization before readings were recorded. The power was increased and the cylinder temperature observed until it stabilized. The potentiometer readings were made, and the readings recorded along with the time. As the power was increased, the direct current generator shunt field circuit temperature increased, and there was a tendency for the generator output to decrease. This effect diminished rapidly, and constant power readings would be obtained within one to two minutes after changing the output. The opposite effect was also observed when decreasing the power while the generator operating temperature was decreasing. Constant thermocouple readings were obtained within 2 to 2.5 minutes after changing the power setting, and a total time of about 5 minutes was allowed for each set of data points. The power was increased in increments of 20 amperes, which gave a flux increase of less than 10%. The final increments leading to burnout were between 6 and 8%, (3 values at 6%, one at 7%, two at 8%), of the last complete reading.

Forced Convection Boiling

The same electrode preparation as in pool boiling was followed in the forced convection studies. The cylinder was fitted with thermocouples, installed in the test section, and the appropriate connections made.

The reservoir was filled with condensed steam, and the system flushed by draining a portion of the water before starting the pump.

The steam was turned on to the coil, and the circulating pump started to maintain a uniform water temperature in the reservoir. Steam was admitted to the tracing upstream from the test section as soon as circulation through the test section was started. The flow rate could be regulated by the main globe valve below 200°F. As the boiling temperature was approached, some flashing was noted in the pump and the by-pass was closed to suppress the flashing and maintain the desired flow rate.

The flow rate thus established, an initial set of thermocouple readings was recorded after the maximum bulk temperature had been reached and before starting the generator. The generator was started and a 10 to 20 minute period, at a flux just sufficient to initiate boiling, was allowed to degas the cylinder surface. The power was then set at the desired starting point, and recordings started.

The power was again increased in increments of 10% or less until the maximum output of the generator was reached, or burnout occurred. In the former situation, additional readings were made while decreasing the power from the maximum. If burnout had taken place, a portion of the cylinder wall was destroyed, water would leak through the thermocouple wire passage in the electrode, and it was necessary to shut down. To shut down, the control valve on the main line was closed, the by-pass and drain valves were opened, the valve downstream from the cell closed, and the cell drained. The generator field could be turned off remotely or at the unit itself. The circulating pump should not be turned off with the water flowing through the cell, as the resultant hammer was found to be sufficient to cause failure of the cell windows.

A water sample was collected at the end of each run, cooled, and the oxygen content and electrical conductivity measured. The oxygen content was found to be between 1.8 to 3.0 ppm, while the average was 2.3 ppm. Since heating the reservoir required approximately 45 minutes and an additional 45 minutes elapsed before initial boiling data were recorded, it is felt that this value is representative of the entire run. The electrical resistivity had an average value of 110 micromhos per centimeter, as compared to 57 micromhos per centimeter for departmental distilled water. This measurement was made when the resistivity was a maximum for the run.

Two forced convection boiling runs were performed for the purpose of obtaining high-speed motion pictures. The film was exposed at a rate of 3000 frames per second with a Fastex camera, using a 0.457 inch O.D. cylinder as the subject. The coolant velocity was 3.42 fps and 5.44 fps, identical to the rest of the forced convection boiling runs. Initial portions of the films are at film speeds less than 3000 frames per second, due to the time required for acceleration, but a significant length of film was exposed at the desired rate. The films were developed and observed on a standard 16 mm projector and measurements were taken from the films with a microfilm reader. The reported bubble diameters and velocities were made in the forward region of the cylinder since the individual bubbles could not be distinguished in the wake region. The bubble velocity reported is the component of the velocity in the flow direction. These velocity components were in agreement with empty channel pitot tube studies. The results of the film studies are given in Appendix D, which also contains data reduction and sample calculations.

CHAPTER VI

EXPERIMENTAL RESULTS

Boiling Curves - Pool Boiling

The pool boiling results are shown as Figs. 8-12, and summarized as Fig. 13. It will be noted that the saturation temperature is used on the abscissa. The wall temperature is the average of the four outside surface temperatures, except for the 0.2497 inch O.D. cylinder, where only a single thermocouple was used inside the cylinder.

In drawing the pool boiling curve where a large amount of scatter exists due to the inclusion of data from more than one set of runs, preference was given to the final points leading to burnout. The pool boiling line in Fig. 8 is such a case, where the data from two successive runs are included: one run covering the low flux range (60,000 to 300,000 Btu/hr.sq.ft.) and the second run the high flux range (125,000 to 350,000 Btu/hr.sq.ft.). Both sets of data become asymptotic to the line shown, a deviation occurring with the initial points of the higher flux tests. A second deviation occurred in the midst of the low flux run. At a flux of 95,500, which was 45 minutes after start-up, the temperature difference remains close to $18^{\circ}F$ for a flux range of 95,500 to 185,000. After the readings were made at 95,500 and the power increased, the potentiometer reading made the expected increase, then abruptly dropped. Above a flux of 185,000, which was after 104 minutes of operation, a definite increase was noted in the

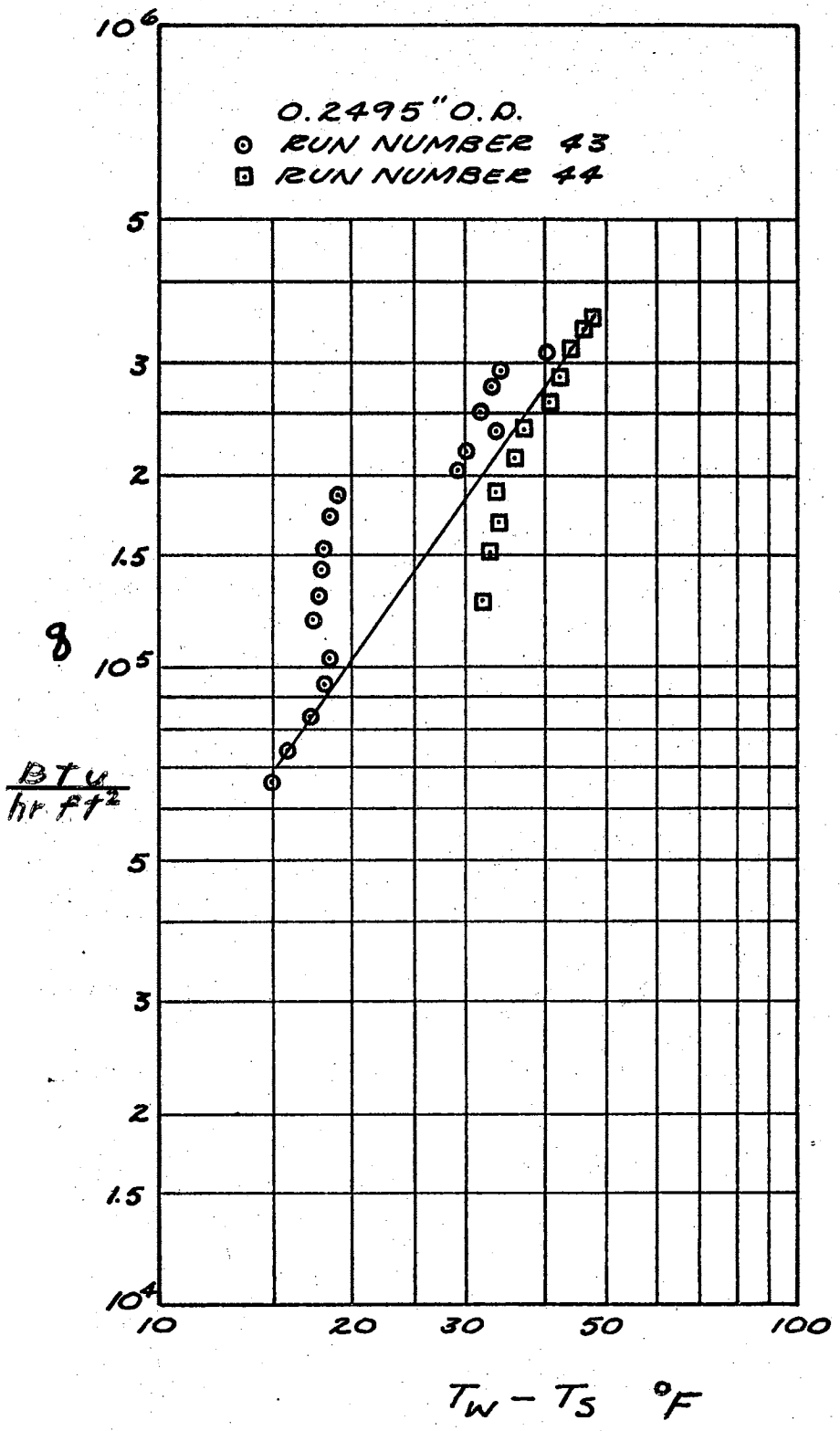

Figure 8. Pool Boiling Curve for 0.2495 in. O.D. Cylinder

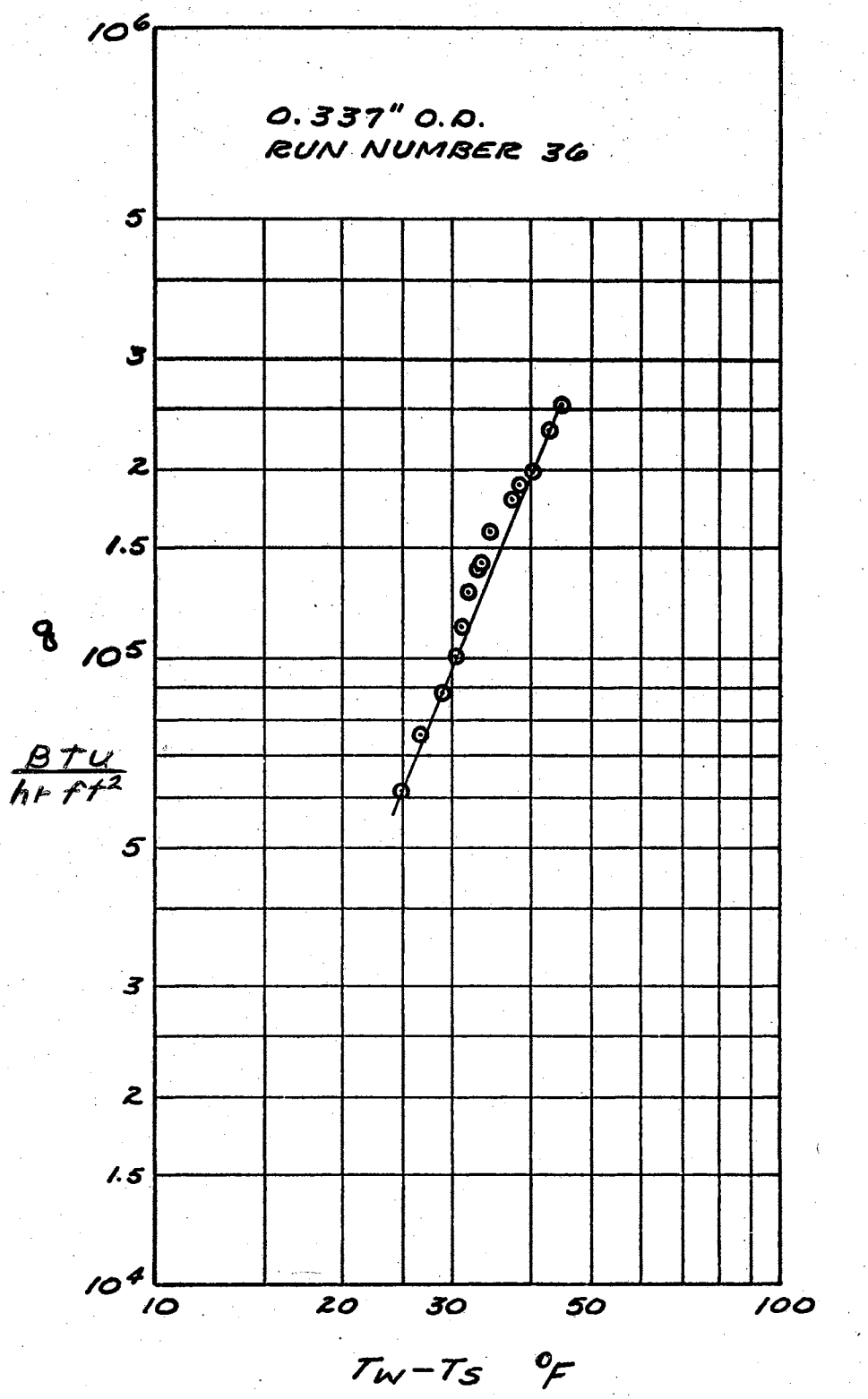

Figure 9. Pool Boiling Curve for 0.337 in. O.D. Cylinder

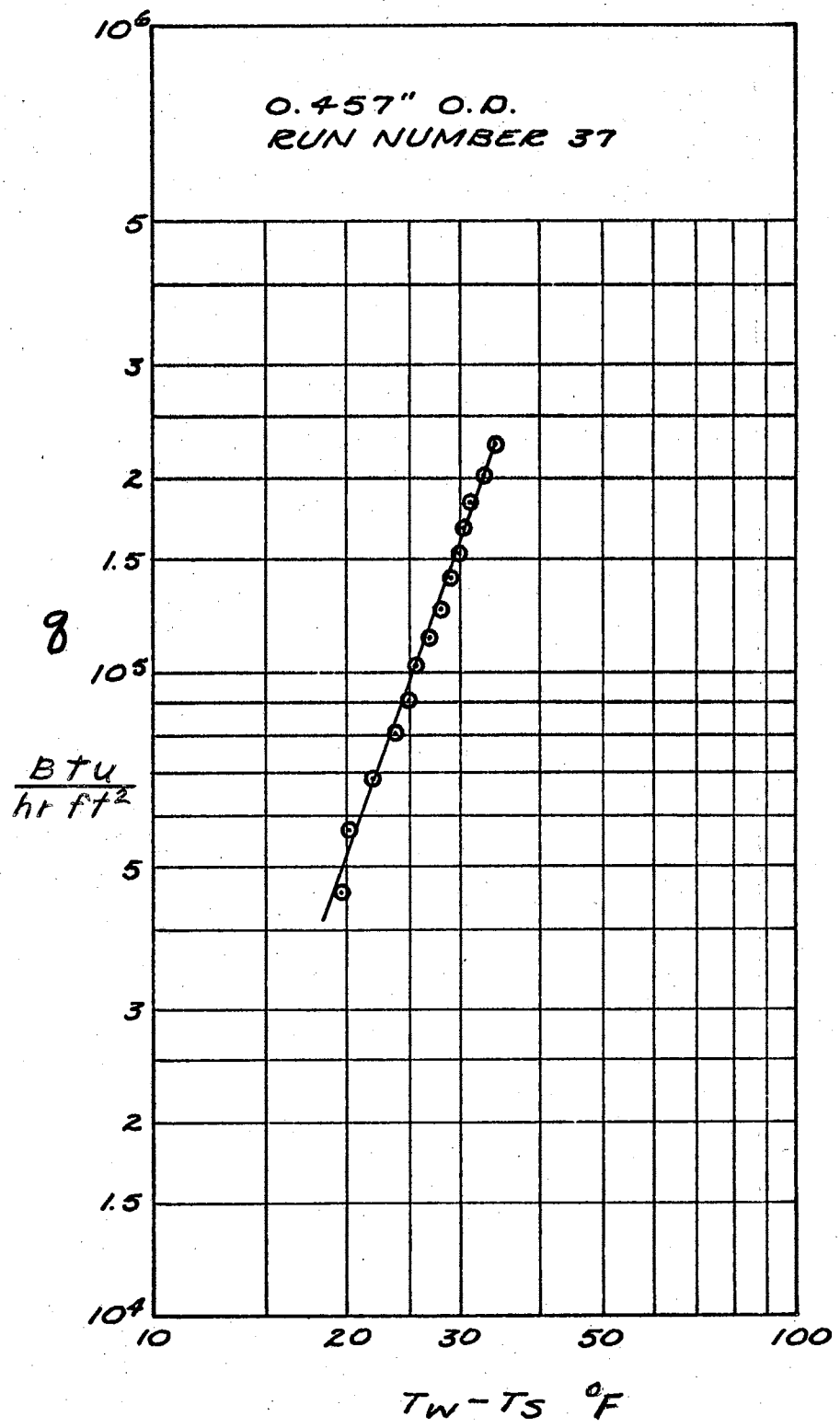

Figure 10. Pool Boiling Curve for 0.457 in. O.D. Cylinder

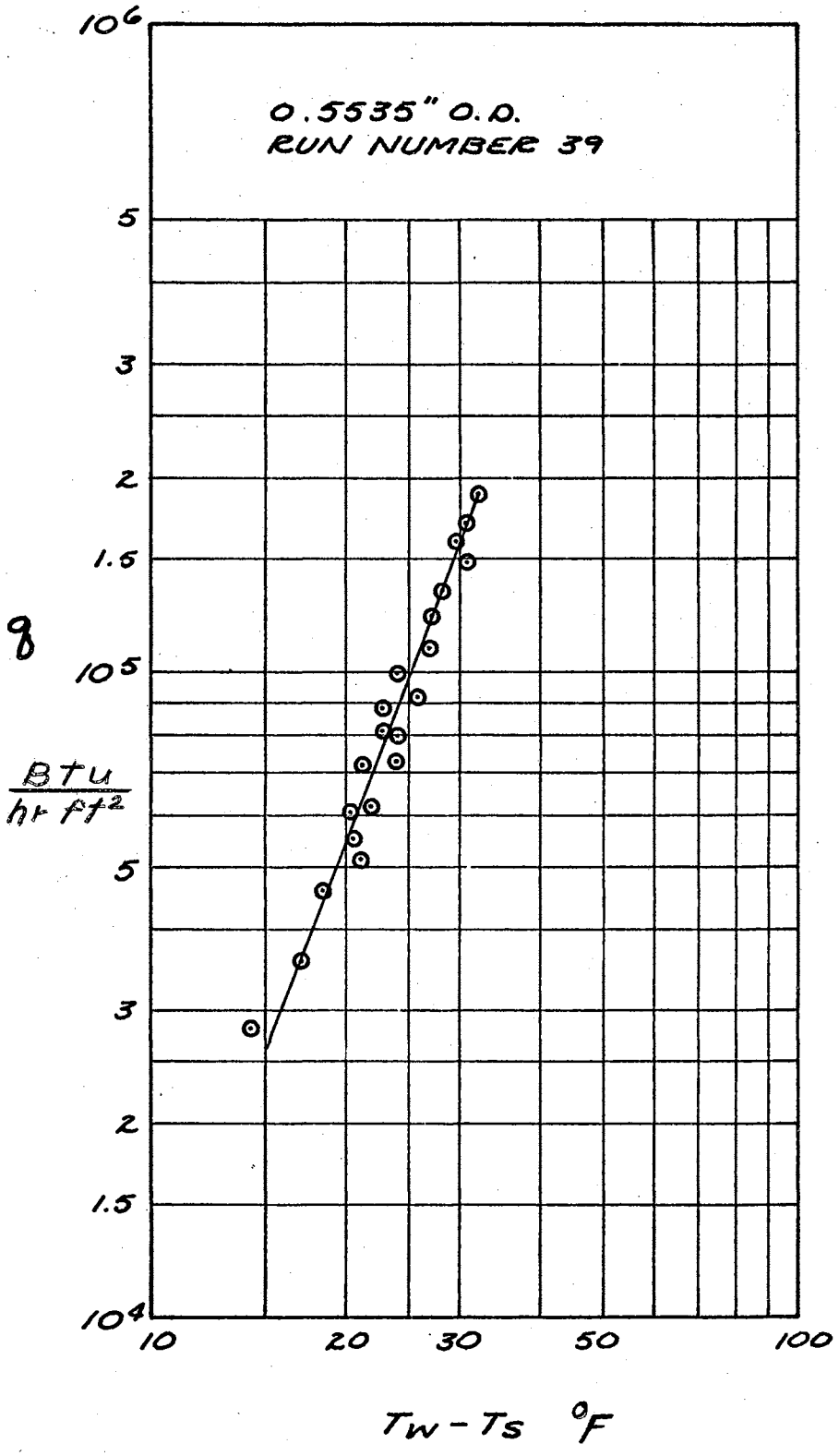

Figure 11. Pool Boiling Curve for 0.5535 in. O.D. Cylinder

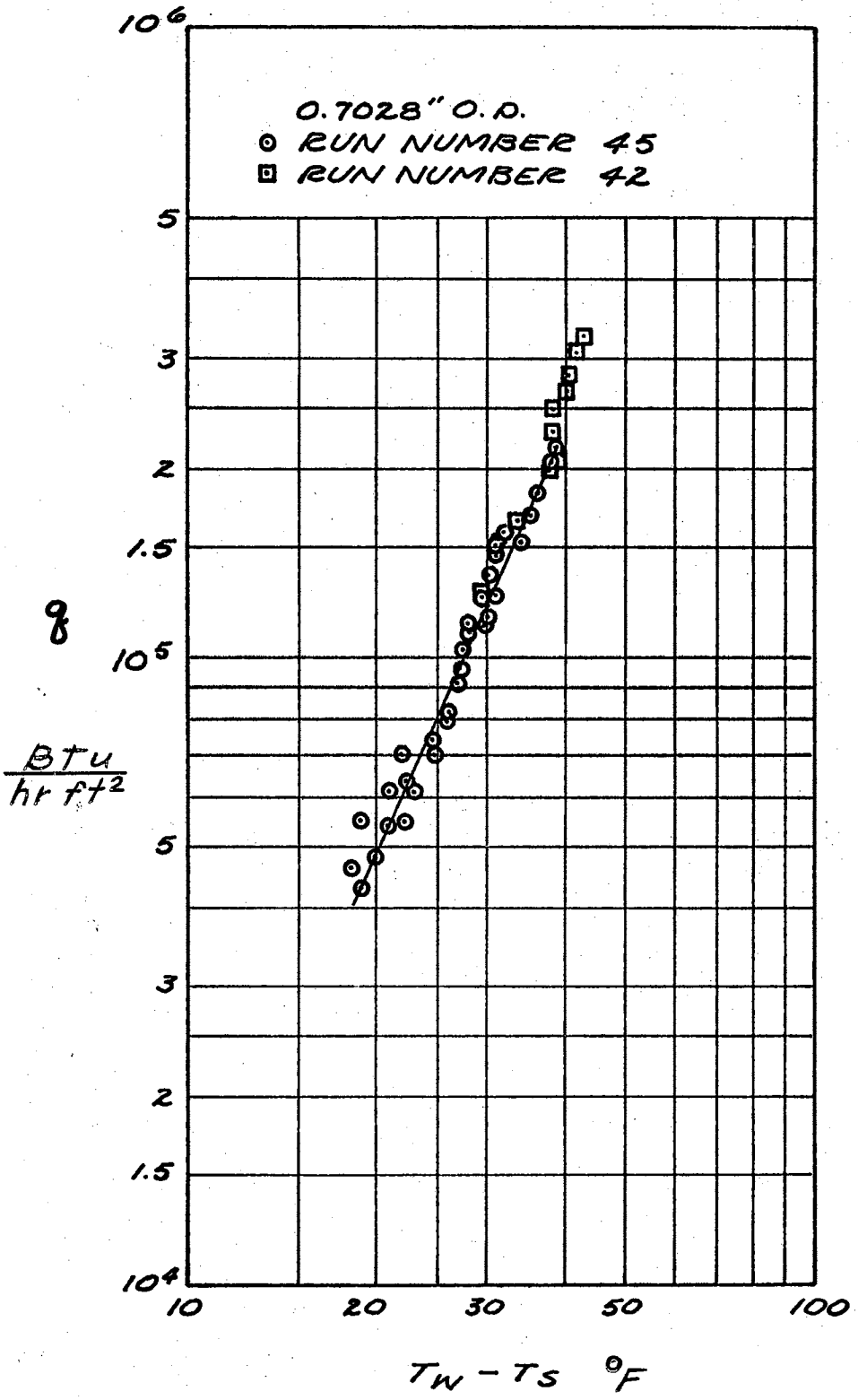

Figure 12. Pool Boiling Curve for 0.7028 in. O.D. Cylinder

potentiometer reading. Neither change was instantaneous, as a faulty connection would cause, but gradual, much the same as the usual change found after increasing or decreasing the power throughout a run. The most significant difference between this run and the others was in surface preparation. The 0.2497 inch O.D. cylinder was not subjected to any machining operations prior to polishing. The existing surface as received from the manufacturer was polished with crocus cloth and then used. Residual surface stresses would vary with the preparation method and could affect the activation rate of nucleation sites with temperature. The variation between the initial points of each run also indicates that inactivation of sites without exposure to air requires time for re-establishment. The surface history role on the boiling process can be seen to be important in pool boiling. Considering only the final points leading to burnout, it is felt that a representative pool boiling curve has been found.

The equations of the pool boiling lines were determined by the method of averages on the assumption that this method would provide satisfactory accuracy to reproduce these curves elsewhere. The equations are:

$$q = 1686\ \Delta T_s^{1.37} \qquad \text{for} \qquad \text{O.D.} = 0.2495'' \qquad (6\text{-}1)$$

$$q = 17.10\ \Delta T_s^{2.54} \qquad \text{O.D.} = 0.337'' \qquad (6\text{-}2)$$

$$q = 15.10\ \Delta T_s^{2.71} \qquad \text{O.D.} = 0.457'' \qquad (6\text{-}3)$$

$$q = 26.77\ \Delta T_s^{2.54} \qquad \text{O.D.} = 0.5535'' \qquad (6\text{-}4)$$

$$q = 43.28\ \Delta T_s^{2.31} \qquad \text{O.D.} = 0.7028 \qquad (6\text{-}5)$$

Attention is drawn to the spread of the pool boiling curves (Fig. 13), and the need for caution in using pool boiling data in generalized correlations. No well-defined diameter effect exists for this diameter range. While the exponents in equations 6-2 to 6-5 are in agreement with published values which vary between 2 to 4, it will be noted that a flux difference of 20,000 to 50,000 exists at a given ΔT_s.

Boiling Curves - Forced Convection

The forced convection boiling data is presented with the reproduced pool boiling curves as Figs. 14-18. The abscissa is the same as on Figs. 8-12, although a $12^{o}F$ subcooling existed for the forced convection boiling studies due to the static head effect on the saturation temperature.

The pool boiling curve in Fig. 14 is remarkably close to the forced convection boiling curve for the 3.42 fps velocity run. The slopes of the curves in the established boiling regions are about equal, and all are less than the slopes of the larger diameter cylinders. The small diameter cylinders used for the forced convection boiling work also did not receive any machining prior to testing. In Fig. 15 the pool boiling curve is in its expected position below both forced convection boiling curves. The 5.44 fps curve in Fig. 16 shows a higher surface temperature than one would expect by comparison with the data from other diameters. A slight amount of tarnishing occurred during this run, but only enough to slightly discolor the surface.

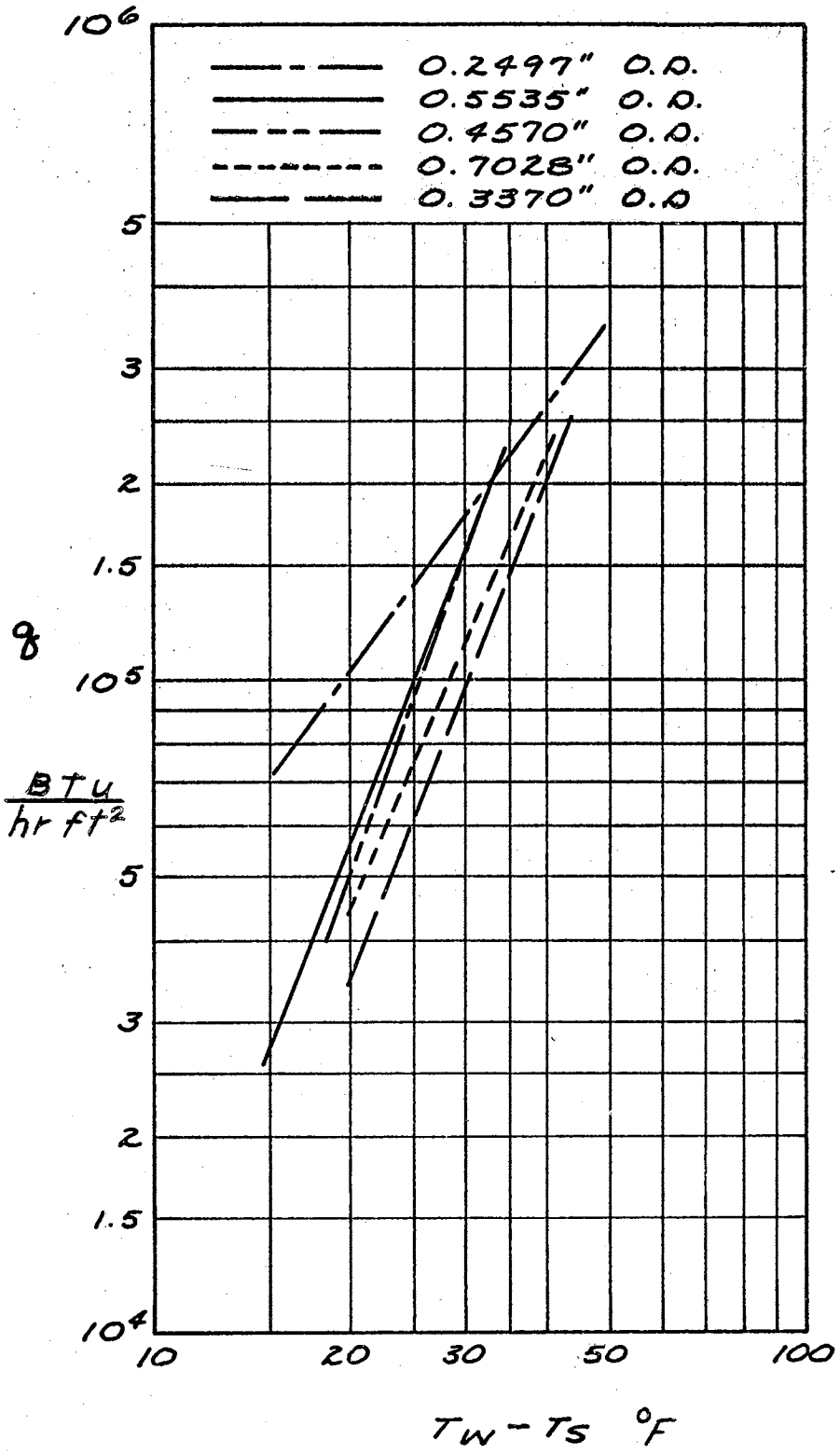

Figure 13. Summary of Pool Boiling Curves

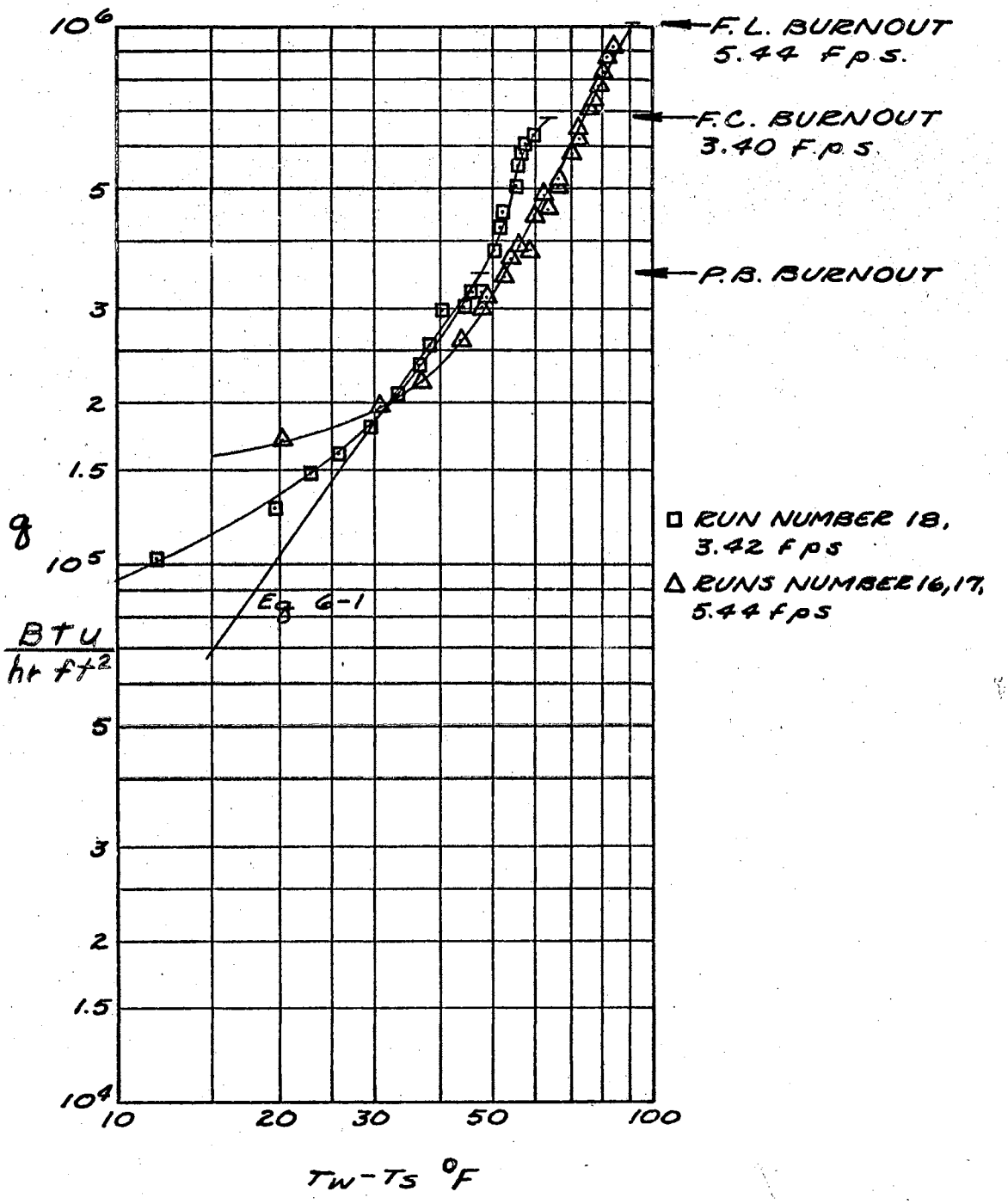

Figure 14. Forced Convection Boiling Curves for 0.2495 in. O.D. Cylinder

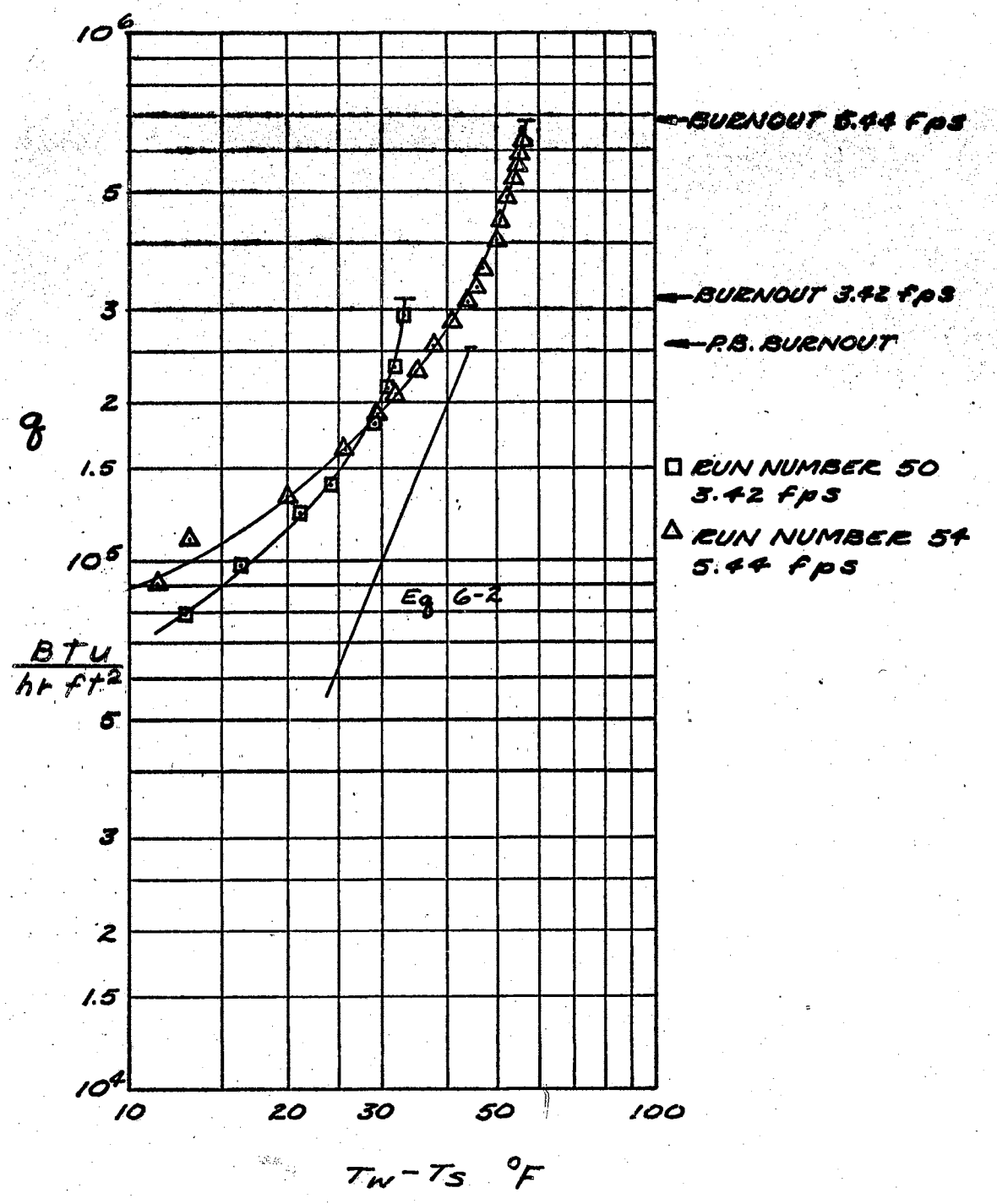

Figure 15. Forced Convection Boiling Curves for 0.337 in. O.D. Cylinder

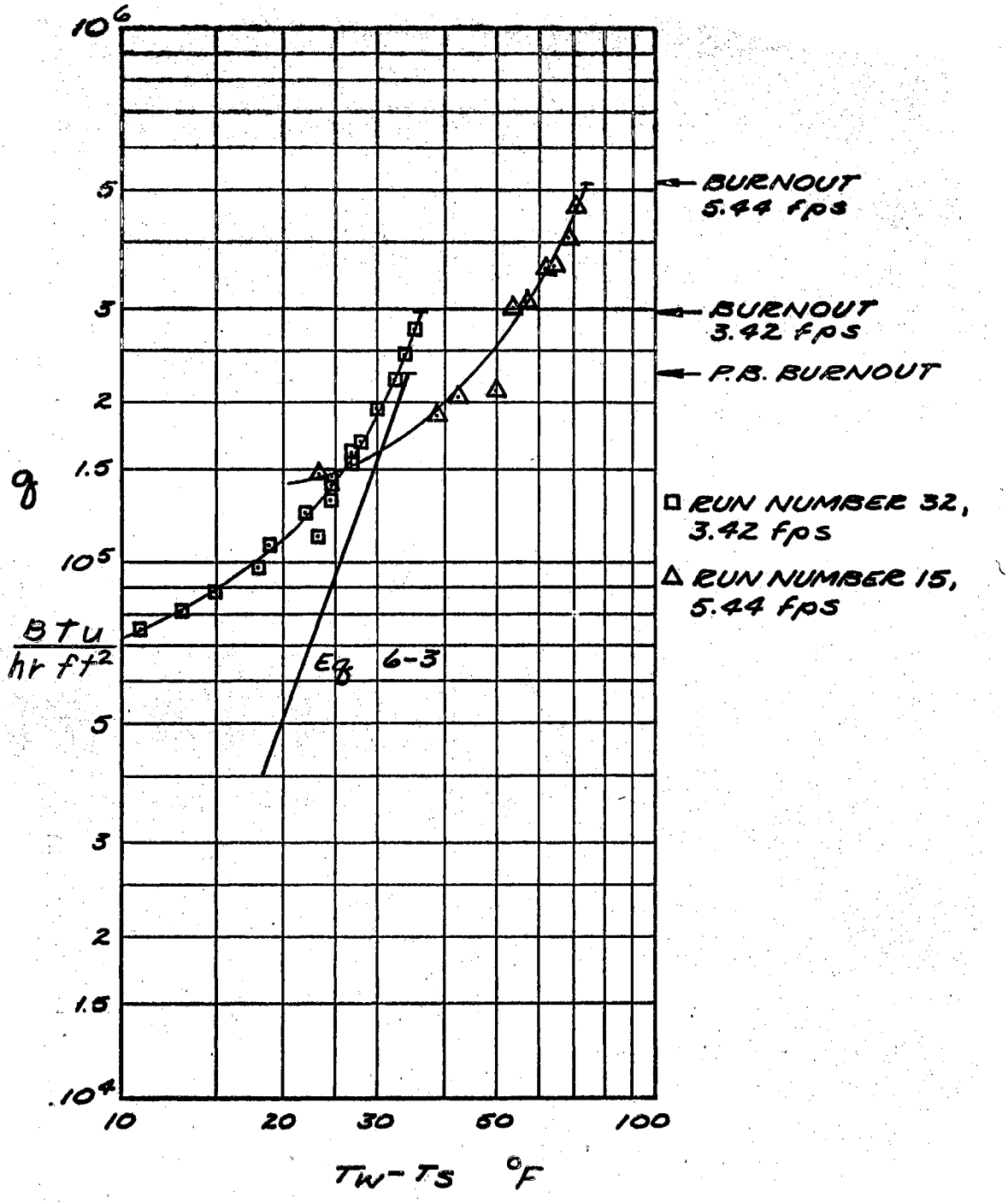

Figure 16. Forced Convection Boiling Curves for 0.457 in. O.D. Cylinder

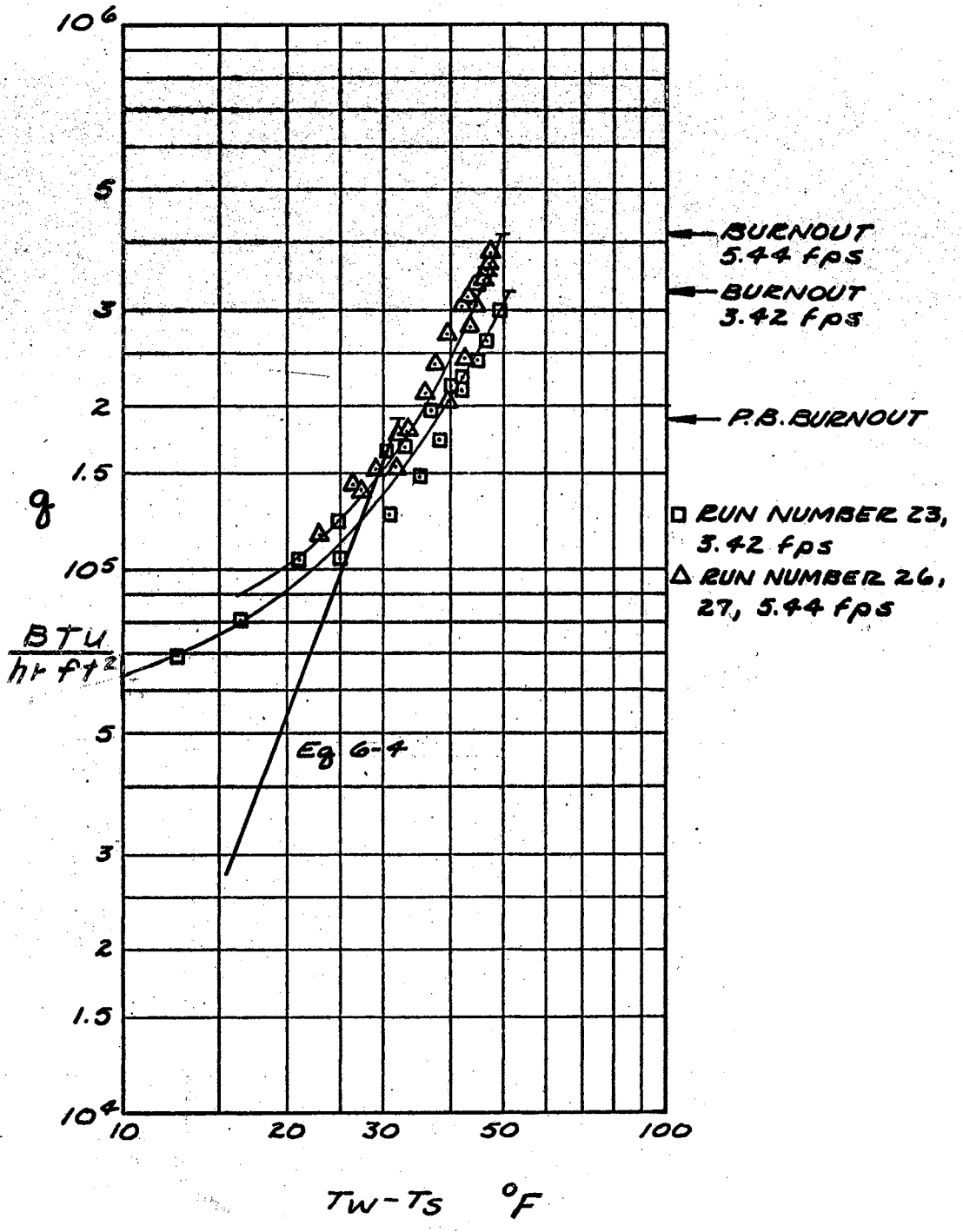

Figure 17. Forced Convection Boiling Curves for 0.555 in. O.D. Cylinder

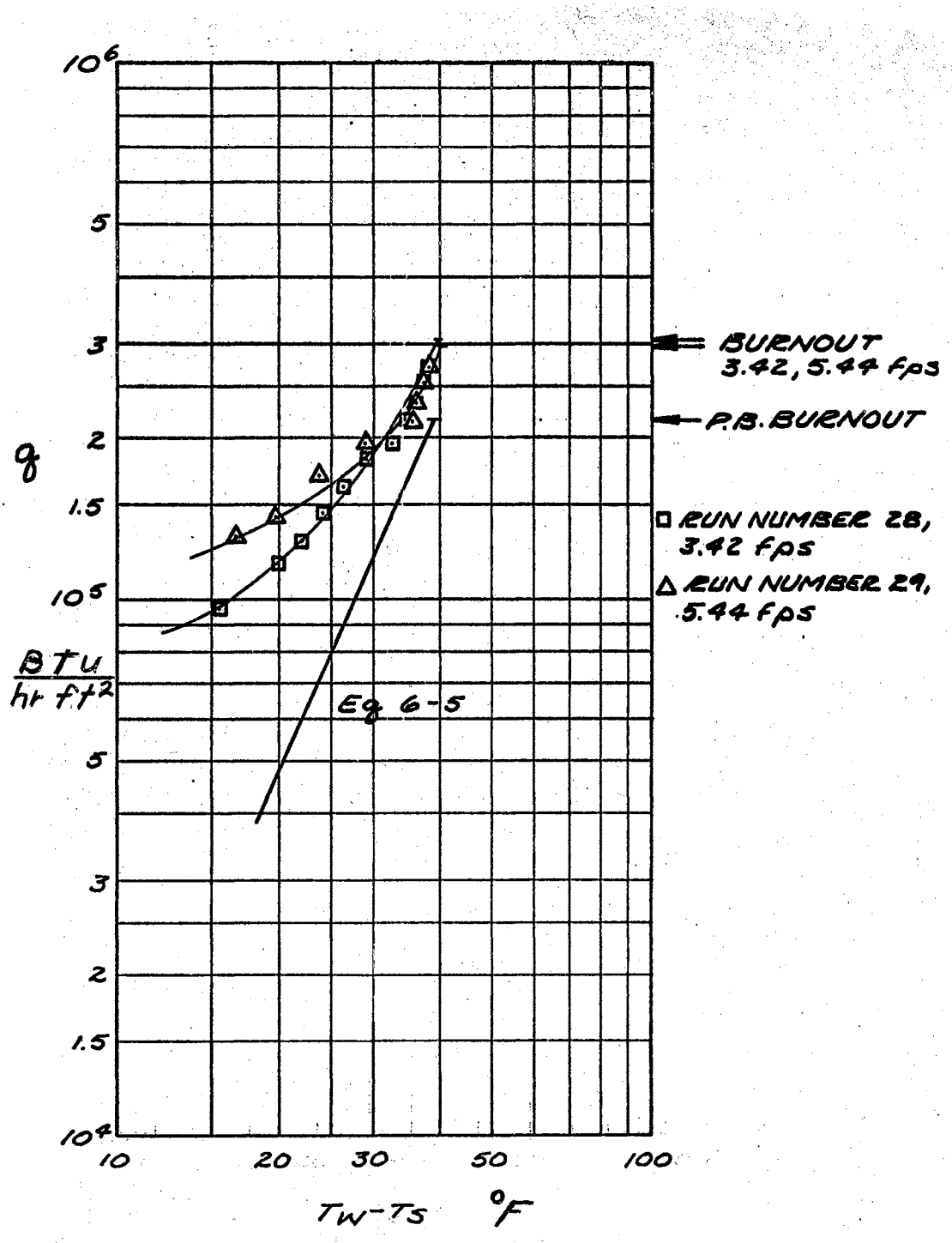

Figure 18. Forced Convection Boiling Curves for 0.707 in. O.D. Cylinder

This was a gradual occurrence, which will influence the shape of the curve more than the position. The pool boiling curve of Fig. 17 was determined from typically random boiling data, and would ideally be slightly to the right of the actual position. The pool boiling curve does merge with the forced convection boiling data. Fig. 18 also shows the approach of the forced convection boiling curves to the extended pool boiling curve.

Fig. 19 shows the flux as a function of the average temperature difference, ΔT_b, for the various diameters at a flow velocity of 3.42 fps. The driving force, ΔT_b, is the difference between the calculated average outside wall temperature and the measured bulk temperature. With the exception of the 0.707" O.D. cylinder, the flux at a constant ΔT_b decreases as the diameter increases. This is in accord with the prediction of the single phase forced convection coefficient equation D-25. This trend does not hold in Fig. 20 which shows the results obtained with a flow velocity of 5.44 fps, (see also Fig. 13 for pool boiling). Since each run was performed on a different cylinder, it can be seen that the individual surface characteristics of a cylinder for boiling overshadow the forced convection contribution which has a well-defined diameter effect.

The same coordinate system as Figures 19 and 20 is used in Figures 21-25 to show the influence of flow velocity on the boiling curve at constant diameter. It is normally expected that an increased flow rate would produce an increased flux for the same outside diameter and ΔT. This is borne out in the lower portion of the boiling curves where they approach the single phase forced convection curves. Departure from pure forced convection single-phase heat transfer produces an inversion

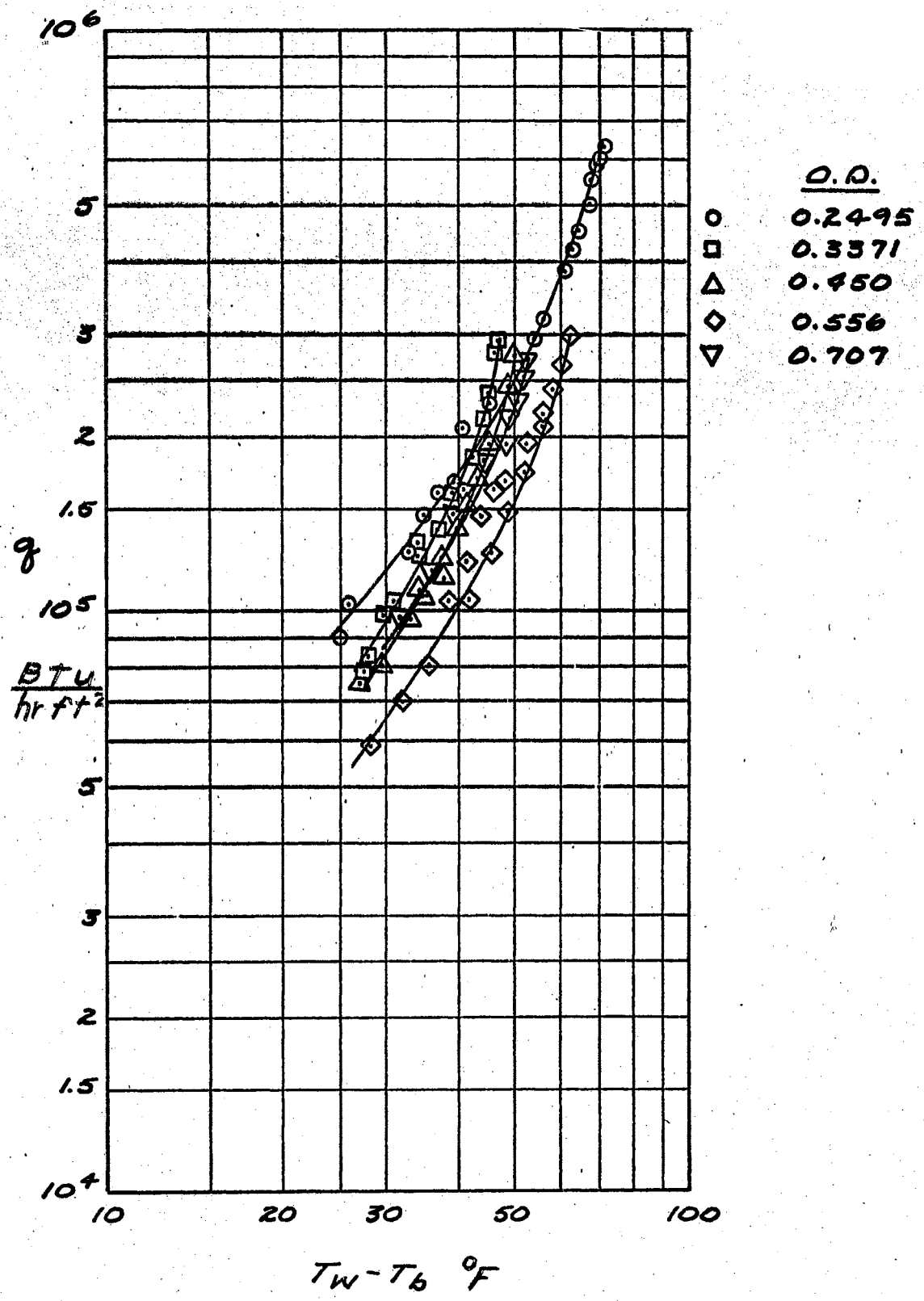

Figure 19. Diameter Effect on Forced Convection Boiling at 3.42 fps

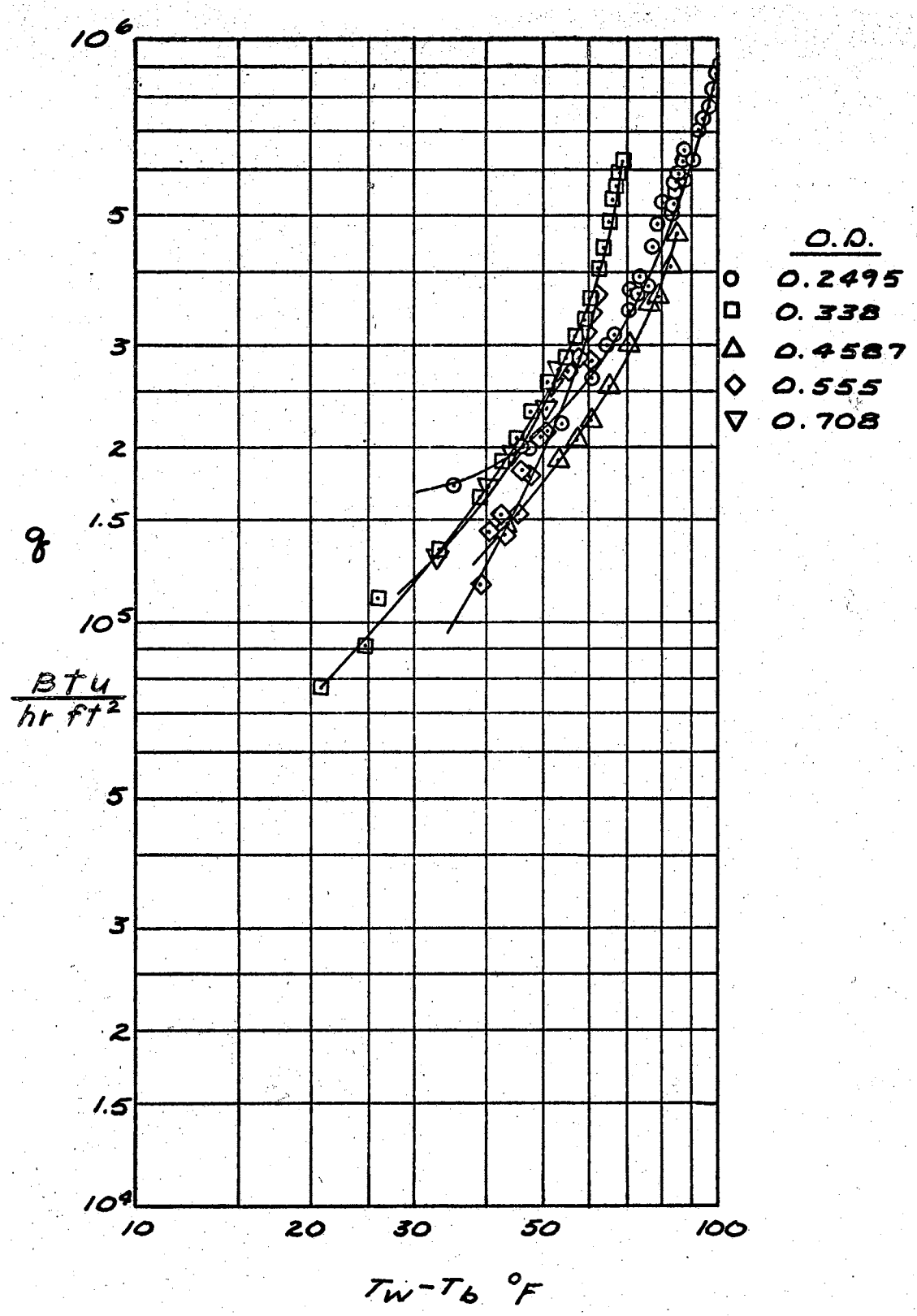

Figure 20. Diameter Effect on Forced Convection Boiling at 5.44 fps

in the expected positions of the curves as shown in Figures 21, 22, and 23. Since each curve represents an individual cylinder, and reasonable agreement is found on the single phase portion of the curves, the inversion of positions must be due to each cylinder having a unique active site distribution. Figures 24 and 25 have the expected positions of the boiling curves with the variation in flow velocity.

Boiling Curves - Local Conditions

The localized boiling curves for four positions around the cylinder are presented in Figures 26-33 for forced convection boiling, and Figures 34-38 for pool boiling.

The complexity of forced convection boiling mechanisms is displayed by two distinct observations from the forced convection boiling data. The first observation is the shape of the curves, other than the front stagnation point (0^o) curve. Only the 0^ocurve, with the exception of Fig. 30, shows no inflection point as the flux is increased. This apparently inidcates one boiling mechanism, nucleate, is operating in conjunction with the flowing liquid which is removing the vapor bubbles before interaction between bubbles occurs. The remaining positions are subject to the bubble-bubble interactions which are typical of other boiling situations. A second observation also bears this interaction influence out; the 90^o (Fig. 32) or 270^o (Figs. 26, 27, 31) position remains the hottest throughout a run. This may be explained as suppression of active sites, for portions of the flux curve, by the moving liquid bubble mixture. A third observation can be made with respect to the forward and rear stagnation points. At low fluxes the forward point, 0^o, is cooler than the trailing point, 180^o, as shown in

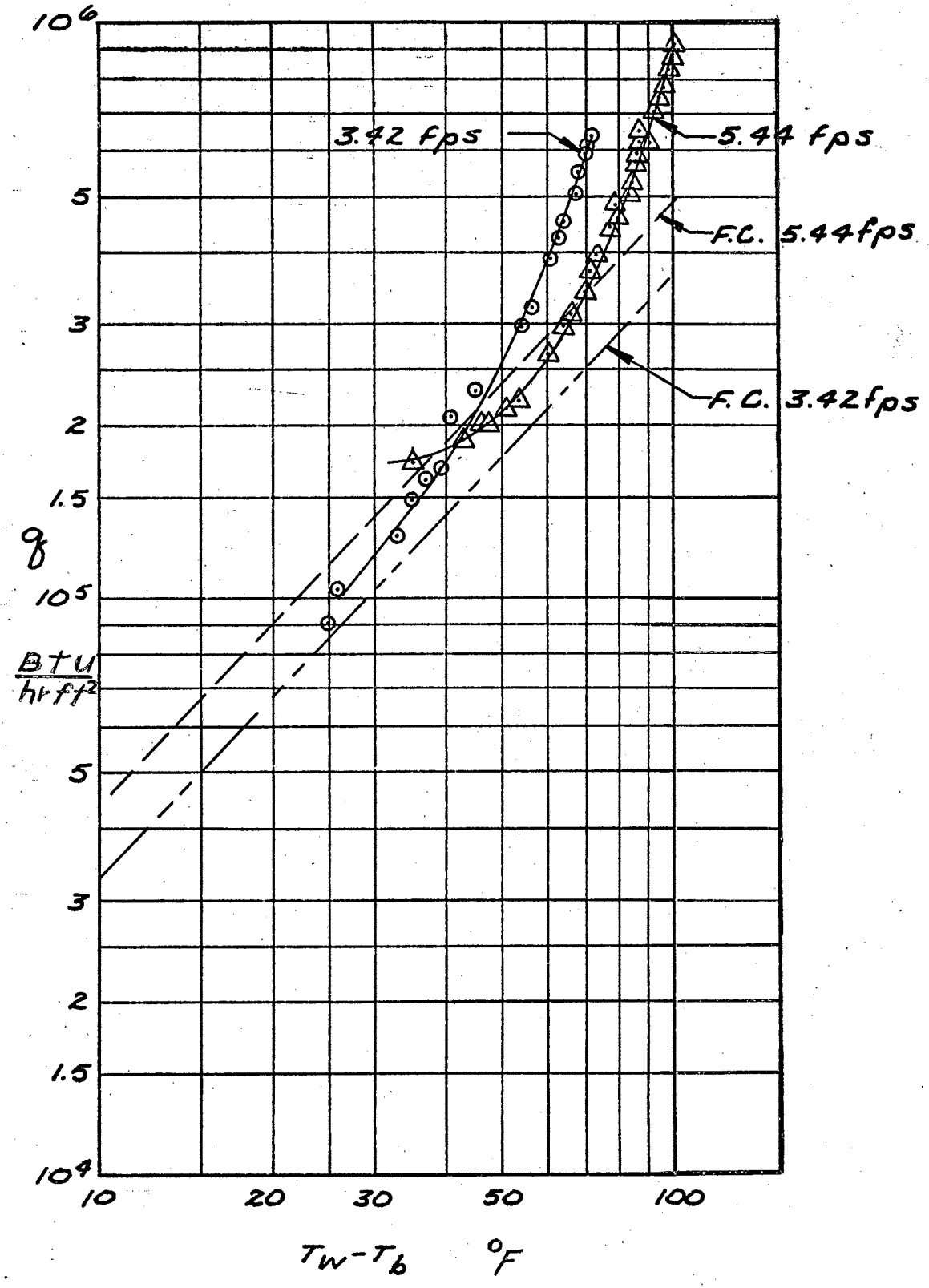

Figure 21. Velocity Effect on Boiling Curves for 0.2495 in. O.D. Cylinder

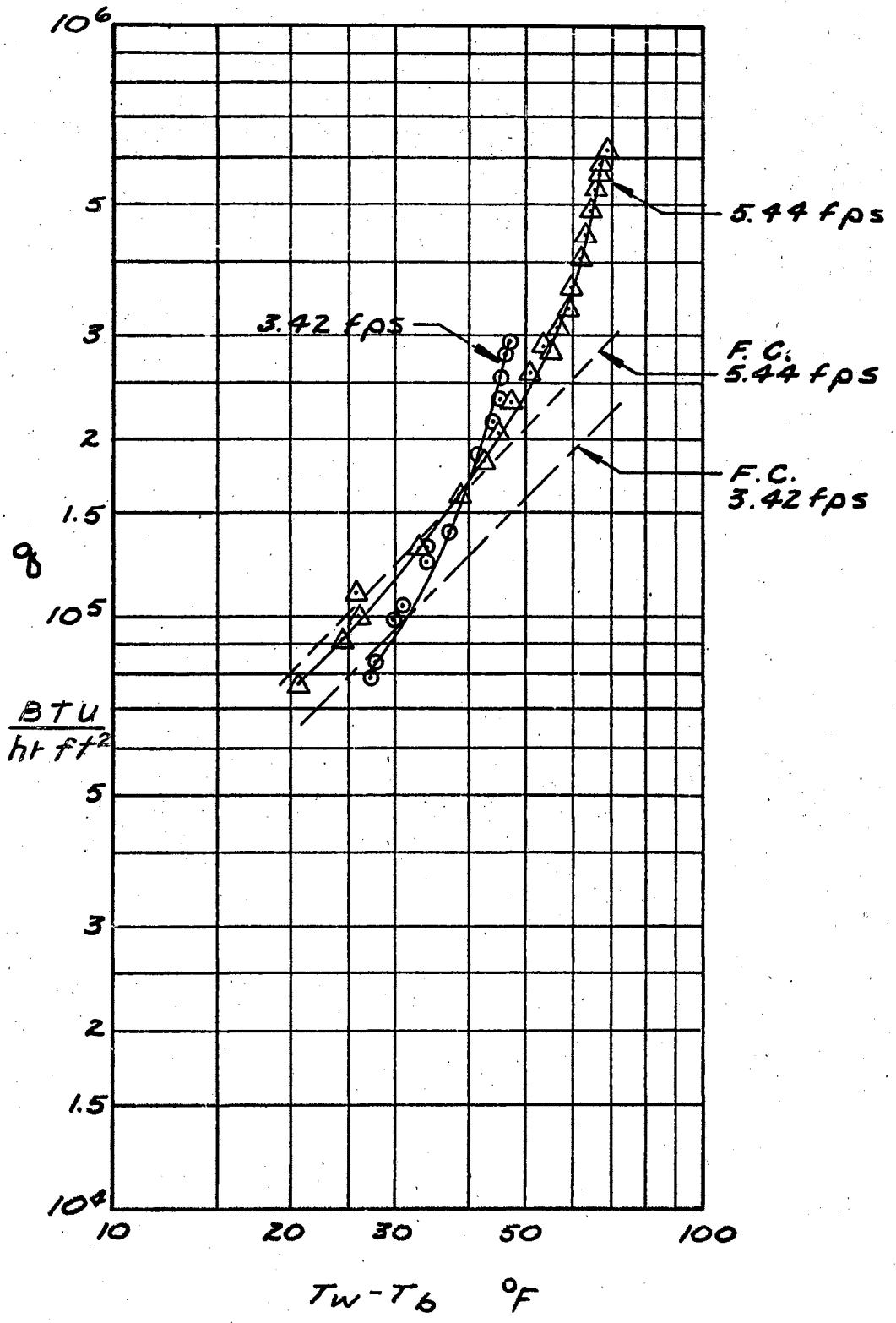

Figure 22. Velocity Effect on Boiling Curves for 0.337 in. O.D. Cylinder

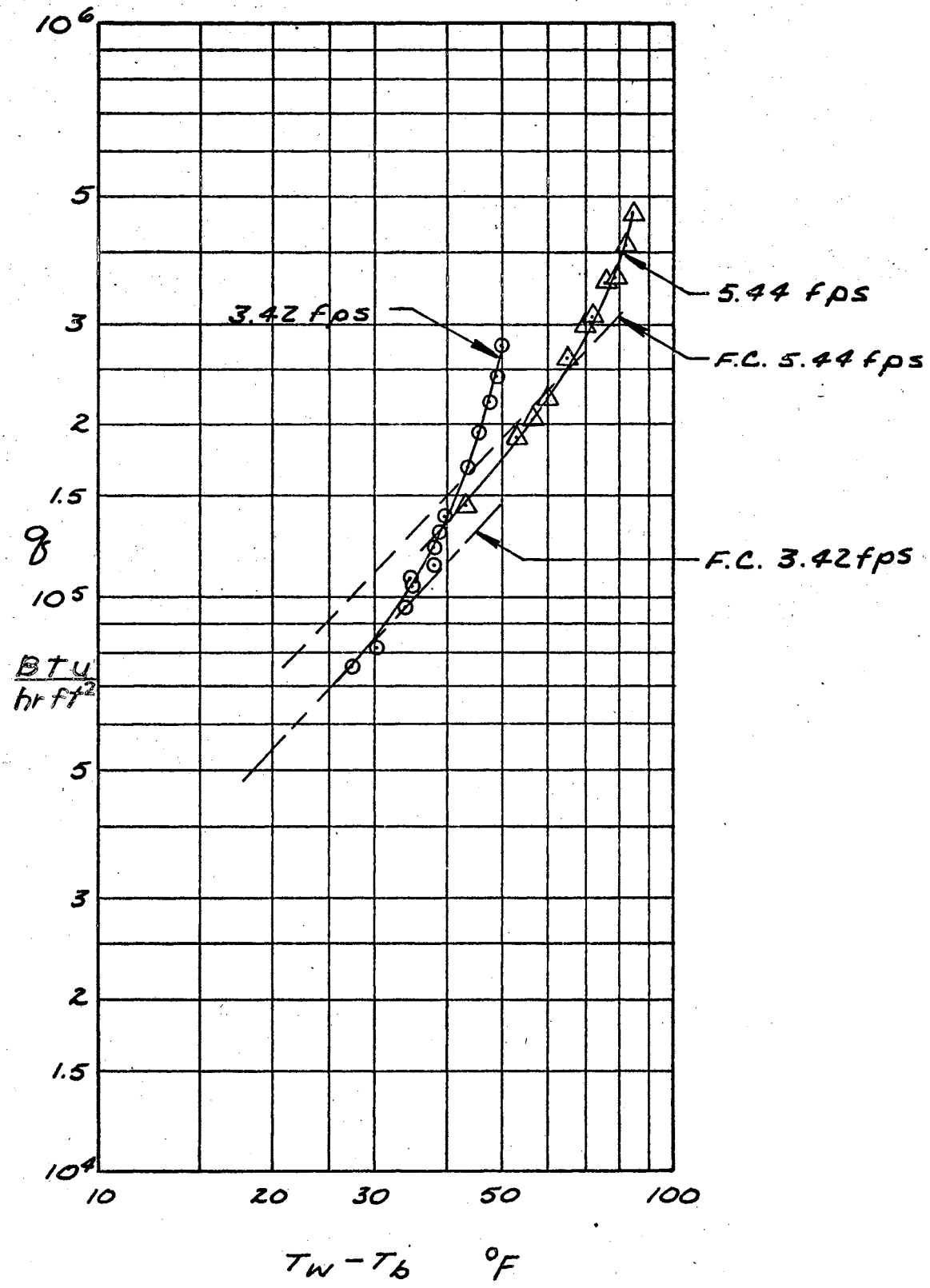

Figure 23. Velocity Effect on Boiling Curves for 0.450 in. O.D. Cylinder

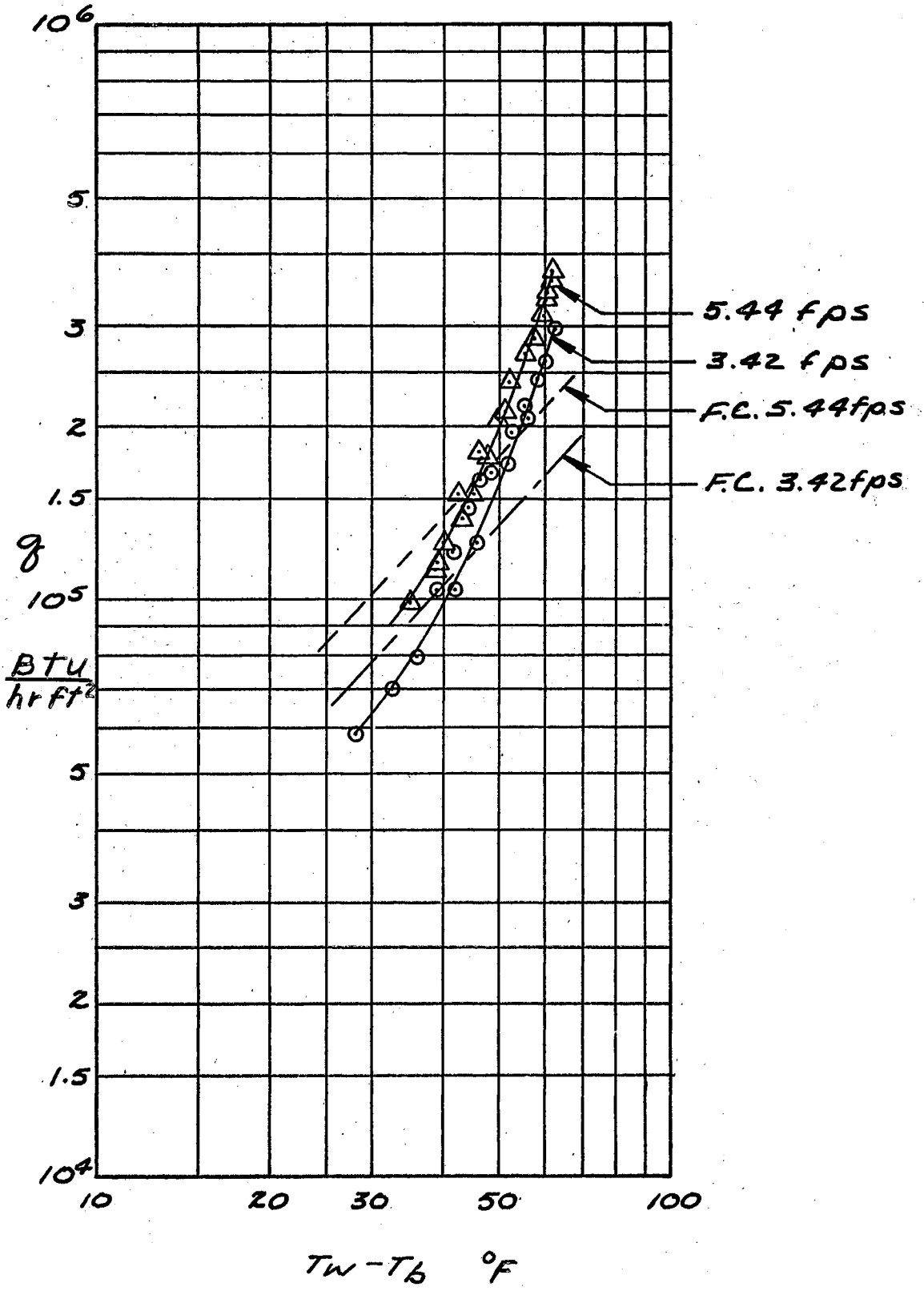

Figure 24. Velocity Effect on Boiling Curves for 0.555 in. O.D. Cylinder

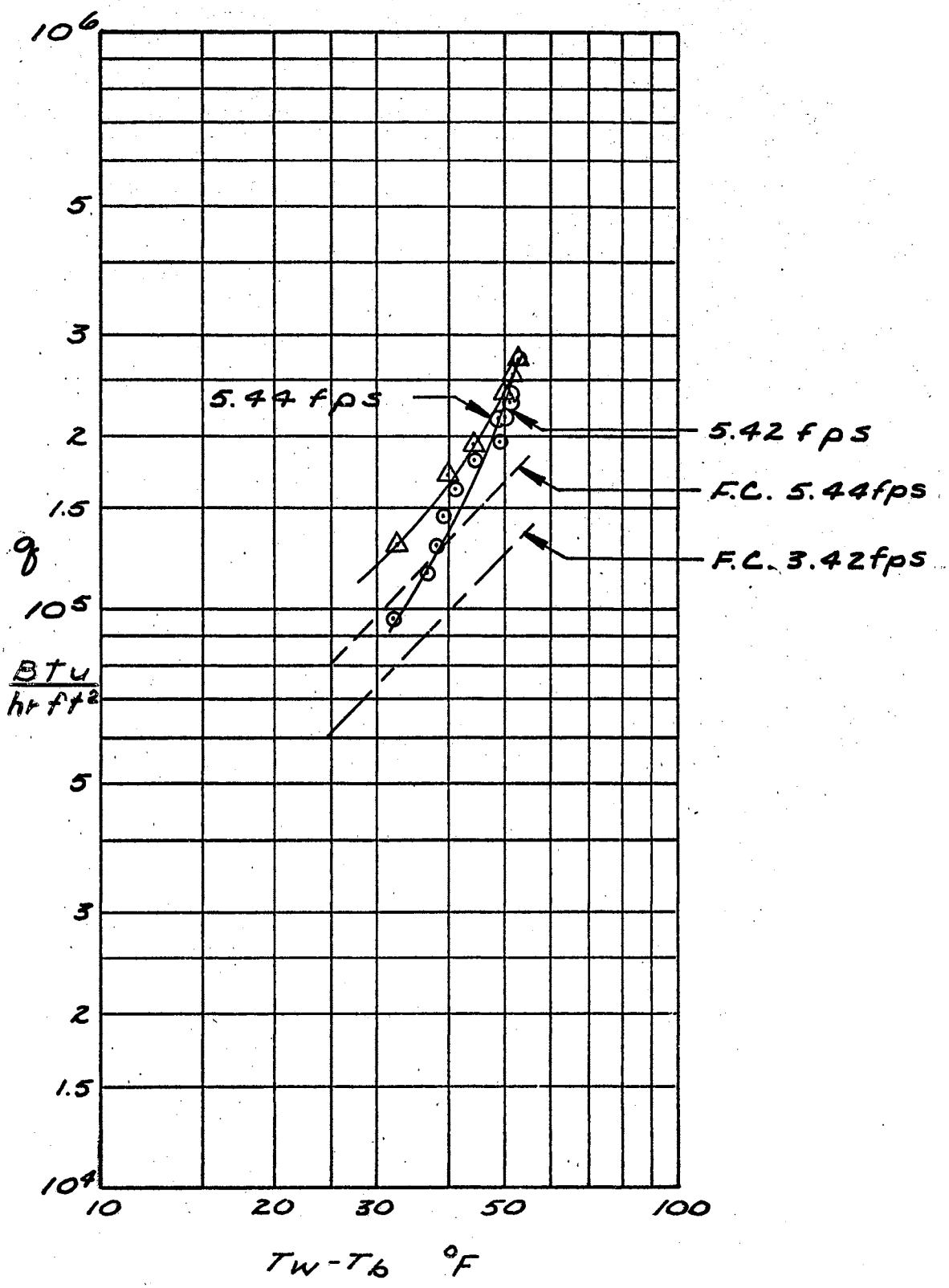

Figure 25. Velocity Effect on Boiling Curves for 0.707 in. O.D. Cylinder

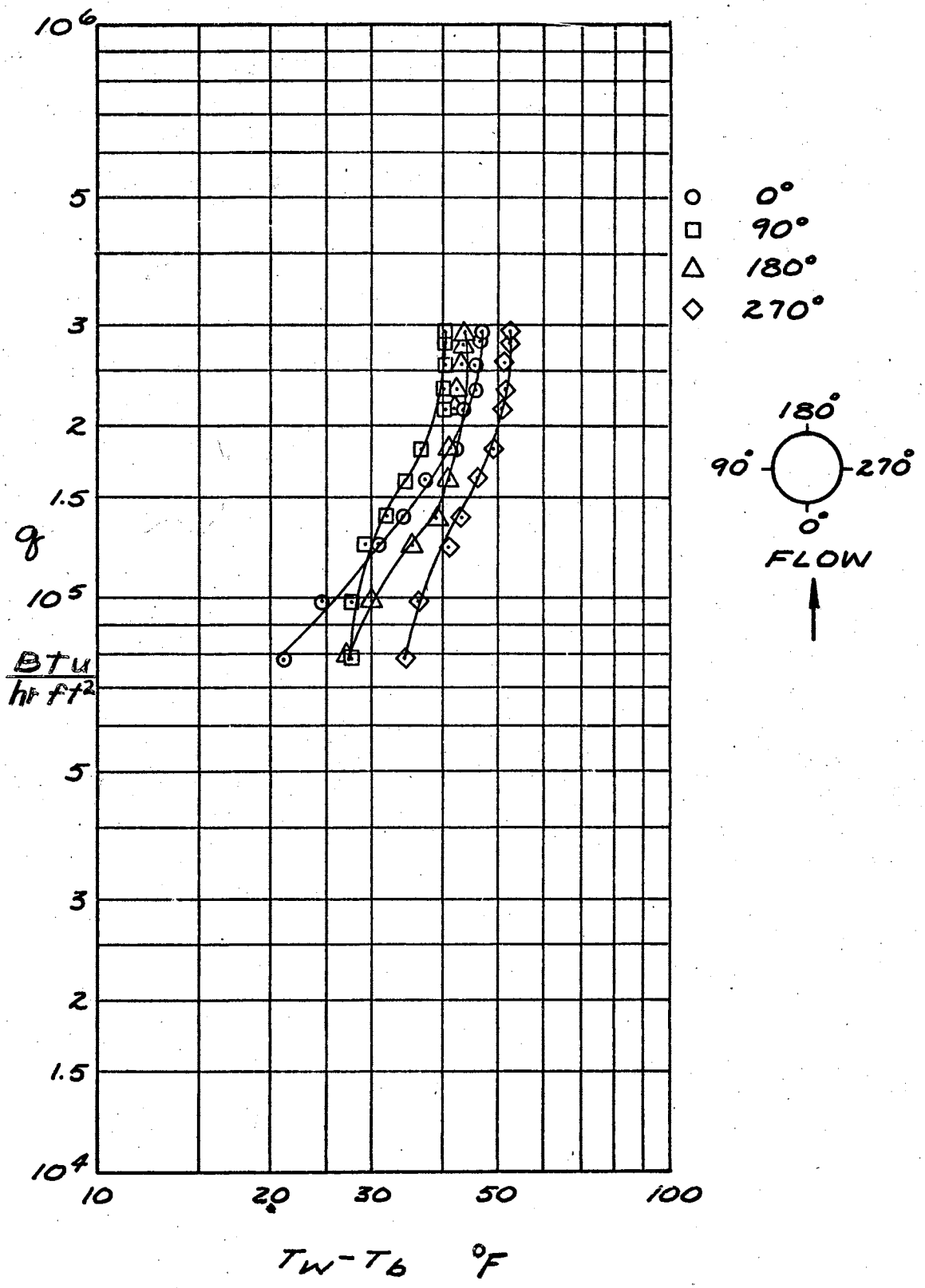

Figure 26. Localized Boiling Curves for 0.337 in. O.D. Cylinder at 3.42 fps

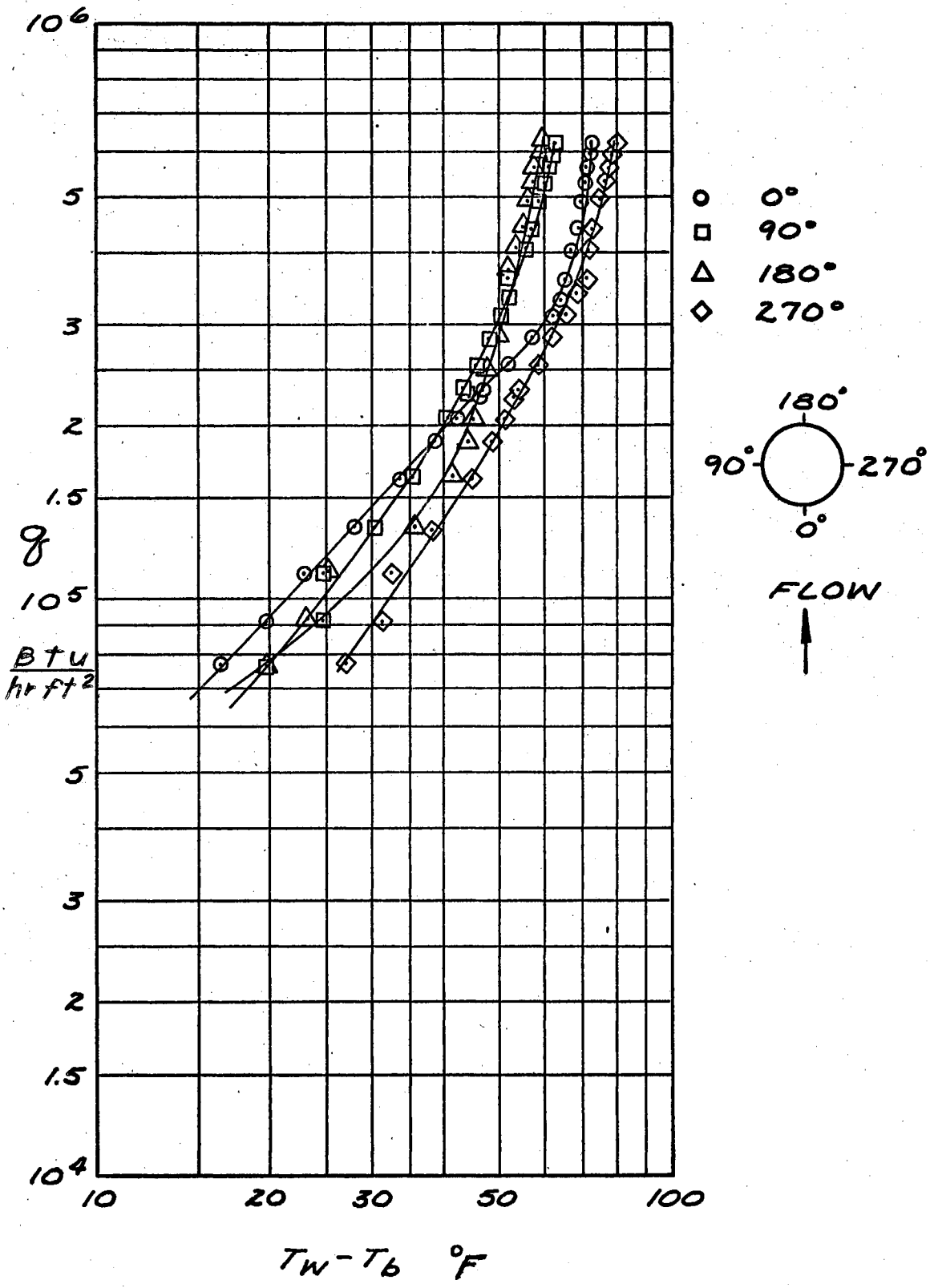

Figure 27. Localized Boiling Curves for 0.338 in. O.D. Cylinder at 5.44 fps

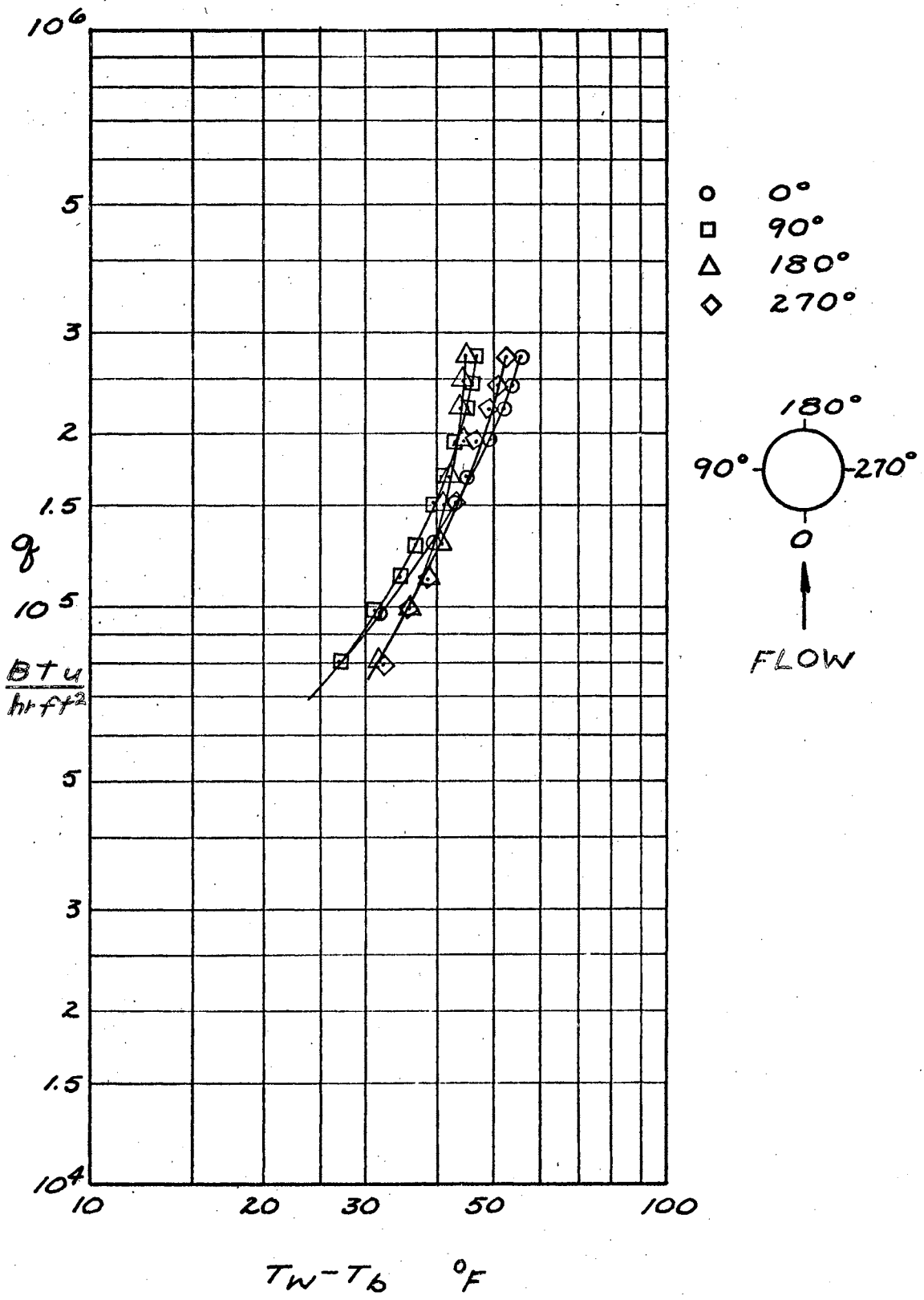

Figure 28. Localized Boiling Curves for 0.450 in. O.D. Cylinder at 3.42 fps

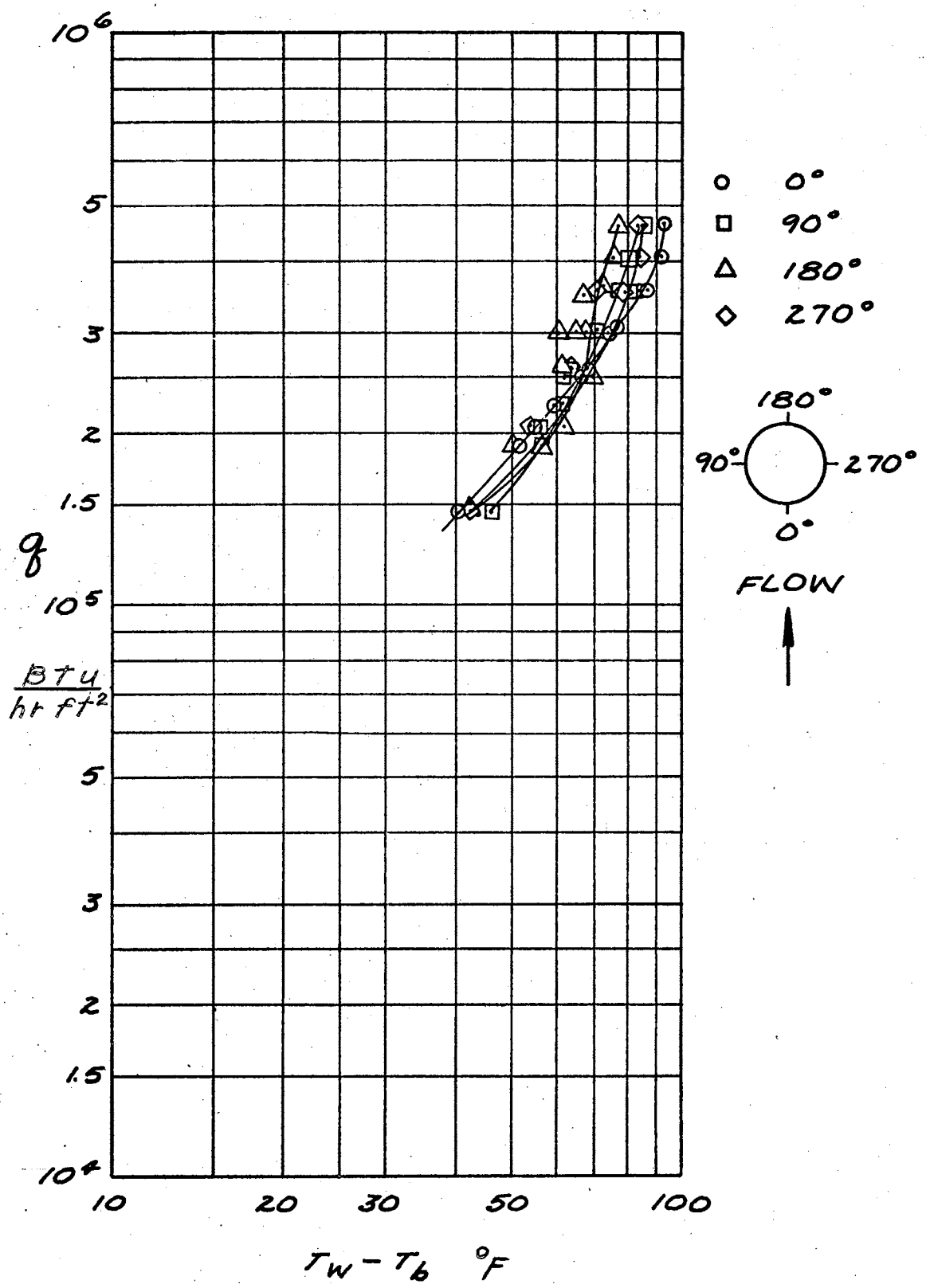

Figure 29. Localized Boiling Curves for 0.458 in. O.D. Cylinder at 5.44 fps

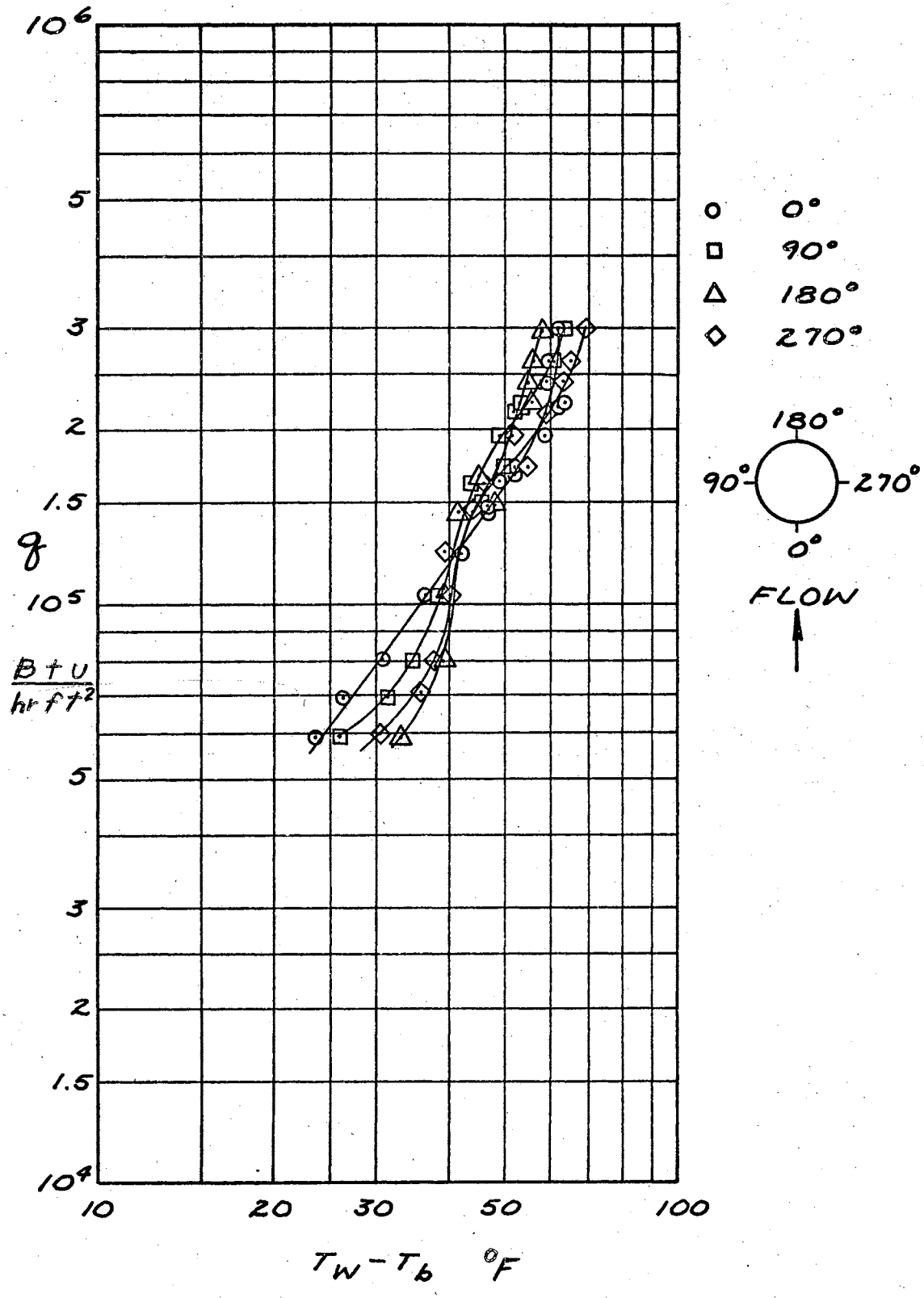

Figure 30. Localized Boiling Curves for 0.556 in. O.D. Cylinder at 3.42 fps

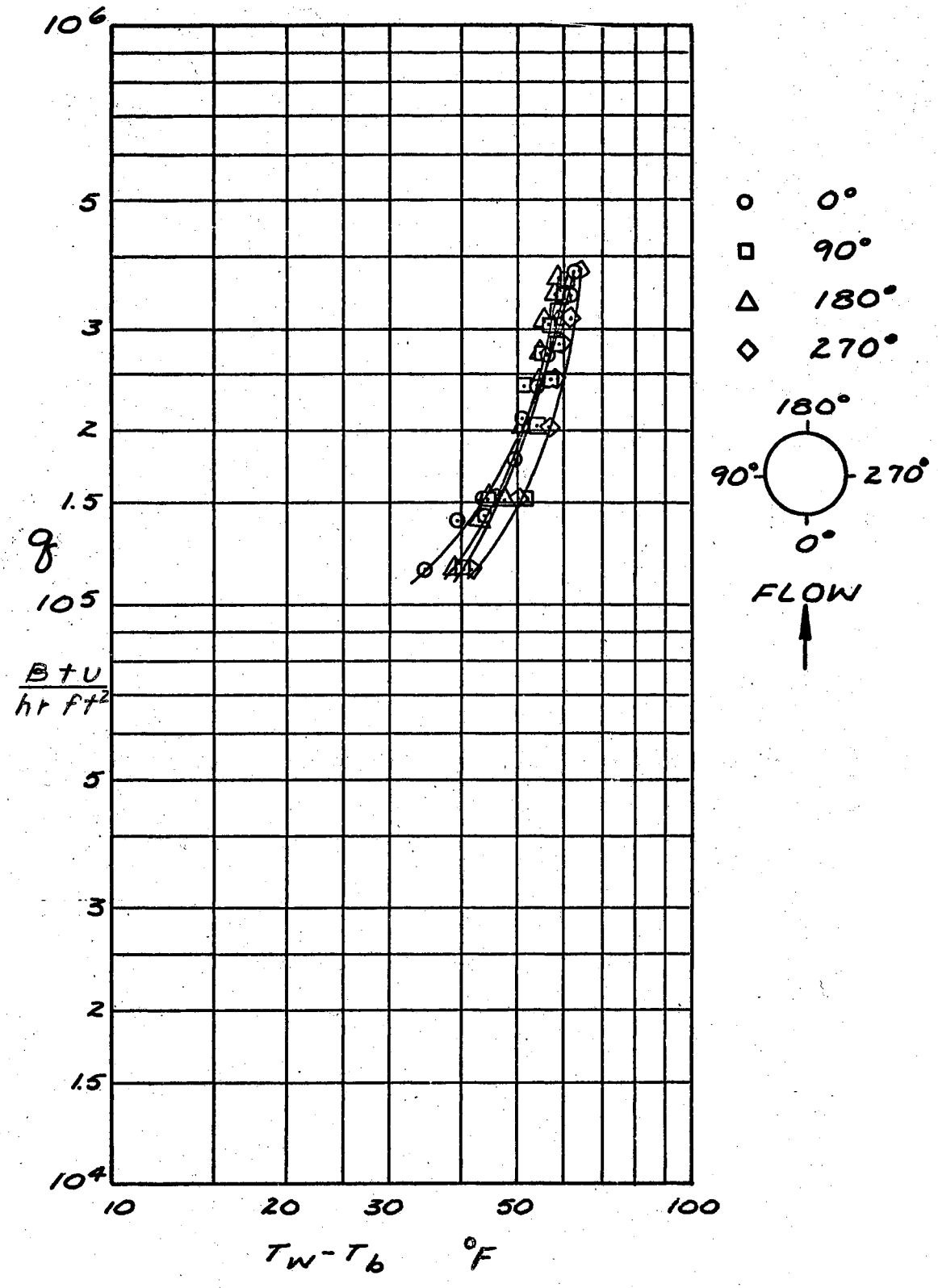

Figure 31. Localized Boiling Curves for 0.555 in. O.D. Cylinder at 5.44 fps

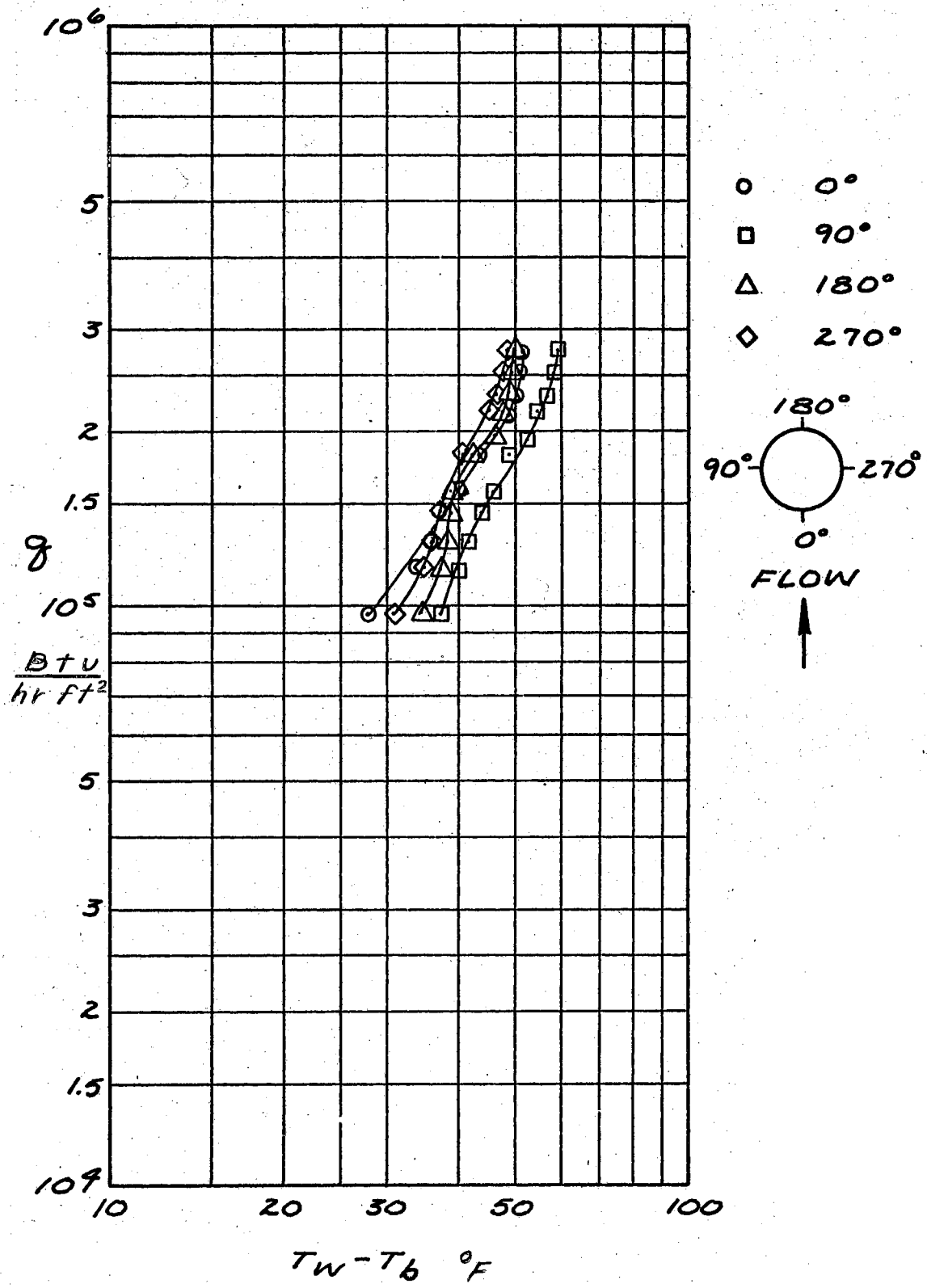

Figure 32. Localized Boiling Curves for 0.707 in. O.D. Cylinder at 3.42 fps

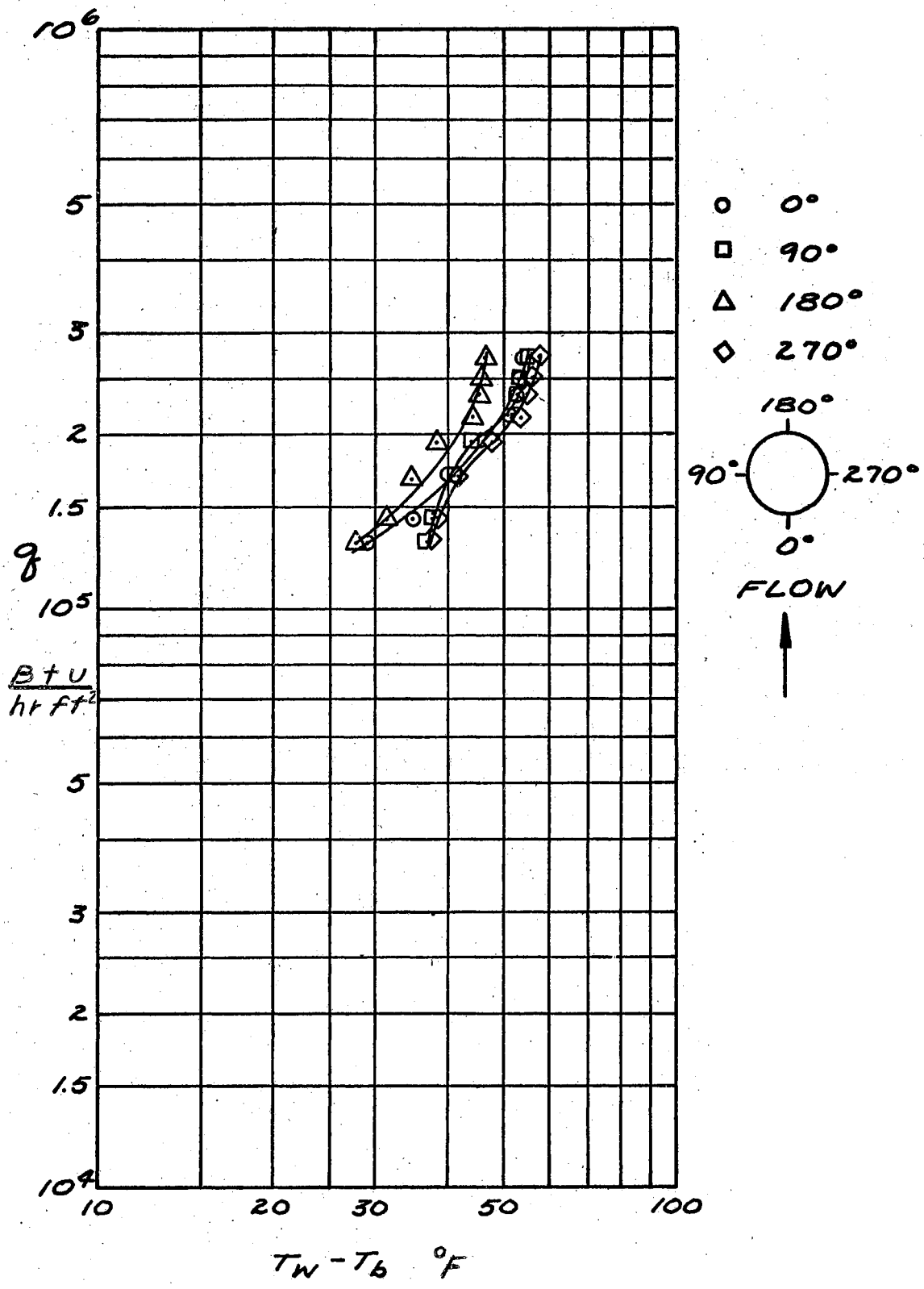

Figure 33. Localized Boiling Curves for 0.700 in. O.D. Cylinder at 5.44 fps

Figures 26-32. At some intermediate flux (150,000 to 250,000) these two points reverse their roles, the boiling in the wake becoming more efficient. The forward stagnation point might be expected to be cooler than the 90^{o} or 270^{o} points at low fluxes, since the laminar boundary layer is the thinnest at this point for single phase flow. Perkins and Leppert (66) show the forward and rear points with varying coefficients depending on channel blockage effects.

The localized boiling curves for pool boiling are included as Figures 34 through 38. In Figures 36 and 37 it is noted that the 270^{o} position is again consistently hotter than the other points.

The temperature distribution in forced convection boiling is dependent upon the distribution and number of activated boiling sites around the cylinder. Momentary interruption of the boiling process, i.e., turning off the power to the cylinder, is sufficient to alter the distribution of sites and temperature. Figure 38 shows this effect in pool boiling. It was necessary to change the power leads during this run. The point most affected is the 0^{o} position. Although there is agreement on the initial points after restarting for the 90^{o}, 180^{o}, and 270^{o} positions, the boiling curve itself is not reproduced.

Photographic Results

The results of the high speed (3000 frames/sec., 0.457" O.D. cylinder) photographic work provided several new pieces of information. The wake region of the cylinder exhibited boiling mechanisms characteristic of pool boiling, i.e., many sites of continuous vapor streams intermixed with periodically erupting vapor patches. This activity

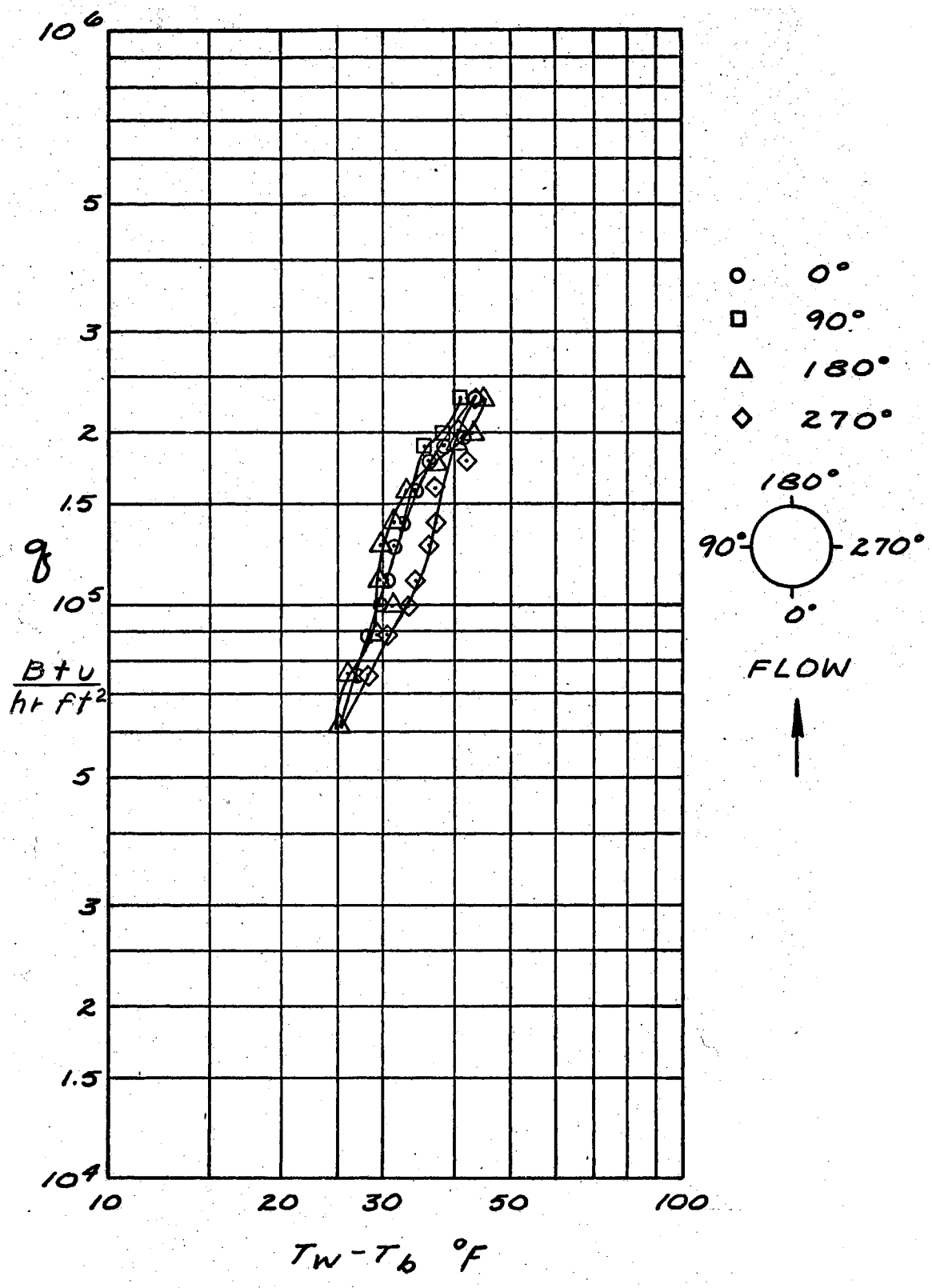

Figure 34. Localized Pool Boiling Curves for 0.337 in. O.D. Cylinder

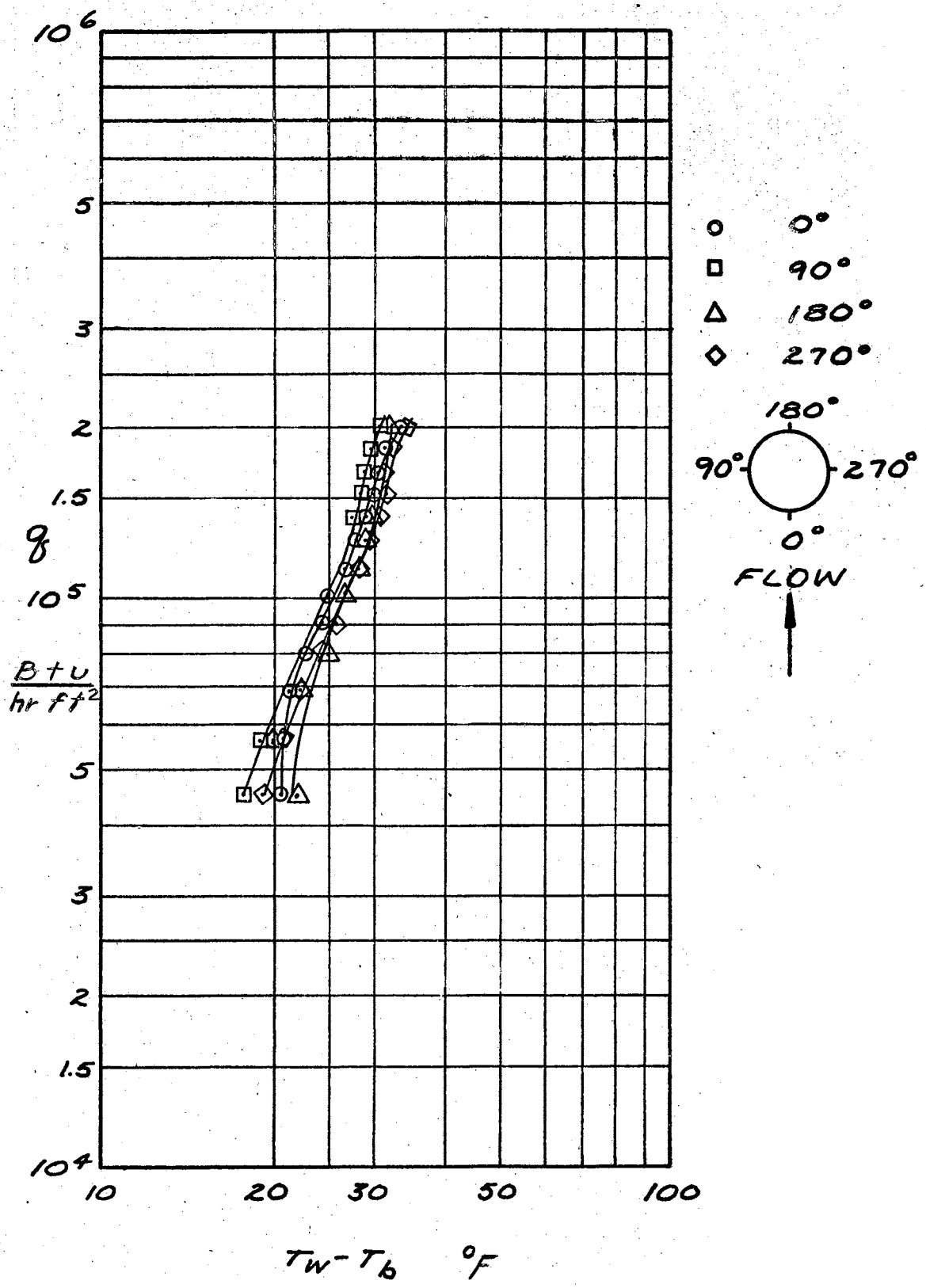

Figure 35. Localized Pool Boiling Curves for 0.457 in. O.D. Cylinder

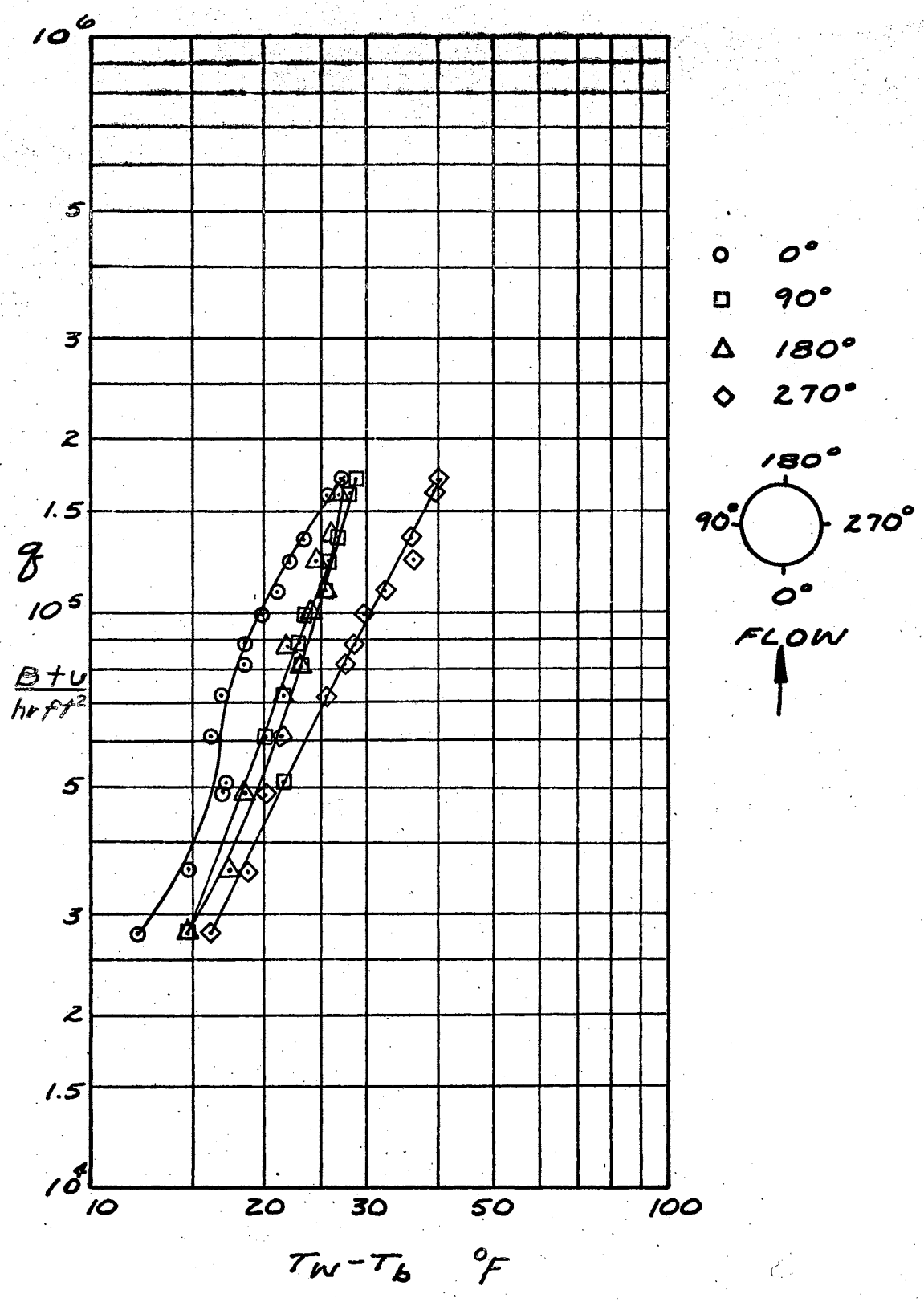

Figure 36. Localized Pool Boiling Curves for 0.553 in. O.D. Cylinder

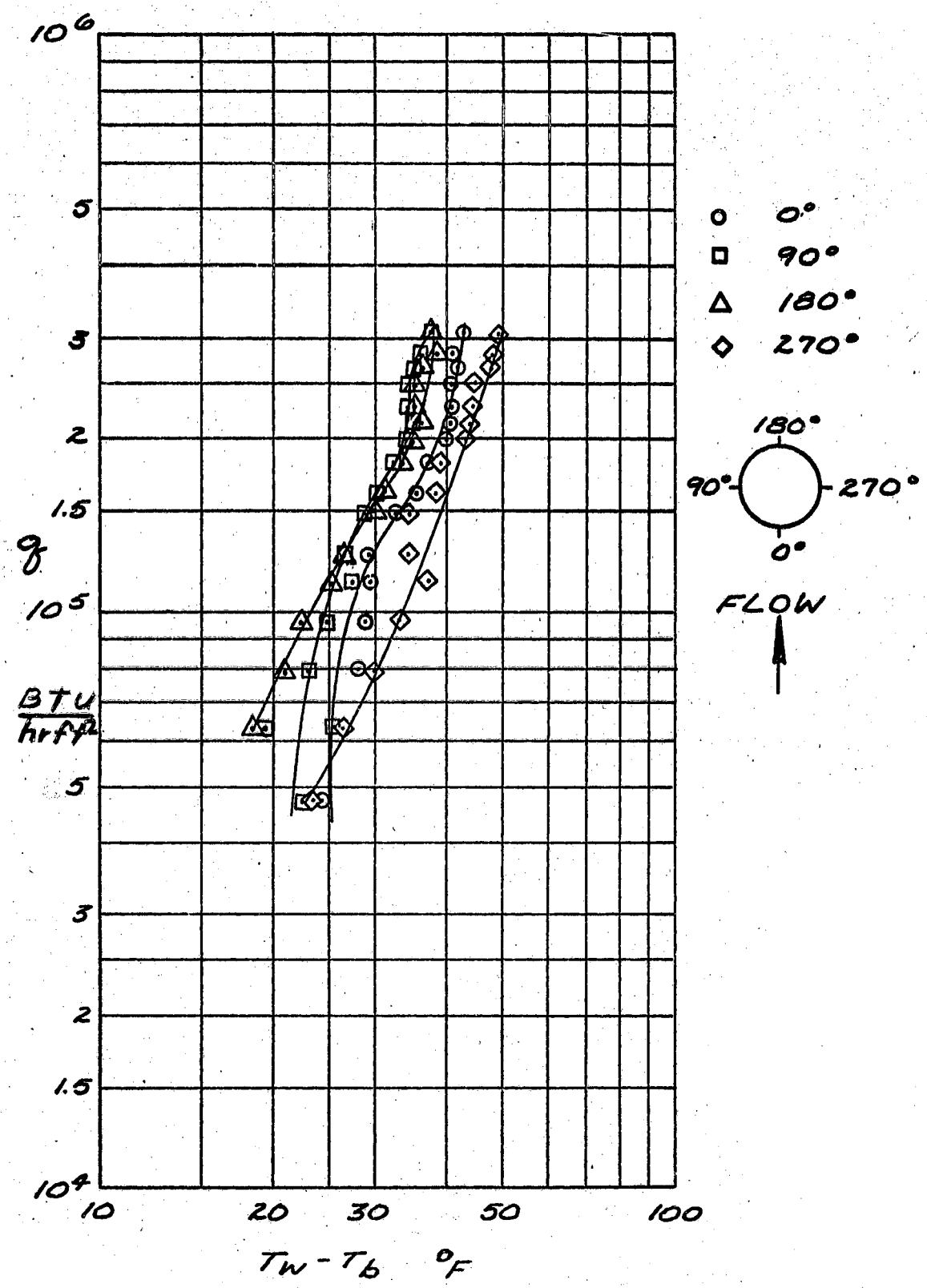

Figure 37. Localized Pool Boiling Curves for 0.7034 in. O.D. Cylinder

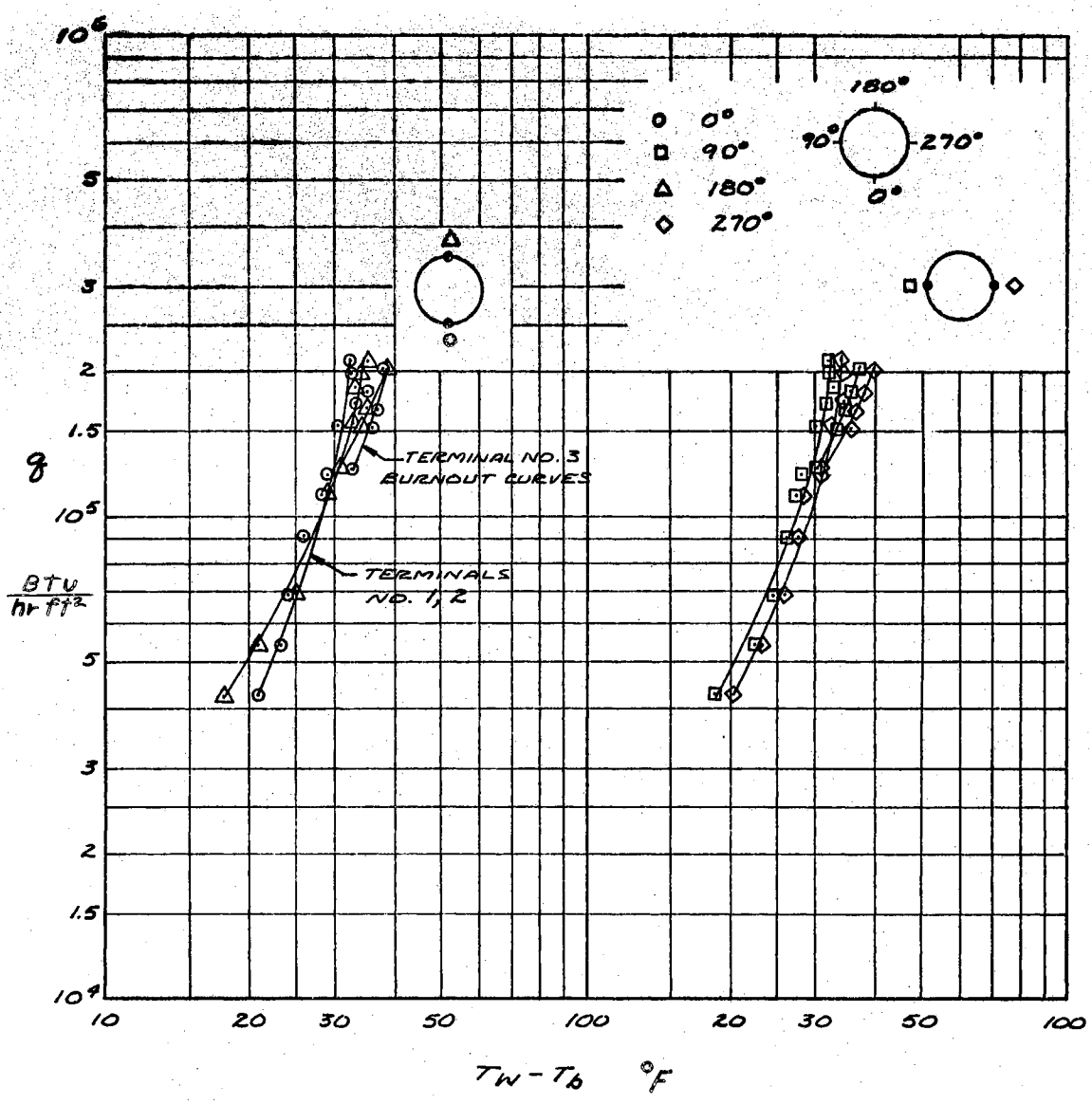

Figure 38. Localized Pool Boiling Curves for 0.7028 in. O.D. Cylinder

does not give a significant difference in the amount of heat removed from this area of the cylinder as compared to the forward region.

Boiling in the forward area of the cylinder displays the influence of the moving liquid. The film of the 3.42 fps run, (q = 187,000, ΔT_b = 54°F) showed a bubble diameter range of 0.036 to 0.061 inches with an average diameter of 0.042 inches. The film of the 5.44 fps run, (q = 238,000, ΔT_b = 55°F) showed a bubble diameter range of 0.025 to 0.043 inches and an average diameter of 0.031 inches. The individual bubbles appeared spherical and separated from each other by varying distances. Bubble coalescence in the vicinity of the active site was also occurring, periodically forming continuous vapor streams. These intermittent vapor streams were of the same width as the individual bubble diameters, showing the influence of the moving fluid on bubble formation.

The vapor bubble velocity in the forward region of the cylinder for the 3.42 fps run varied between 3.8 and 5.2 fps with an average of 4.07 fps. The bubble velocity for the 5.44 fps run varied between 5.4 and 8.6 fps with an average of 6.5 fps. Pitot tube investigations showed the maximum empty channel velocity for the latter flow rate to be 6.1 fps. Buoyant effects were estimated from Levich (76) as contributing less than 1 fps. Since shadows could be observed behind the bubbles as they approached the 90° position of the cylinder, the majority of the bubble volume is traveling outside the laminar boundary layer. The laminar boundary layer for the 3.42 fps run (Re = 44,000), was estimated to vary between 0.0037 inch at 60° from stagnation to 0.0041 inch at 90° from stagnation. The 5.44 fps run (Re = 70,000)

had a laminar boundary layer thickness of 0.0029 inch at 60^{o} from stagnation and 0.0033 inch at 90^{o} from stagnation.

The frequency of bubble departure and the distribution of active sites in this area were both too random to obtain any meaningful data.

Data Presentation - Method of Superposition

The superposition model states that the forced convection boiling curve of flux vs ΔT_s can be predicted by combining the single phase forced convection heat flux line with the pool boiling line. There are three distinct portions of the boiling curve. Starting with low wall superheat, single-phase forced convection dominates; there is an intermediate or combination forced convection-boiling zone as the wall superheat is increased, and finally a region completely dominated by the boiling process. The predicted boiling curve joins the single phase forced convection curve at one extreme and the extended pool boiling curve at the other end. The methods of constructing the intermediate zone have been summarized by Bergles and Rohsenow (74). The total heat flux then is a function of the magnitude of the wall superheat, which determines the dominating heat flux mechanism. The use of an equation such as:

$$q_{tot.} = q_{f.c.} + q_{pb} \qquad 6\text{-}6$$

should be used only in context with the descriptive material accompanying it, since it is only symbolic of the method used in constructing the boiling curve.

Figures 39 through 48 show the combination of liquid phase forced convection and pool boiling to produce a forced convection boiling

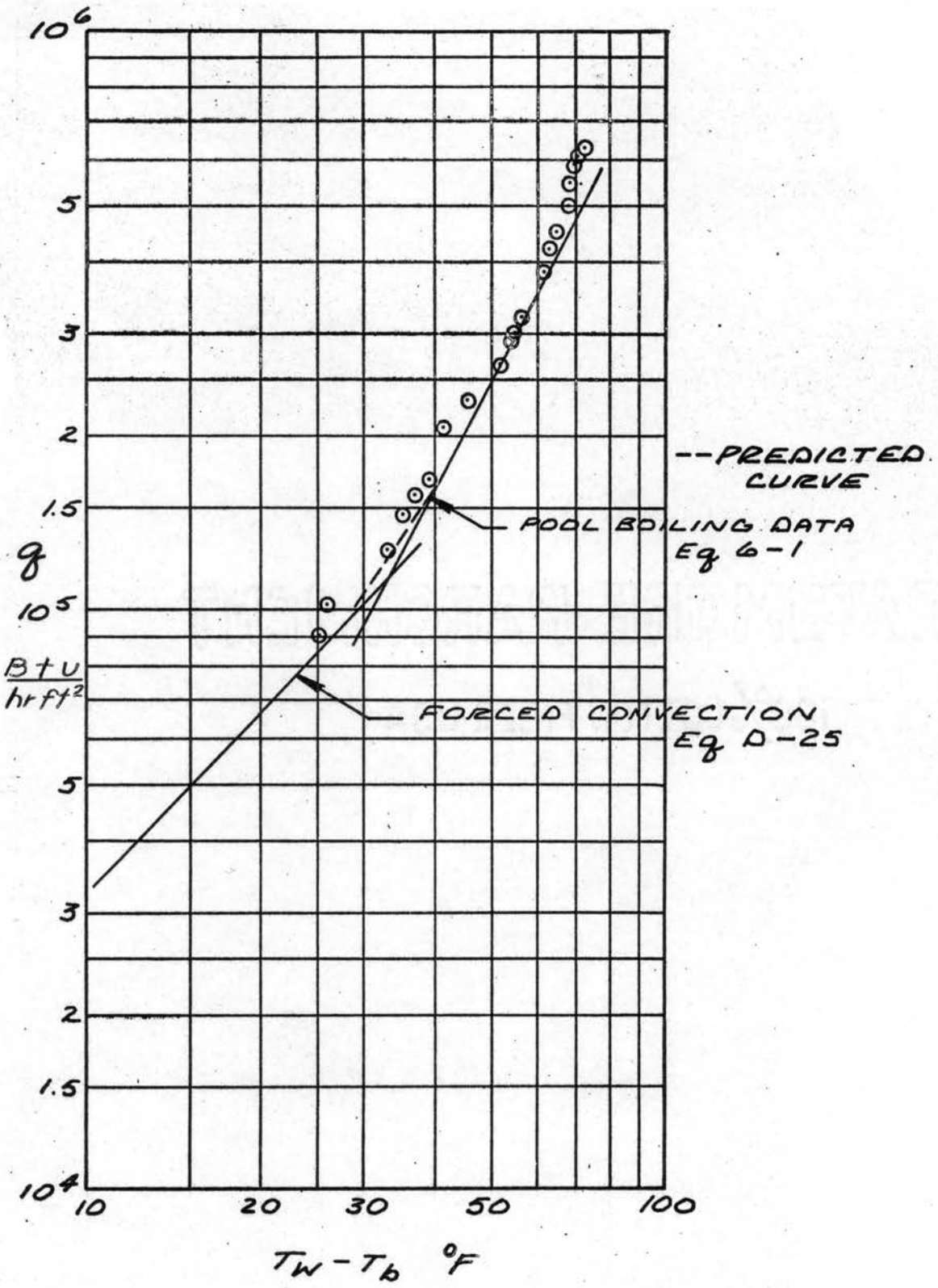

Figure 39. Method of Superposition for 0.2495 in. O.D. Cylinder at 3.42 fps

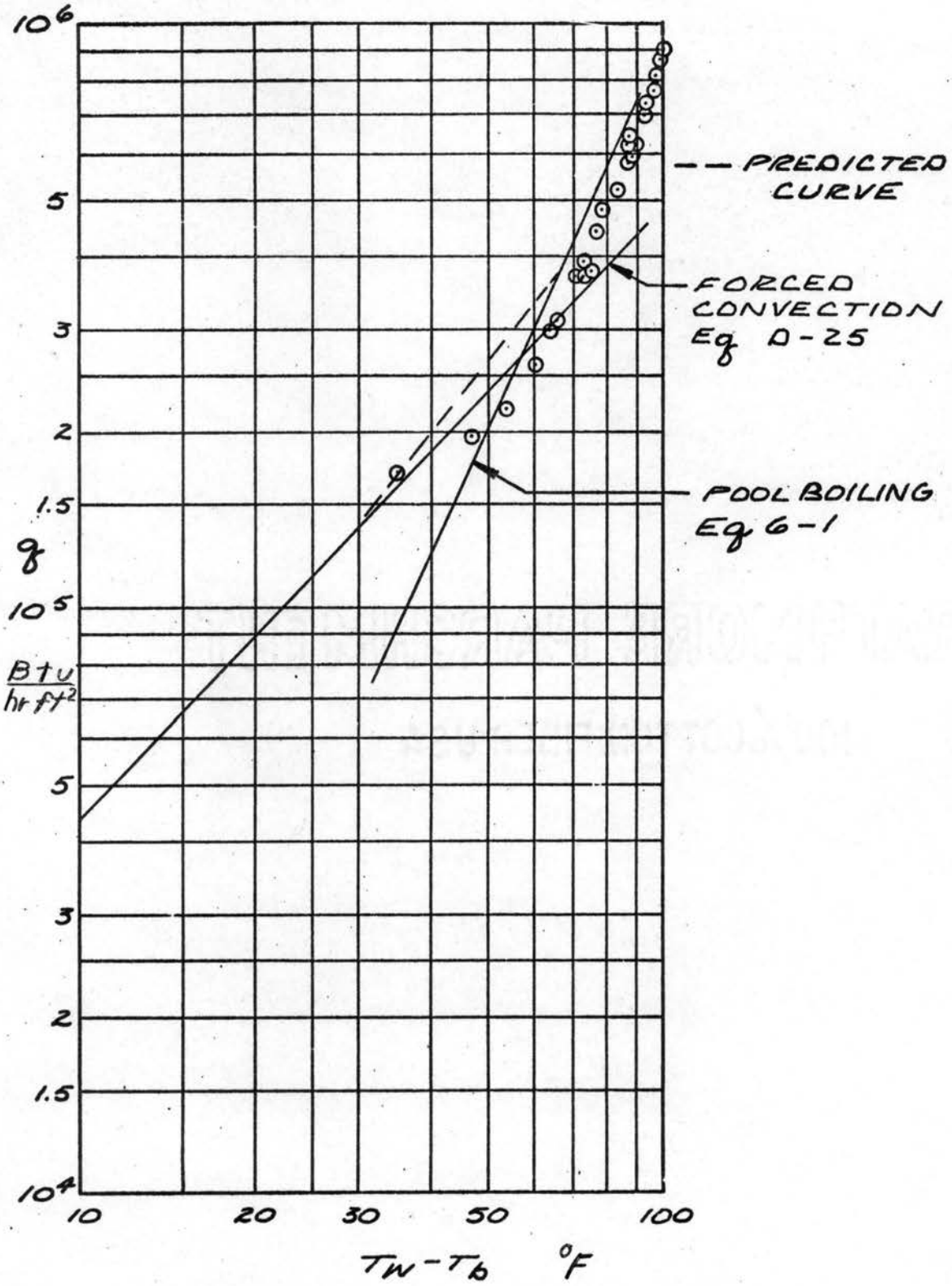

Figure 40. Method of Superposition for 0.2495 in. O.D. Cylinder at 5.44 fps

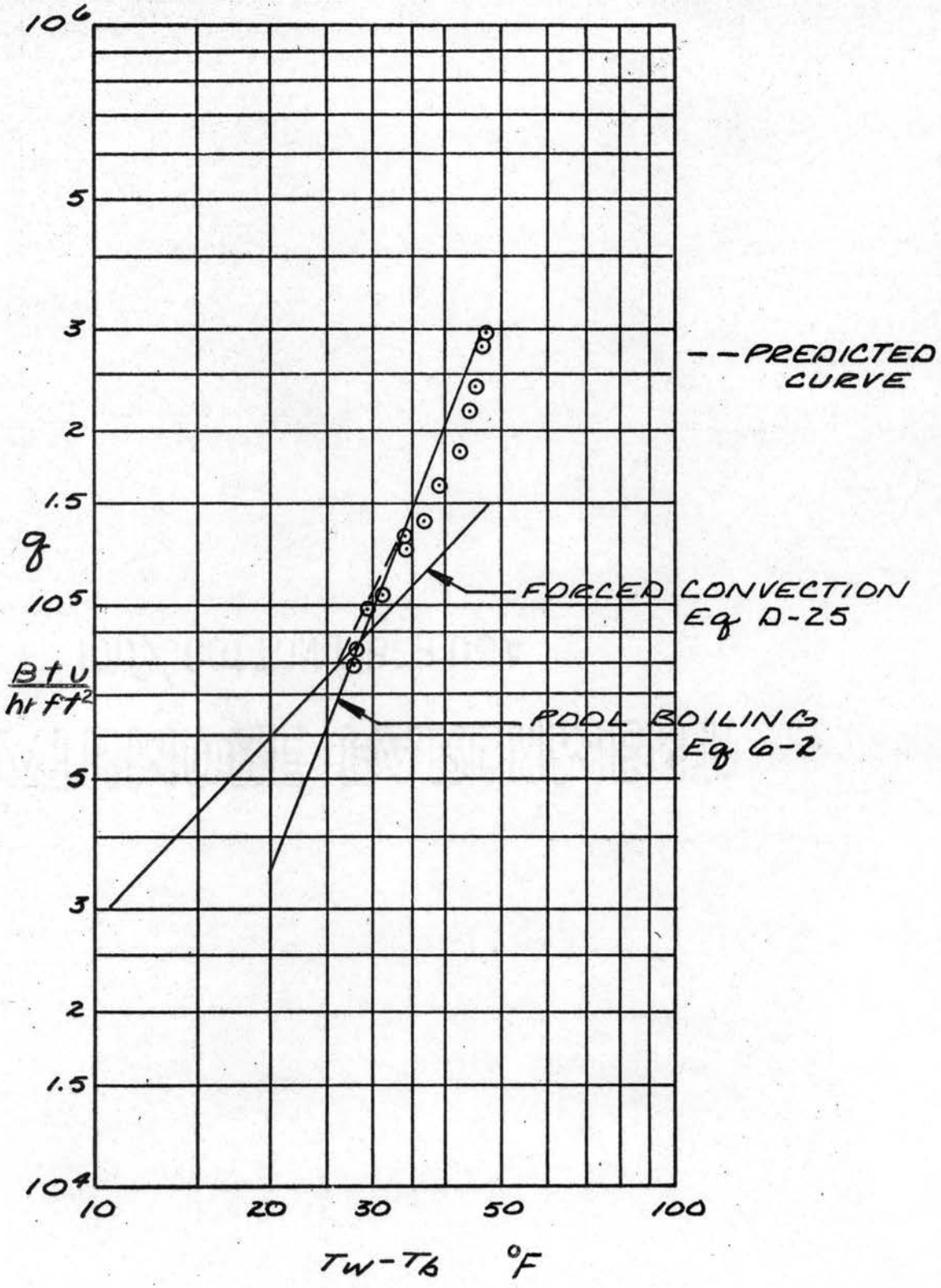

Figure 41. Method of Superposition for 0.337 in. O.D. Cylinder at 3.42 fps

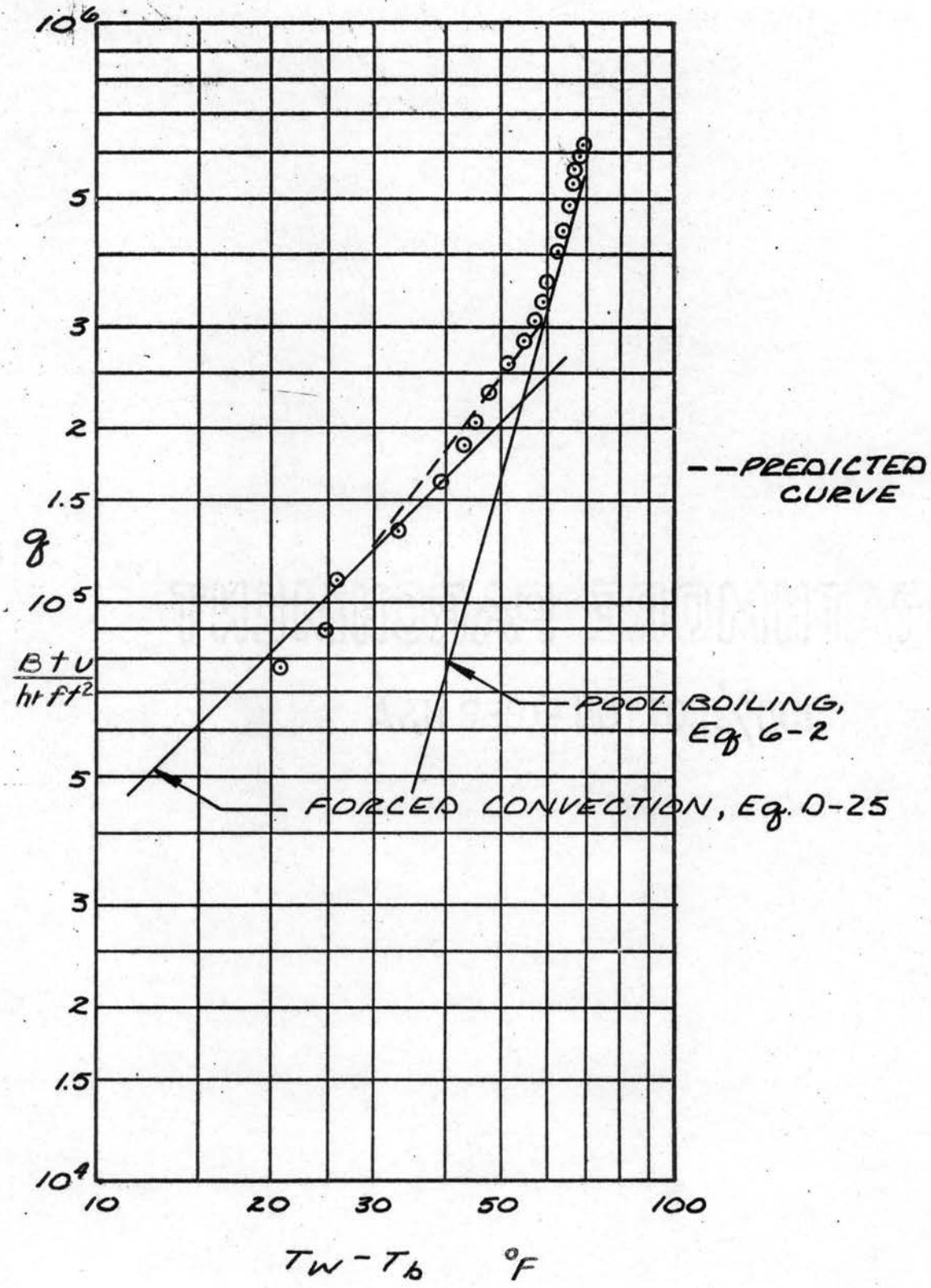

Figure 42. Method of Superposition for 0.338 in. O.D. Cylinder at 5.44 fps

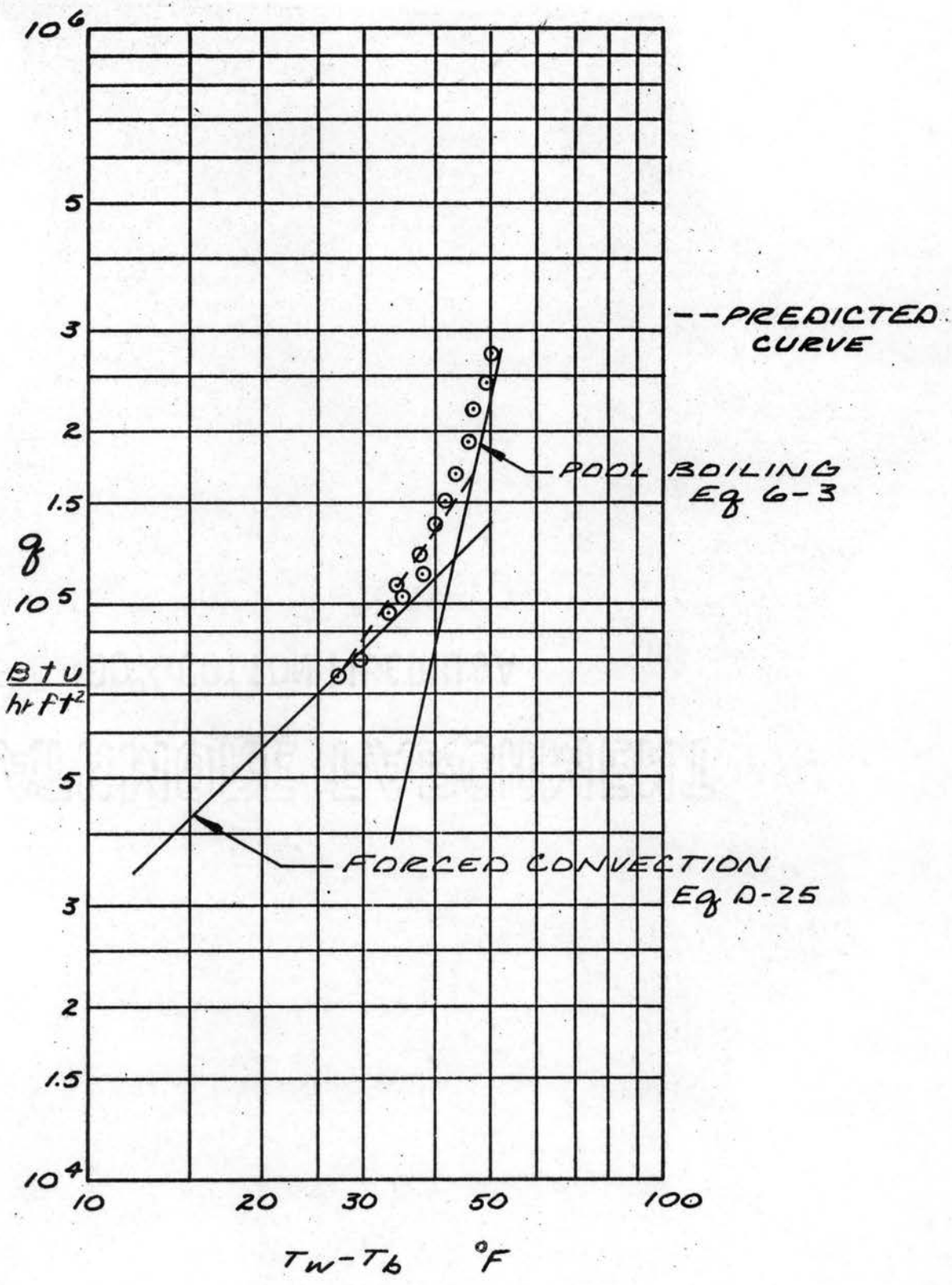

Figure 43. Method of Superposition for 0.450 in. O.D. Cylinder at 3.42 fps

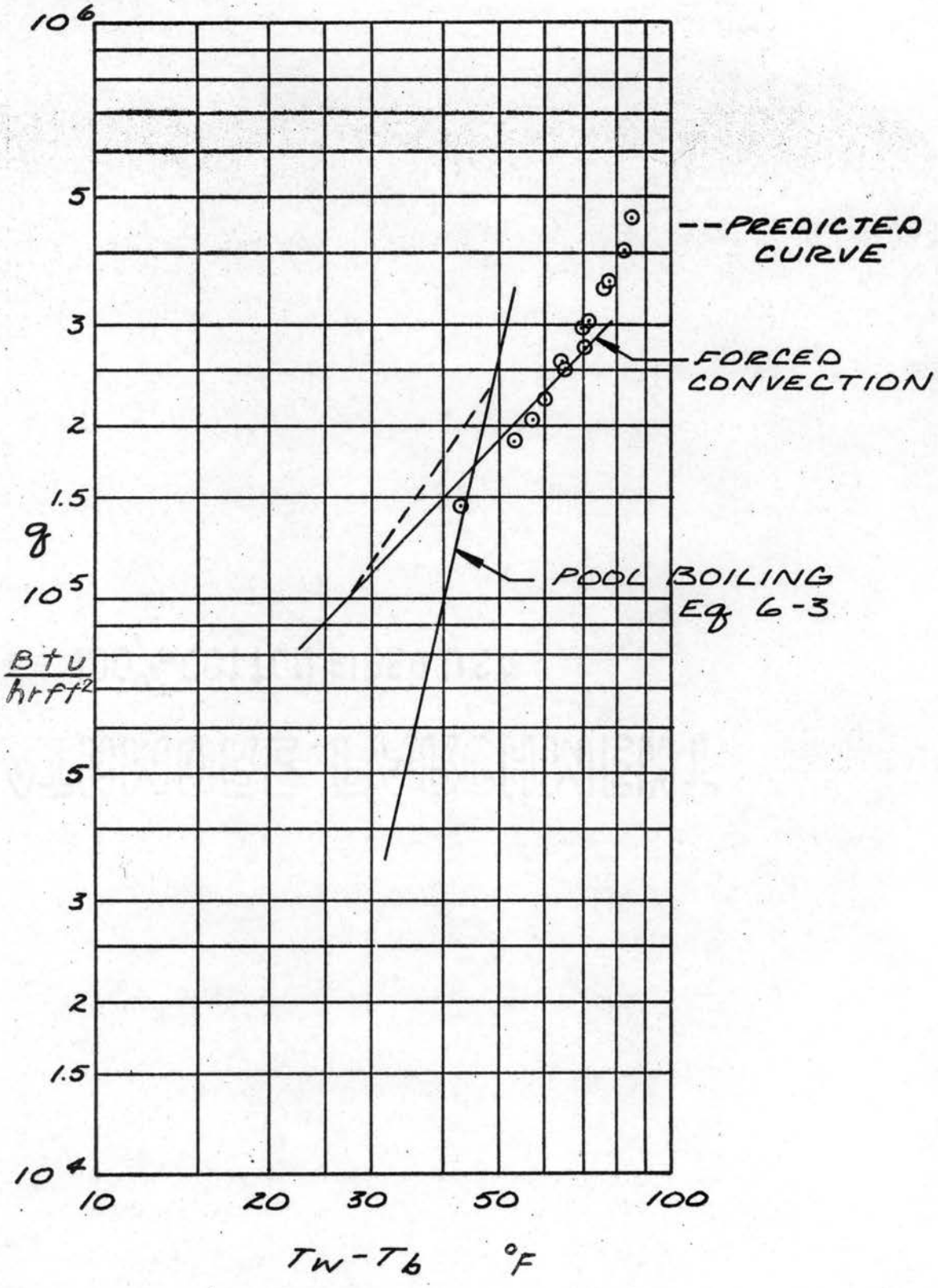

Figure 44. Method of Superposition for 0.458 in. O.D. Cylinder at 5.44 fps

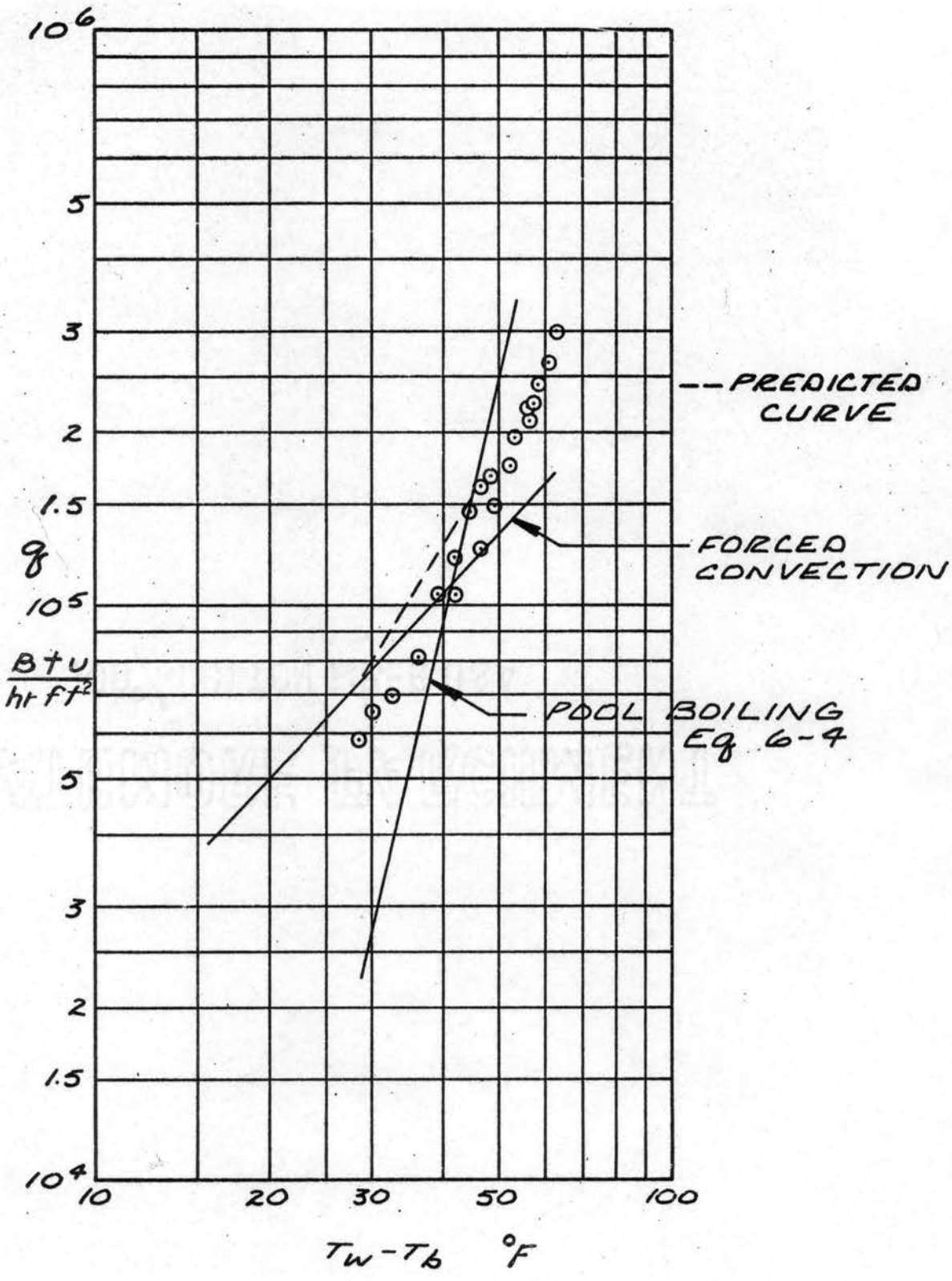

Figure 45. Method of Superposition for 0.556 in. O.D. Cylinder at 3.42 fps

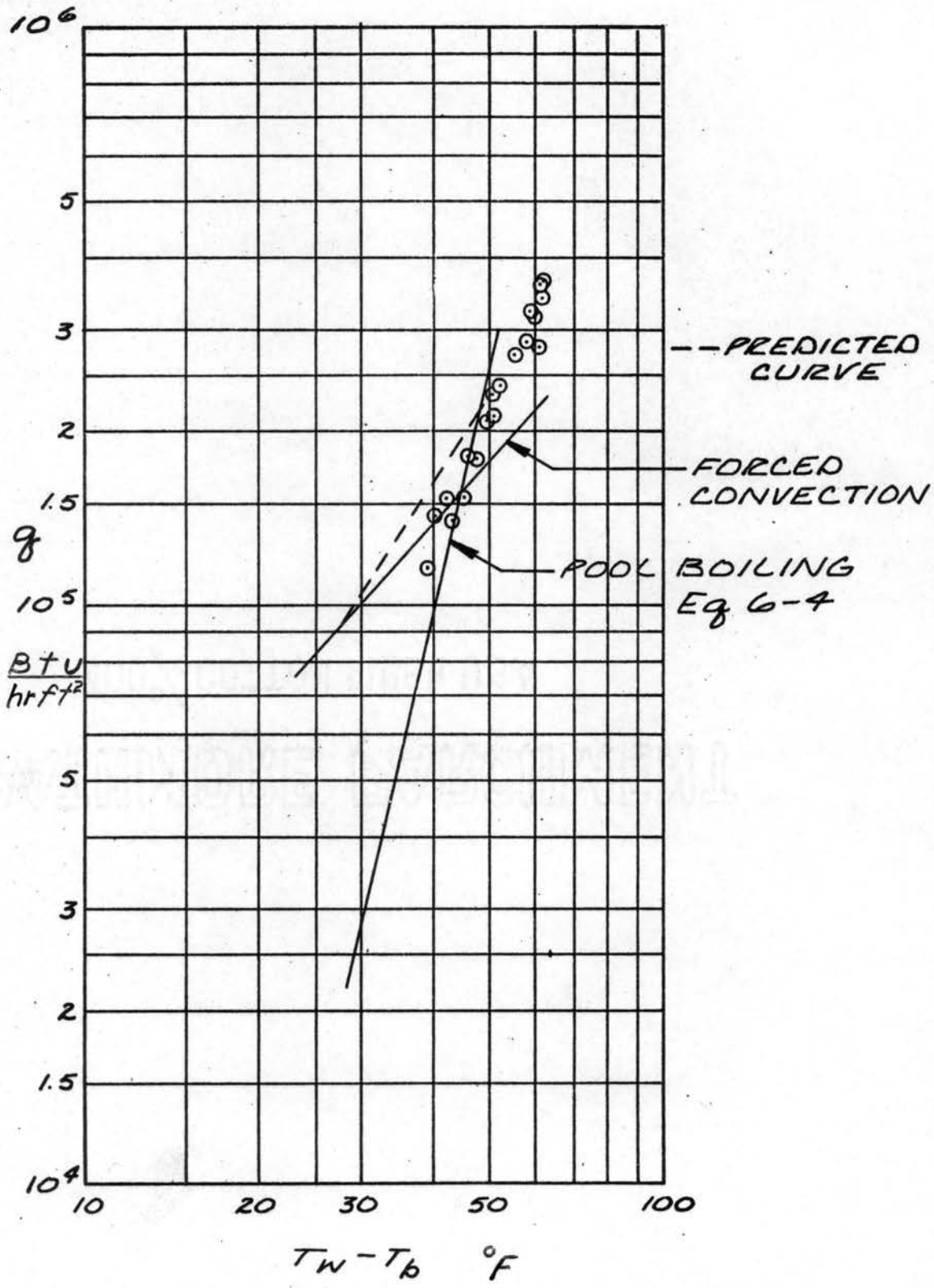

Figure 46. Method of Superposition for 0.555 in. O.D. Cylinder at 5.44 fps

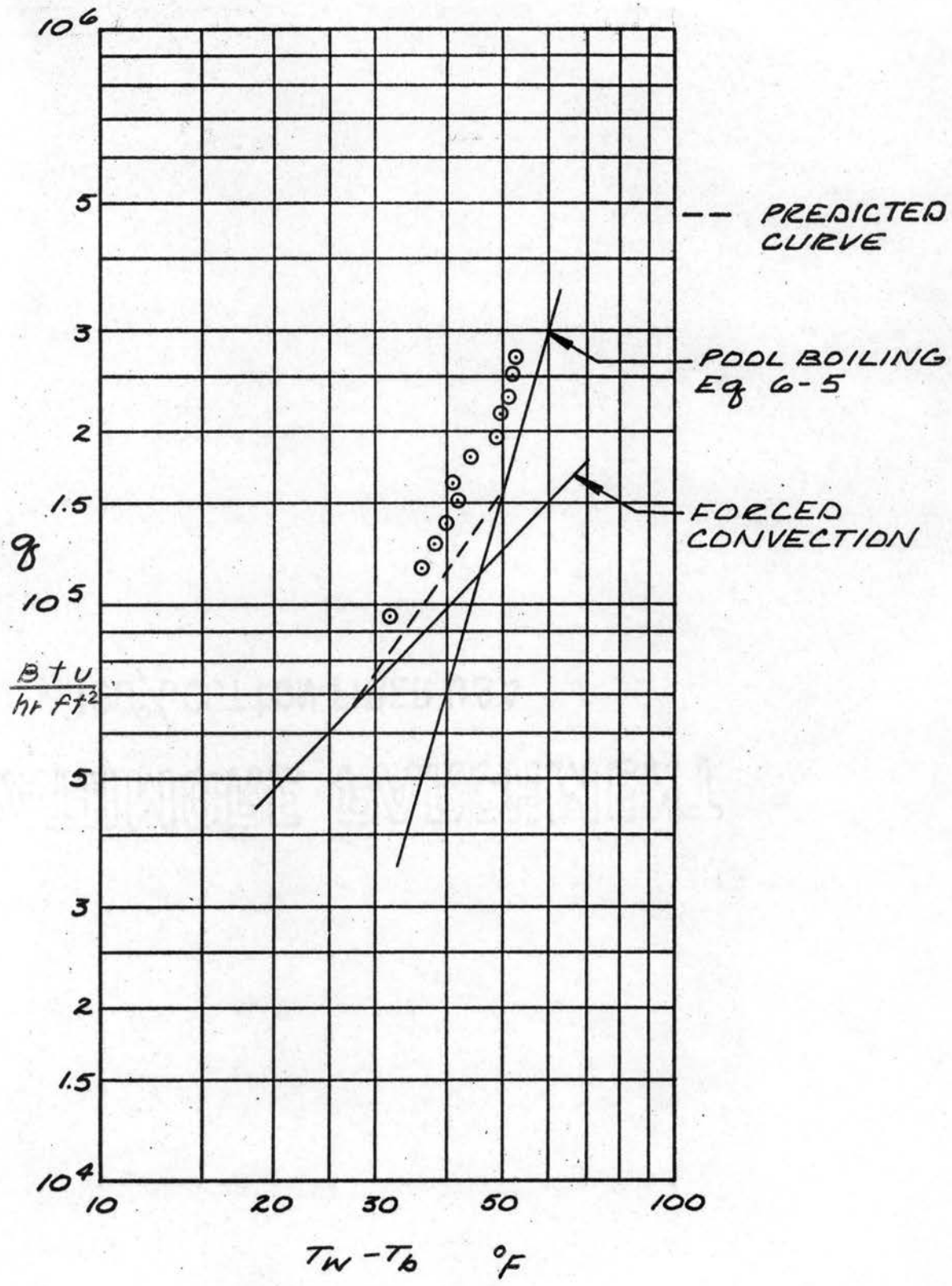

Figure 47. Method of Superposition for 0.707 in. O.D. Cylinder at 3.42 fps

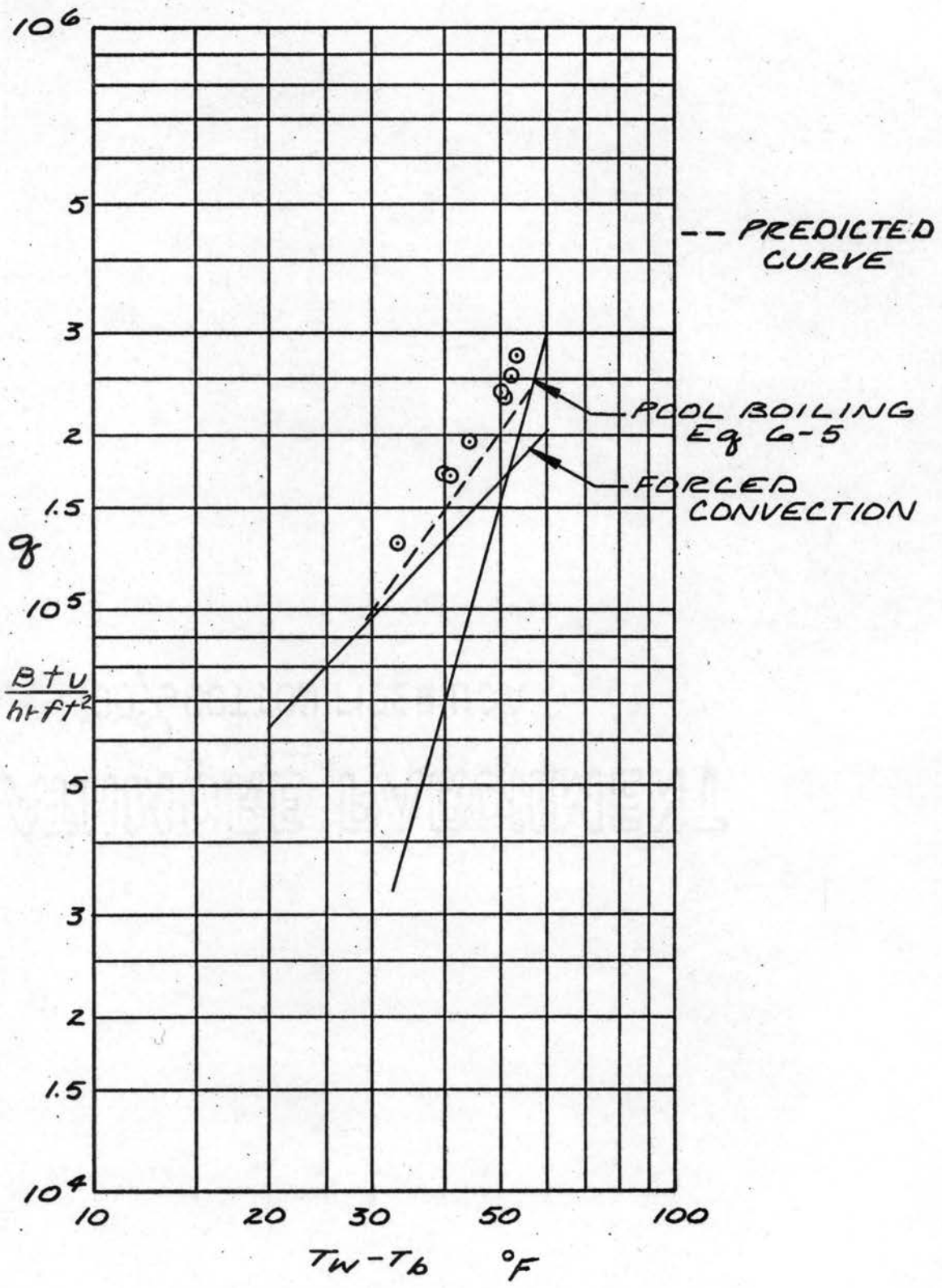

Figure 48. Method of Superposition for 0.708 in. O.D. Cylinder at 5.44 fps

curve, and the agreement with actual measured data. The single phase forced convection curves were obtained from equation D-25 for flow normal to a cylinder. The pool boiling curves are reproductions of the curves on Fig. 13, by use of equations 6-1 through 6-5, with the corresponding correction for bulk temperature which is used on the abscissa. The correction was obtained by subtracting the existing forced convection boiling bulk temperature from the wall temperature at a given flux. The coordinates of Figures 13-18 could have been used directly if the forced convection curve were altered to compensate for the substitution of saturation temperature for bulk temperature. The predicted curve was constructed by locating the point of incipient boiling which had been recorded in the original laboratory data for most runs. The point of intersection of the predicted curve with the extended pool boiling curve was determined after the procedure of Forster and Greif (72). The flux at the pool boiling-predicted curve intersection is found by multiplying the flux at the forced convection - pool boiling curve intersection by 1.4. Further discussion of this method (72) is shown in Appendix D.

Good agreement is found between the predicted and actual data for Figures 39, 42, 43, 47, and 48. Use of the superposition method in these cases would either reasonably represent the actual forced convection boiling curve or give conservative results. The remaining curves show the forced convection boiling data between the extended pool boiling curve and the single phase curve. Reasonable agreement exists between the slopes of the pool boiling and forced convection boiling curves. If the superposition method is used to predict the boiling curves for Figures 39, 41, 44, 45, and 46, the results will be disappointing for at least a portion of the boiling region. The single

phase forced convection portion of Figures 40, 41, and 44, show fairly good agreement with the forced convection boiling data for this region.

Data Presentation - Method of Distinct Areas

The forced convection boiling curves can also be represented by the following expression:

$$q_{tot.} = q_{f.c.} + \frac{A_b}{A_t} (q_b - q_{f.c.}) \qquad 6\text{-}7$$

where

$$q_b = 2.84 \times 10^9 \exp \left[-3.28 \times 10^9 / T_w^3\right]$$

$$\frac{A_b}{A_t} = \exp \left[0.0848 \, \Delta T_s - 5.38\right]$$

$$q_{f.c.} = h_{f.c.} \, \Delta T_b$$

This curve is shown with the experimental data on Figure 49 for a flow velocity of 3.42 fps and as Figure 50 for 5.44 fps. Equation 6-7 is derived in Appendix D and is based upon the assumption that the total flux can be expressed as the sum of the forced convection single phase flux multiplied by the area under the influence of single phase heat transfer plus the boiling flux multiplied by the boiling area.

The single phase forced convection flux was determined by Equation D-25 for $h_{f.c.}$, multiplied by the actual temperature difference.

The boiling flux, q_b, was determined by evaluating the following expression:

$$q_b = \rho L V f n \qquad 6\text{-}8$$

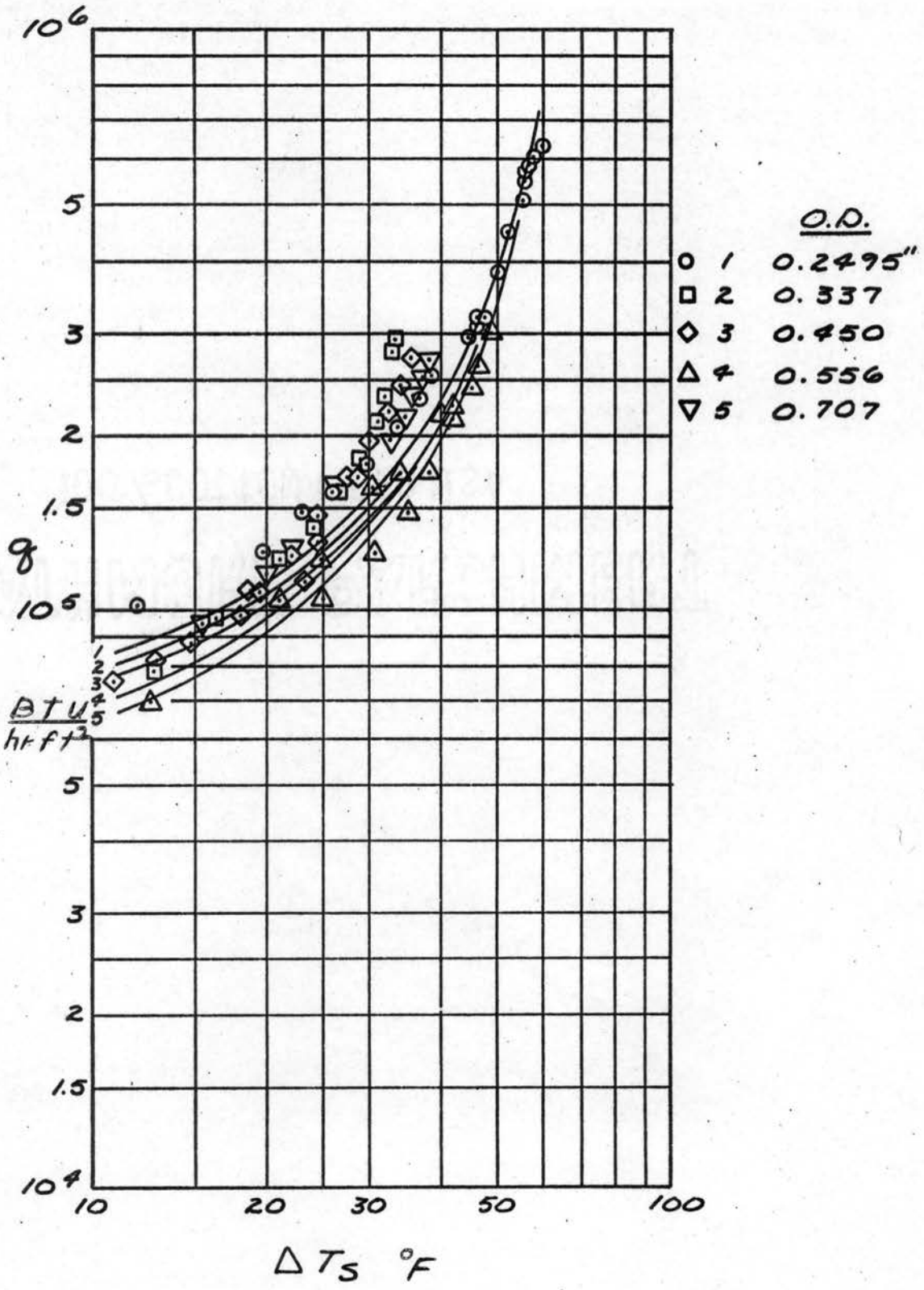

Figure 49. Correlation of Data at 3.42 fps by Method of Distinct Areas

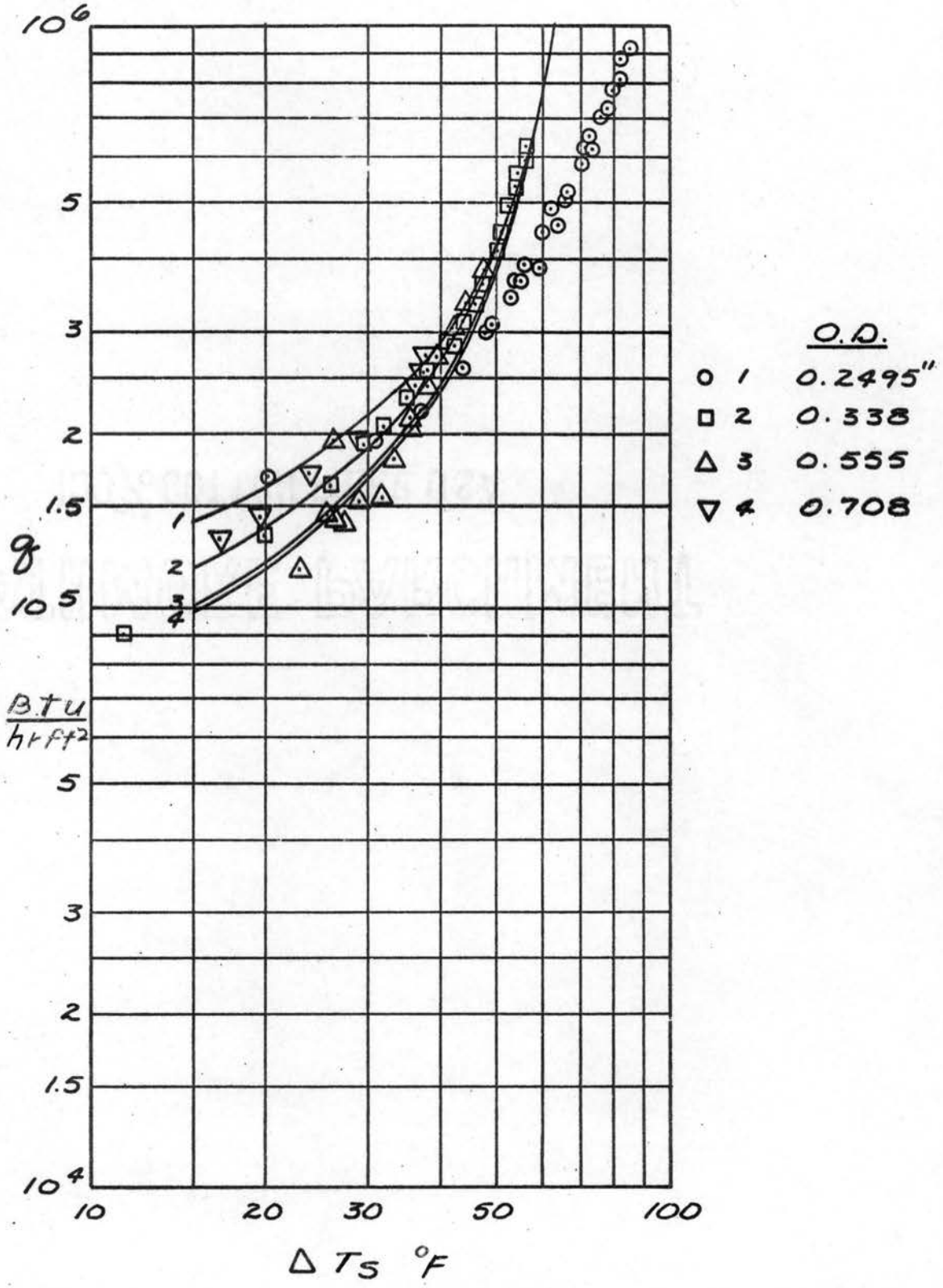

Figure 50. Correlation of Data at 5.44 fps by Method of Distinct Areas

where

ρ = vapor density

L = latent heat of vaporization

V = bubble volume

f = bubble departure frequency

n = number of active sites per unit area

The number of active sites has been found by Gaertner (75) to be a function of the wall temperature. The function has the form:

$$n = a\, e^{-\frac{b}{T_w^3}} \qquad 6\text{-}9$$

where

a,b are constants characteristic of the surface

T_w = wall temperature, ^oR

The value of "b" was determined from the pool boiling data, one value for each experiment, and the smallest value was selected. The value of "a" was estimated by assuming in the forward region, one active site per bubble diameter squared per unit surface area, and one active site per bubble diameter squared per unit of projected area in the wake region. The wall temperature was selected at a ΔT_s of 37^oF for the 3.42 fps data, and 47^oF for the 5.44 fps data. These temperature differences represent the point at which the slope of the forced convection boiling curve approaches the pool boiling curve slope. Bubble diameters were measured from the photographic studies.

The bubble departure frequency, f, was estimated from the frequency of a continuous stream of bubbles, which is the bubble velocity divided by the bubble diameter.

The bubble volume was calculated using the average of the measured diameters and assuming the bubbles to be spheres.

This allowed the evaluation of the boiling flux in Eq. 6-8. The total flux in Eq. 6-7 was known from the experimental data, and the remaining term, $A_B/A_{tot.}$, was found empirically as a function of ΔT_s.

Pool Boiling Burnout

The relationship of ϕ_c to outside diameter is shown in Figure 51. Included on this figure are representative data from the literature for smaller tubes and wires. The limiting case as the diameter increases would be burnout data from flat plates (strips), which give burnout fluxes of 140,000 to 220,000 Btu/hr.sq.ft. at atmospheric pressure. The general scatter of the data shown on Fig. 48 shows the need for further investigation into the important factors determining pool boiling burnout. Cylinder diameter is not a major variable.

This conclusion has been supported by Pitts and Leppert (78) who have stated that for diameters above 0.05 inches, the critical flux is not a function of diameter. These authors have also decided that in the diameter range of 0.01 to 0.05 inches, ϕ_c increases with an increase in diameter. This is due to a decrease in the insulating effects of bubbles which have diameters of about this size range. In the diameter range of 0.003 to 0.01 inches, the bubble diameter becomes large compared to the wire, giving a large insulated area, and ϕ_c remains fairly constant. Below 0.003 inches, ϕ_c increases as the diameter decreases. This is attributed to the fact that the bubble spacing along the wire increases as the wire diameter decreases, and coalescence becomes more difficult.

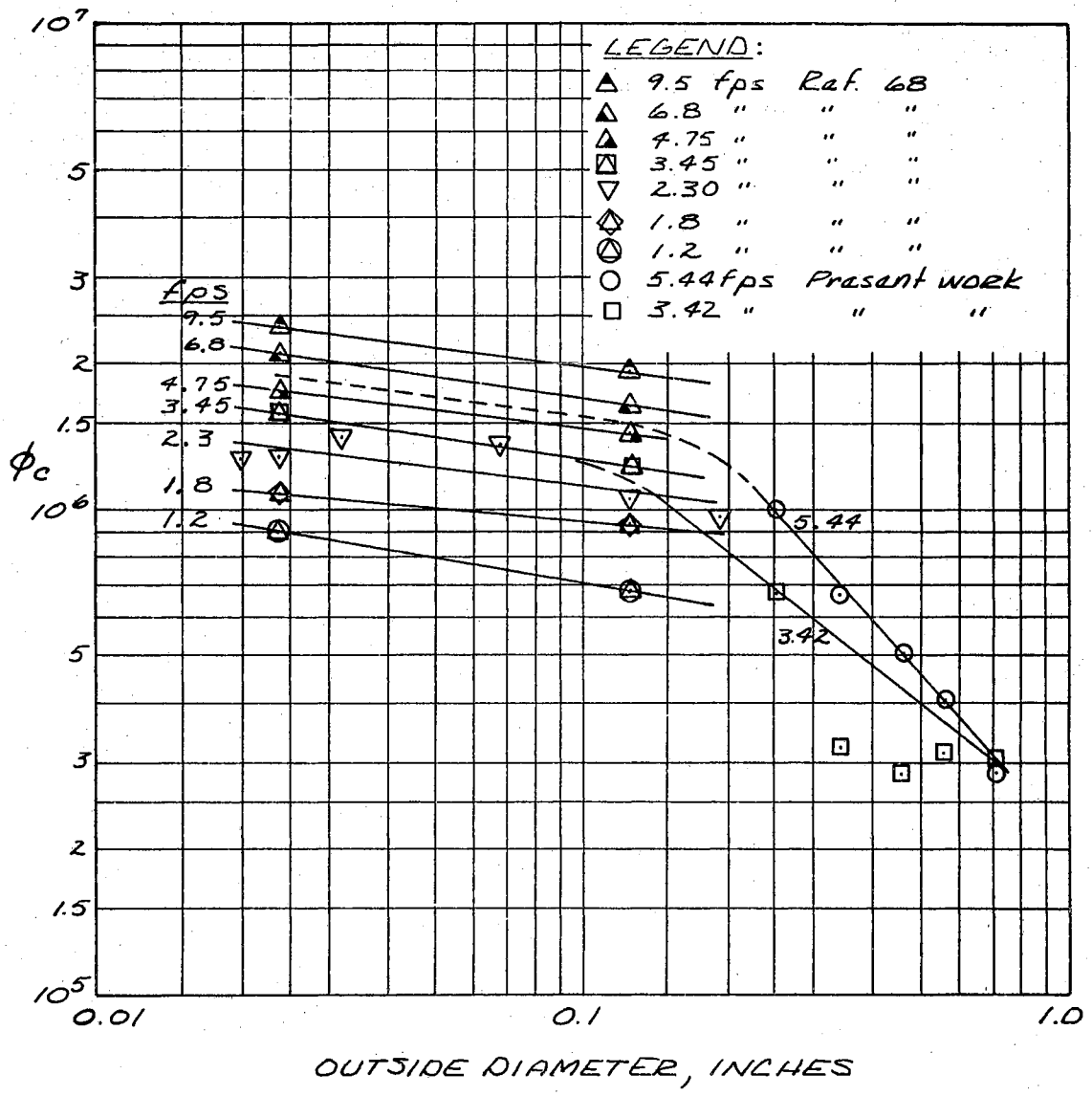

Figure 51. Velocity Effect on Forced Convection Burnout

The work of Gambill (61) brilliantly illustrates the problem of trying to correlate pool boiling burnout flux as a function of diameter, particularly for diameters above 0.1 inch. Burnout flux variations are determined by elusive surface conditions, other than roughness variations, which seem to affect the wettability of the fluid coolant. This non-hydrodynamic factor has manifested itself in the surface aging effects in which older surfaces tend to display higher values of ϕ_c.

The large variation in the burnout flux at 0.7 inch falls into this category. Both specimens had been undergoing boiling for periods greather than three hours, so that rapid aging effects should have vanished. No known changes were made in performing the two tests, and the data for the other diameters would indicate the lower value of ϕ_c to be the more realistic one.

It is possible the large diameters are approaching the case of a flat strip insulated from below. This case was part of an investigation by Howell and Bell (81) who determined ϕ_c with a 0.75 inch wide strip as a function of pressure. Their data at atmospheric pressure gives ϕ_c in the order of 180,000 Btu/hr.sq.ft.

Forced Convection Burnout

The critical or burnout flux, ϕ_c, is presented together with the results of Vliet and Leppert (68) in Figures 51, 52, and 53.

Figure 52 shows the relationship of ϕ_c to diameter at various bulk velocities. The higher velocity burnout data lie on a straighter line than the lower velocity data. This indicates that the forced convection influence on ϕ_c is dominating the inherent randomness found in pool boiling burnout values of ϕ_c. The lower velocity data at diameters

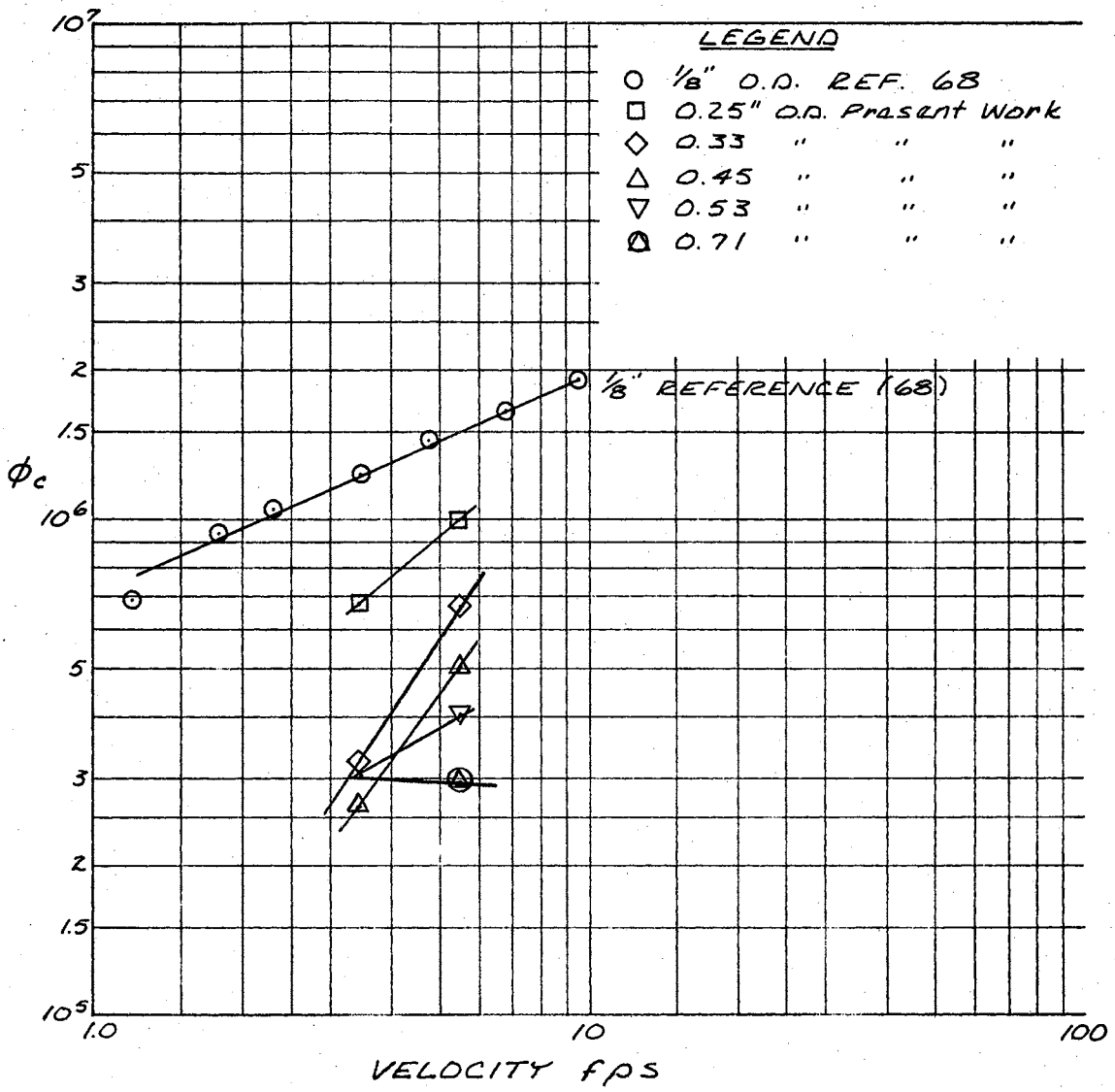

Figure 52. Diameter Effect on Forced Convection Burnout

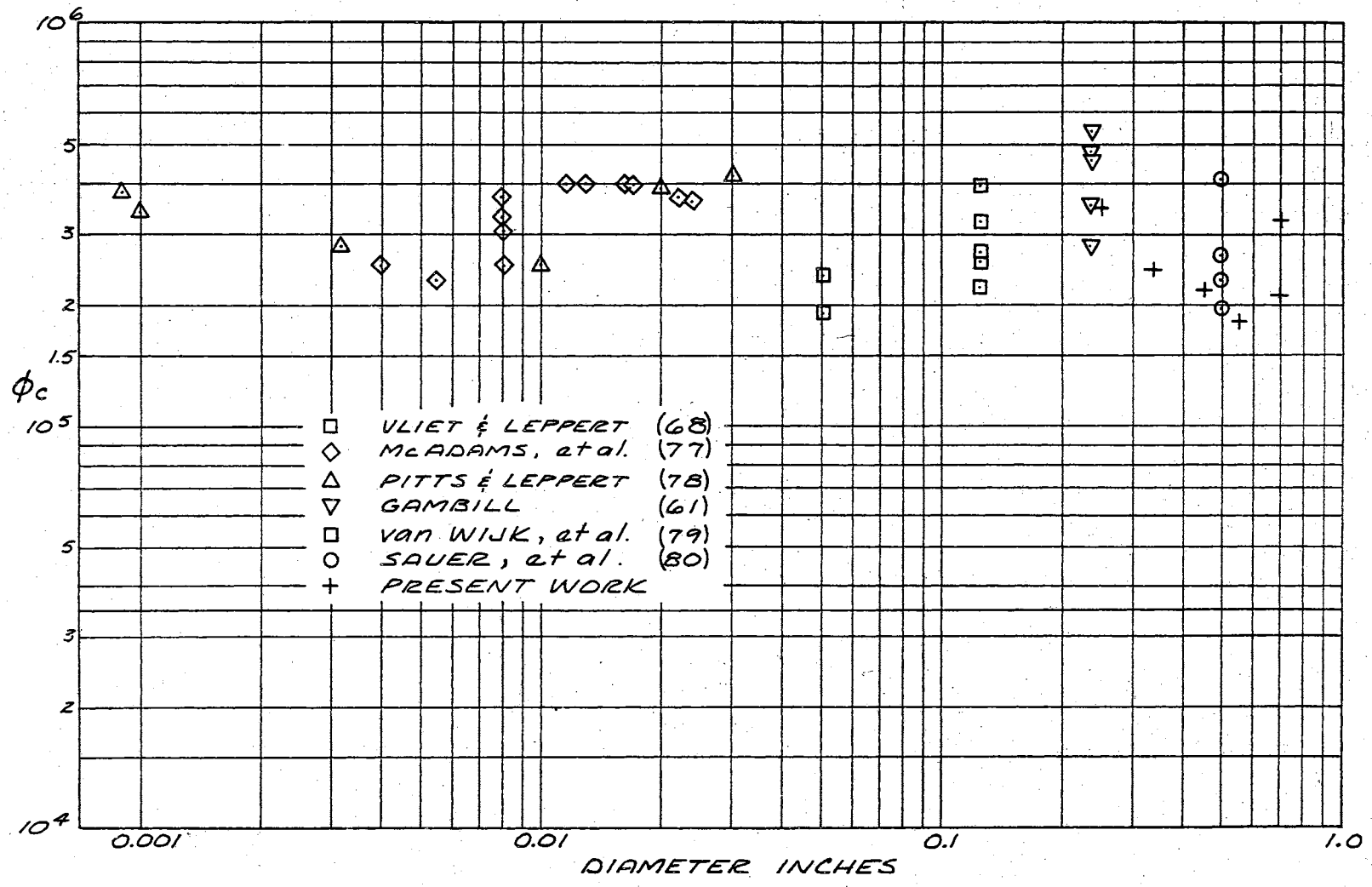

Figure 53. Diameter Effect on Pool Boiling Burnout

greater than 0.25 inches show the characteristic scatter found in pool boiling burnout data. The decrease in ϕ_c as the cylinder diameter increases can be attributed to the fact that larger cylinder diameters allow larger vapor bubble diameters to form in the wake region; thus the likelihood of local overheating is also increased. Bubbles in the wake region of the large cylinders are less affected by the forced flow, and boiling in the wake becomes similar to pool boiling.

In Figure 53 the diameter is the parameter for the relationship between critical flux and velocity.

The critical flux for flow inside tubes can be calculated by numerous methods. Kutateladze's (82) correlation is independent of length and diameter. It is:

$$\phi_c = \left\{ 0.023 L \rho_v \left[\frac{g g_c (\rho_L - \rho_v)}{\rho_v^2} \right]^{0.25} \left[U \left(\frac{\rho_L + \rho_v}{g g_c} \right)^{0.25} \right]^{0.5} \right\} \times \left[1 + \left(\frac{\rho_L}{\rho_v} \right)^{0.85} \left(\frac{c_p \Delta T_{sub}}{2.22 L} \right) \right] \qquad 6\text{-}10$$

Equation (6-10) gives ϕ_c = 304,000 and 400,000 Btu/hr.ft^2 at 3.42 and 5.44 fps respectively.

The method of Gambill (63) adds a convective flux to a pool boiling flux to obtain the forced convection burnout flux for subcooled liquids. Following this procedure, the forced convection coefficient is the usual single phase liquid coefficient, and the burnout wall temperature is obtained from Bernath's (83) correlation. The convective flux is:

$$(\phi_c)_{nb} = h_L \, (t_w - t_b)_c \qquad 6\text{-}11$$

Zuber's relationship (84) for the pool boiling burnout is:

$$\phi_c = \frac{\pi}{24} L \rho_v \left[\frac{g g_c (\rho_L - \rho_v)}{\rho_v^2} \right]^{0.25} \left[\frac{\rho_L + \rho_v}{\rho_L} \right]^{0.5} \qquad 6\text{-}12$$

This gives a value of 388,000 Btu/hr.ft^2 for the burnout flux. The sum of (6-11) and (6-12) is shown in Table I with the experimental values obtained in this work.

Burnout Temperatures

The temperatures of the cylinder surface at burnout were estimated from Figures 9-13. The flux at burnout was measured in each case, but the rapidity of the burnout process did not allow time for temperatures to be measured. Therefore, the curves were extrapolated to the burnout flux and the temperature noted. The results are shown in Table II. Average values are the average of all the thermocouples used in the cylinder. The average minimum and maximum ΔT_b for pool boiling is 35°F and 41°F. At 3.42 fps the average minimum and maximum ΔT_b is 48.6°F and 60°F, and at 5.44 fps they are 62°F and 77°F, respectively. The average pool boiling ΔT_b is 39.8°F which is in agreement with published values (61).

TABLE I

BURNOUT FLUX SUMMARY

Run No.	O.D. inches	Velocity fps	Φ_c Experimental Btu/hr.ft^2	Φ_c Eq (6-11)+(6-12) Btu/hr.ft^2
44	0.2497	0.00	350,000	
18	0.2495	3.42	673,000	623,000
17	0.2495	5.44	990,000	684,000
36	0.337	0.00	245,000	
50	0.337	3.42	321,000	598,000
54	0.338	5.44	664,000	656,000
37	0.457	0.00	219,000	
32	0.450	3.42	294,000	579,000
15	0.4587	5.44	502,000	630,000
39	0.5535	0.00	183,000	
23	0.556	3.42	314,000	563,000
27	0.555	5.44	402,000	611,000
46	0.7028	0.00	212,700	
28	0.707	3.42	301,500	554,000
29	0.708	5.44	287,000	500,000

TABLE II

BURNOUT TEMPERATURE SUMMARY

Run No.	O.D. inches	Velocity fps	T_s	T_b	Avg. T_w	Min. T_w	Max. T_w	Avg. ΔT_s	Avg. ΔT_b	Min. ΔT_b	Max. ΔT_b
44	0.2497	0.00	211.5	211.5	259.0			47.5	47.5		
18	0.2495	3.42	223.7	212.2	286.7			63.0	74.5		
17	0.2495	5.44	223.7	207.0	314.7			91.0	107.7		
36	0.337	0.00	211.7	211.7	255.7	254.2	258.7	44.0	44.0	42.5	47.0
50	0.3371	3.42	223.7	210.4	257.7	251.4	262.9	34.0	47.3	41.0	52.5
54	0.338	5.44	223.7	210.7	281.2	270.7	289.7	57.5	70.5	60.0	79.0
37	0.457	0.00	212.5	212.5	247.0	244.5	249.0	34.5	34.5	32.0	36.5
32	0.450	3.42	223.7	208.2	260.2	253.7	265.7	36.5	52.0	45.5	57.5
15	0.4587	5.44	223.7	209.3	296.2	289.3	302.3	72.5	86.9	80.0	93.0
39	0.5335	0.00	213.5	213.5	246.0	242.5	255.5	32.5	32.5	29.0	42.0
23	0.556	3.42	223.7	208.8	275.2	266.8	278.8	51.5	66.4	58.0	70.0
27	0.555	5.44	223.7	209.2	274.2	269.2	274.2	50.5	65.0	60.0	65.0
46	0.7028	0.00	212.2	212.2	251.7	248.2	252.2	39.5	39.5	36.0	40.0
28	0.707	3.42	223.7	208.4	263.7	258.4	268.4	40	55.3	50.0	60.0
29	0.708	5.44	223.7	208.1	263.7	255.1	269.1	40	55.6	47.0	61.0

CHAPTER VII

CONCLUSIONS AND RECOMMENDATIONS

Boiling heat transfer from horizontal cylinders with flow normal to the major axis was studied for cylinders from 0.25 in. O.D. to 0.70 in. O.D. The coolant was 12^{o}F subcooled water approaching the cylinders at bulk velocities of 3.42 fps and 5.44 fps. Inside wall temperatures were measured at four points on the cylinder circumference, and the results presented as the localized or point boiling curve of flux vs. ΔT_b. Cylinders of the same size range were also subjected to pool boiling studies.

The temperature profile investigations show that the surface temperature is nearly independent of position for forced convection boiling, and completely independent of position for pool boiling. The pool boiling temperature profiles produced an intermixing of individual boiling curves which attests to the random distribution of active sites on the cylinder's surface. In forced convection boiling as the wall temperature increases, there is a definite tendency for the forward and rear stagnation points to exchange temperature roles. At low average wall temperatures, the forward point is cooler than the rear point. At higher average wall temperatures the rear point becomes cooler, but burnout inevitably occurs in the wake region. The four individual boiling curves again display the randomness typical of boiling curves in general. These curves do justify the use of an average

temperature, which is common practice. Until more is known about surface characteristics, the extension of a model describing flux as a function of the system variables, based on the forward region into the wake region will also yield reasonable results, even though the hydrodynamic patterns are different.

The pool boiling burnout studies show agreement with published data with respect to wall temperature. A general decrease in the critical flux with increasing diameter was noted. The pool boiling burnout fluxes were between reported values for small tubes or wires, and flat strips which could be regarded as cylinders of infinite diameter.

The forced convection burnout studies also displayed a decrease in burnout flux with an increase in diameter. Since the larger diameter tubes provide a greater amount of blockage to the flowing fluid than the smaller diameter tubes, the opportunity for vapor coalescence and local wall overheating in the wake region increases with cylinder diameter.

The photographic studies have shown that the major part of the visible bubble volume is outside the boundary layer. The maximum bubble diameter in the forward region of the cylinder was determined by the fluid velocity, the larger diameters appearing at the lower flow rate. The range of major bubble diameters was smaller than the bubble velocity range. The bubble velocity in the forward region is greater than the bulk fluid velocity, but more extensive photographic work at greater magnifications and higher film speeds will be required to determine the contribution of the departure velocity to final velocity. This effect in pool boiling has been estimated by Darby (85) to be about 20 fps in the region of 1 to 3 bubble diameters from the surface.

Areas which are recommended for further research include: the characteristics of a surface during the boiling process; the hydrodynamics and thermodynamics of a growing vapor bubble in a moving liquid stream; the mechanism of activation of nucleation sites with temperature; and the area of influence of a departing vapor bubble in a liquid stream. Since the basic boiling curves for the nucleate boiling region with flow normal to the cylinder have been demonstrated to be similar to the curves for other flow geometries, a logical extension of this work would be into the effects of a tube bank on the boiling curve and critical flux.

The use of pool boiling data in formulating forced convection boiling expressions has the inherent weakness of encompassing the randomness of pool boiling data. The source of this randomness lies with the inadequate description of the surface characteristics. Likewise, the use of boiling data for wires and small tubes for larger diameters should be done with caution.

A SELECTED BIBLIOGRAPHY

(1) Nukiyama, S. "The Maximum and Minimum Values of Heat q Transmitted From Metal Surface to Boiling Water Under Atmospheric Pressure." J. Soc. Mech. Eng., Japan, Vol. 37, No. 206, (1934) 367-74.

(2) Bonilla, Chas. F. Nuclear Engineering. McGraw-Hill Book Co., Inc. New York, N. Y. (1957) 399-431.

(3) Emmerson, G. S. "Heat Transmission With Boiling." Nuclear Engineering. Vol. 5, (November 1960) 493-500.

(4) Roberts, H. A., and R. W. Bowring. "Boiling Effects in Liquid-cooled Reactors." Nuclear Power. Vol. 4, (March 1959) 96-101, 118.

(5) Lottes, P. A., M. Petrick, and J. F. Marchaterre. "Lecture Notes on Heat Extraction From Boiling Water Power Reactors." ANL 6063 (August 1959).

(6) Gambill, W. R. "A Survey of Boiling Burnout." British Chemical Engineering. Vol. 8, No. 2, 93-98 (February 1963).

(7) Gambill, W. R. "Burnout in Boiling Heat Transfer." Nuclear Safety. Vol. 6, No. 2 (Winter 1964-65) 152-60.

(8) Kepple, R. R., and T. V. Tung. "Bibliography on Heat Transfer and Hydraulics." ANL 6734 (July 1964).

(9) Eckert, E. R. G., E. M. Sparrow, W. E. Ibele, and R. J. Goldstein. "Heat Transfer-A Review of Current Literature." International Journal of Heat and Mass Transfer. Vol. 8, No. 8. (August 1965) 1053-83.

(10) Ibid. Vol. 7, No. 8 (August 1964) 827-52.

(11) Ibid. Vol. 6, No. 9 (September 1963) 761-91.

(12) Eckert, E. R. G., T. F. Irvine, E. M. Sparrow, and W. E. Ibele. "Heat Transfer-A Review of Current Literature." International Journal of Heat and Mass Transfer. Vol. 5. (October 1962) 1023-50.

(13) Ibid. Vol. 3, No. 3 (October 1961) 222-48.

(14) Eckert, E. R. G., E. M. Sparrow, W. E. Ibele, and R. J. Goldstein. "Heat Transfer Bibliography." International Journal of Heat and Mass Transfer. Vol. 8, No. 1. (January 1965)

(15) Ibid. Vol. 8, No. 2 (February 1965) 359-71.

(16) Ibid. Vol. 8, No. 5 (May 1965) 845-55.

(17) Ibid. Vol. 8, No. 9 (September 1965) 1235-51.

(18) Ibid. Vol. 8, No. 12 (December 1965) 1537-53.

(19) Ibid. Vol. 7, No. 2 (February 1964) 257-65.

(20) Ibid. Vol. 7, No. 4 (April 1964) 485-98.

(21) Ibid. Vol. 7, No. 8 (August 1964) 931-48.

(22) Ibid. Vol. 6, No. 1 (January 1963) 91-112.

(23) Ibid. Vol. 6, No. 7 (July 1963) 621-42.

(24) Ibid. Vol. 6, No. 11 (November 1963) 971-86.

(25) Eckert, E. R. G., E. M. Sparrow, and W. E. Ibele. "Heat Transfer Bibliography." International Journal of Heat and Mass Transfer. Vol. 5, No. 3 (May 1962) 413-24.

(26) Ibid. Vol. 5, No. 4 (June 1962) 561-70.

(27) Ibid. Vol. 3, No. 4 (December 1961) 351-57.

(28) Ibid. Vol. 3, No. 1 (August 1961) 68-75.

(29) Ibid. Vol. 2, No. 4 (June 1961) 342-47.

(30) Eckert, E. R. G., J. P. Hartnett, and E. M. Sparrow. "Heat Transfer Bibliography." Heat and Mass Transfer. Vol. 2, No. 2 (March 1961) 163-72.

(31) Ibid. Vol. 1, No. 4 (January 1961) 336-56.

(32) Ibid. Vol. 1, No. 3 (August 1960) 255-68.

(33) Eckert, E. R. G., J. P. Hartnett, and T. F. Irvine. "Heat Transfer Bibliography." Heat and Mass Transfer. Vol. 1, No. 1 (June 1960) 102-112.

(34) Luikov, A. V. "Heat Transfer Bibliography-Russian Works." International Journal of Heat and Mass Transfer. Vol. 8, No. 6 (June 1965) 955-70.

(35) Ibid. Vol. 8, No. 2 (February 1965) 337-57.

(36) Ibid. Vol. 7, No. 3 (March 1964) 371-96.

(37) Ibid. Vol. 6, No. 4 (April 1963) 309-24.

(38) Ibid. Vol. 5, No. 4 (June 1962) 571-82.

(39) Ibid. Vol. 5, No. 9 (November 1962) 1121-29.

(40) Ibid. Vol. 2, No. 2 (March 1961) 173-84.

(41) Sato, T. "Heat Transfer Bibliography." International Journal of Heat and Mass Transfer. Vol. 8, No. 6 (June 1965) 953-54.

(42) Ibid. Vol. 7, No. 2 (February 1964) 267-68.

(43) Ibid. Vol. 7, No. 10 (October 1964) 1141-42.

(44) Ibid. Vol. 6, No. 3 (March 1963) 243-44.

(45) Ibid. Vol. 5, No. 7 (September 1962) 883-84.

(46) Ibid. Vol. 3, No. 4 (December 1961) 358.

(47) Wiley, John S. "Burnout in Steam-water Mixtures." Power Reactor Technology. Vol. 7, No. 4 (Fall 1964) 335-53.

(48) Anon. "Two-phase Systems." Power Reactor Technology. Vol. 8, No. 3 (Summer 1965) 164-71.

(49) Wiley, John S. "Burnout in Multirod Geometry." Power Reactor Technology. Vol. 7, No. 2 (Spring 1964) 154-66.

(50) Rohsenow, W. M. Developments in Heat Transfer. Chapter 8. The M. I. T. Press, Cambridge, Massachusetts (1964).

(51) Rohsenow, W. M. "A Method of Correlating Heat-Transfer Data For Surface Boiling of Liquids." Trans. Amer. Soc. Mech. Eng. Vol. 74 (August 1952) 969.

(52) Forster, H. K., and N. Zuber. "Dynamics of Vapor Bubbles and Boiling Heat Transfer." Amer. Inst. Chem. Engrs. Jour. Vol. 1 (December 1955) 531.

(53) Zuber, N., and M. Tribus. "Stability of Boiling Heat Transfer." AECU 3631, No. 11 (January 1958)

(54) Madejski, J. "Theory of Nucleate Pool Boiling." International Journal of Heat and Mass Transfer. Vol. 8, No. 1 (January 1965) 155-71.

(55) Han, C., and P. Griffith. "The Mechanism of Heat Transfer in Nucleate Pool Boiling - Part I. Bubble Initiation, Growth, and Departure." International Journal of Heat and Mass Transfer, Vol. 8, No. 6 (June 1965) 887-904.

(56) Ibid. "Part II. The Heat Flux-Temperature Difference Relation." Vol. 8, No. 6 (June 1965) 905-14.

(57) Cole, R. "A Photographic Study of Pool Boiling in the Region of the Critical Heat Flux." Amer. Inst. Chem. Engrs. Jour. Vol. 6, No. 4 (December 1960) 533-38.

(58) Gaertner, R. F. "Photographic Study of Nucleate Pool Boiling on a Horizontal Surface." Trans. Amer. Soc. Mech. Eng. Jour. Heat Transfer. Vol. C87, No. 1 (February 1965) 17-29.

(59) Lance, R. P., and J. E. Myers. "Local Boiling Coefficients on a Horizontal Tube." Amer. Inst. Chem. Engrs. Jour. Vol. 4, No. 1 (March 1958) 75-80.

(60) Zuber, N., M. Tribus, and J. W. Westwater. "The Hydrodynamic Crisis in Pool Boiling of Saturated and Subcooled Liquids." Inter. Developments in Heat Transfer. Part II (January 1962) 230-36.

(61) Gambill, W. "An Experimental Investigation of the Inherent Uncertainty in Pool Boiling Critical Heat Fluxes to Saturated Water." Amer. Inst. Chem. Engrs. Jour. Vol. 10 No. 4 (July 1964) 502-08.

(62) Irvine, T. F., and J. P. Hartnett. Advances in Heat Transfer. Vol. 1, Academic Press, New York (1964).

(63) Gambill, W. R. "Generalized Prediction of Burnout Heat Flux For Flowing, Subcooled, Wetting Liquids." Chemical Engineering Progress Symposium Series. Vol. 59, No. 41 (1963) 71-87.

(64) Longo, J. "Statistical Study of Subcooled Burnout." KAPL 1744 (October 1957)

(65) Perkins, H. C., and G. Leppert. "Forced Convection Heat Transfer From a Uniformly Heated Cylinder." Trans. Amer. Soc. Mech. Eng. Jour. Heat Transfer. Vol. 84C (1962) 257-63.

(66) Perkins, H. C., and G. Leppert. "Local Heat-Transfer Coefficients on a Uniformly Heated Cylinder." International Journal of Heat and Mass Transfer. Vol. 7, No. 2 (February 1964) 143-58.

(67) Richardson, P. D. "Heat and Mass Transfer in Turbulent Separated Flows." Chemical Engineering Science. Vol. 18 (1963) 149-55.

(68) Vliet, G. C., and G. Leppert. "Critical Heat Flux For Nearly Saturated Water Flowing Normal to a Cylinder." Trans. Amer. Soc. Mech. Eng. Jour. Heat Transfer. 85C (February 1964) 59-67.

(69) Becker, K. M. "Burnout Conditions For Flow of Boiling Water in Vertical Rod Clusters." Amer. Inst. Chem. Engrs. Jour. Vol. 9, No. 2 (1963) 216-222.

(70) Bromley, L. A., N. R. LeRoy, and J. A. Robbers. "Heat Transfer in Forced Convection Film Boiling." Industrial and Engineering Chemistry. Vol. 45, No. 12, 2639-46.

(71) Schlichting, H. Boundary Layer Theory. 4th Ed. McGraw-Hill, New York (1960).

(72) Forster, K. E., and R. Greif. "Heat Transfer to a Boiling Liquid, Mechanism and Correlations." Amer. Soc. Mech. Engr. 58-HT-11 (1958).

(73) Chang, Yan Po. "Some Possible Critical Conditions in Nucleate Boiling." Amer. Soc. Mech. Eng. Jour. Heat Transfer. 85C (1963) 89-100.

(74) Bergles, A. E., and W. M. Rohsenow. "The Determination of Forced-Convection Surface-Boiling Heat Transfer." Trans. Amer. Soc. Mech. Eng. Jour. Heat Transfer. 85C (August 1965) 365-72.

(75) Gaertner, R. F. "Distribution of Active Sites in the Nucleate Boiling of Liquids." CEP Symp. Ser. Vol. 59, No. 41 (1963) 52-61.

(76) Levich, V. G. Physicochemical Hydrodynamics. Prentice-Hall (1962).

(77) McAdams, W. H., J. N. Addoms, P. M. Rinaldo, and R. S. Day. Chemical Engineering Progress. Vol. 44, No. 8 (August 1948) 639-46.

(78) Pitts, C. C., and G. Leppert. "The Critical Heat Flux For Electrically Heated Wires in Pool Boiling." International Journal of Heat and Mass Transfer. Vol. 9 (1966) 365-77.

(79) van Wijk, W. R., A. S. Vos, and S. J. D. Van Stralen. "Heat Transfer to Boiling Binary Liquid Mixtures." Chemical Engineering Science. Vol. 5 (1956) 68-80.

(80) Sauer, E. T., H. B. H. Cooper, G. A. Akin, and W. H. McAdams. "Heat Transfer to Boiling Liquids." Mechanical Engineering. Vol. 60 (September 1938) 669-75.

(81) Howell, J. R., K. J. Bell. "An Experimental Investigation of the Effect of Pressure Transients of Pool Boiling Burnout." Chem. Eng. Symp. Ser. Vol. 59, No. 41 (1963) 88-91.

(82) Tong, L. S. Boiling Heat Transfer and Two-Phase Flow. Wiley and Son, New York (1965) p. 8173, Table 6-7.

(83) Bernath, L. "A Theory of Local-Boiling Burnout and Its Application to Existing Data." CEP Sym. Ser. Vol. 56, No. 30 (1960) 95.

(84) Zuber, N. "On the Stability of Boiling Heat Transfer." Trans. Amer. Soc. Mech. Eng. Vol. 80 (1958) 711.

(85) Darby, R. "The Dynamics of Vapour Bubbles in Nucleate Boiling." Chem. Eng. Sci. Vol. 19, No. 1 (1964) 39.

(86) Owens, W. L., Jr. "An Analytical and Experimental Study of Pool Boiling with Particular Reference to Additives." British Report AEEW-R-180 (May 1963).

(87) Forster, H. K., and N. Zuber. "Growth of a Vapor Bubble in a Superheated Liquid." Journal of Applied Physics. Vol. 25, No. 4 (1954) 474.

(88) Moore, F. D., and R. B. Mesler. "The Measurement of Rapid Surface Temperature Fluctuations During Nucleate Boiling of Water." Amer. Inst. Chem. Engrs. Jour. Vol. 7 (1961) 620-24.

APPENDIX A

CALIBRATION DATA

TABLE A-I

CALIBRATION OF THERMOCOUPLES FOR MEASUREMENT OF WATER TEMPERATURE

Actual Temperature National Bureau of Standards Platinum Resistance Thermometer °F	Thermocouple Number	Thermocouple Indicated Temperature °F
203.5748	7A	204.333
203.5880	7B	204.419
203.7475	7C	204.515
203.8372	7D	204.551
272.3639	7A	273.315
272.0820	7B	273.167
272.2459	7C	273.236
272.1672	7D	273.249
324.0251	7A	325.682
324.1006	7B	325.724
324.1289	7C	325.695
324.2547	7D	325.782

TABLE A-II

CORRECTION FACTOR MILLIVOLTS FOR DEVIATION OF CYLINDER THERMOCOUPLE READING FROM WATER TEMPERATURE THERMOCOUPLE READING

Run No.	Bulk Water Thermocouple	Thermocouple Number 2	3	4	5
8	7A	0.007	0.009	0.004	0.012
9	7A	0.007	0.009	0.004	0.012
15	7A	0.007	0.009	0.004	0.012
16	7A				0.020
17	7A				0.020
18	7A				0.020
22	7B	0.035	0.038	0.038	0.051
23	7B	0.035	0.034	0.037	0.051
26	7B	0.070	0.062	0.062	0.061
27	7B	0.048	0.026	0.026	0.038
28	7B	0.006	0.036	0.018	0.026
29	7B	0.041	0.041	0.042	0.032
30	7C	0.004	0.007	0.002	0.114
31	7C	0.008	0.008	0.009	0.014
32	7C	0.031	0.030	0.030	0.042
36	7C	0.005	-0.028	0.005	-0.003
37	7C	-0.028	-0.029	-0.012	-0.012
38	7C	-0.022	-0.030	-0.029	-0.043
39	7C	-0.022	-0.030	-0.029	-0.043
40	7C	0.034	0.020	0.004	0.019
41	7C	0.079	0.075	0.072	0.072
42	7C	0.022	0.013	0.008	0.007
43	7C				0.091

TABLE A-II (Continued)

Run No.	Bulk Water Thermocouple	Thermocouple Number 2	3	4	5
44	7C				0.000
45	7C	-0.010	-0.029	-0.030	-0.032
46	7C	-0.001	-0.015	-0.008	-0.006
48	7C	0.040	0.034	0.042	0.043
50	7D	0.000	-0.106	0.002	0.003
54	7D	0.011	0.004	0.004	0.012

Note: The above correction factors are to be subtracted from the indicated thermocouple readings.

TABLE A-III

ORIFICE CALIBRATION DATA

Orifice Diameter: 1.60 inches

Water Temperature: 70°F

Points 1-13: Original Calibration
Points 14-22: Recalibration

Calibration Tank Dimensions: 60" x 30.4" x 37" length x width x depth

Point No.	Manometer Reading inches of mercury		Time	Water Level Change	Flow Rate
	Left	Right	min. sec.	inches	gpm
1	- 1.2	1.2	3:38.7	24	59.9
2	- 2.5	2.5	2:33.9	24	73.6
3	- 3.4	3.4	2:10.7	24	86.8
4	- 2.0	2.0	2:51.2	24	66.1
5	- 2.5	2.5	2:08.5	20	72.6
6	- 4.0	3.9	1:41.2	20	93.5
7	- 5.6	5.4	1:25.1	20	111.0
8	- 6.5	6.4	1:19.2	20	119.3
9	- 8.6	8.4	1:09.2	20	136.7
10	- 9.5	9.2	1:06.5	20	142.3
11	-10.8	10.5	1:02.7	20	150.8
12	- 5.0	4.9	1:29.9	20	105.0
13	- 9.0	8.8	1:07.7	20	139.8
14	- 0.8	0.7	3:47.5	20	1.48
15	- 1.7	1.6	2:35.5	20	2.16
16	- 3.1	3.0	1:54.5	20	2.94
17	- 5.1	5.0	1:29.3	20	4.13
18	- 8.1	7.9	1:10.9	20	4.75
19	-10.7	10.5	1:01.7	20	5.48
20	-12.2	12.0	0:57.6	20	5.85
21	-14.2	14.0	0:53.7	20	6.28
22	-13.2	13.0	0:55.4	20	6.08

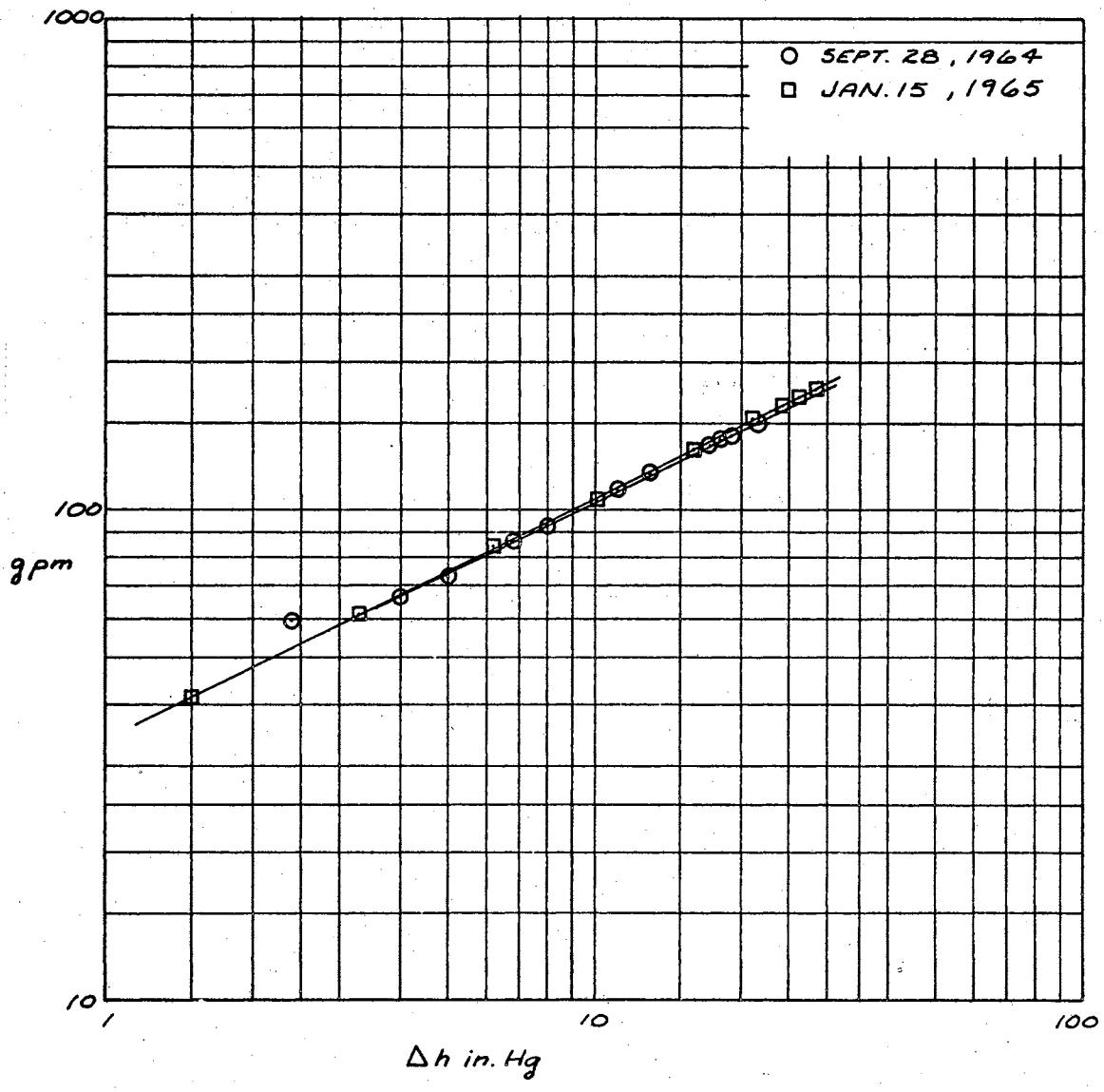

Figure A-1. Orifice Calibration

TABLE A-IV

VOLTMETER CALIBRATION

Voltmeter Reading	Actual Potential	Difference	%
1.00	1.0254	0.0254	2.54
1.50	1.5355	0.0355	2.36
1.99	2.0288	0.0388	1.95
2.77	2.8227	0.0527	1.90
3.98	4.0543	0.0743	1.87

Average % deviation 2.12%

APPENDIX B

VELOCITY PROFILE DATA

TABLE B-I

Date: October 18, 1964

Orifice Manometer: 2.8 in. Hg (61.5 gpm)

Pitot Tube: Normal to longitudinal cylinder axis at midpoint, test section empty.

Point No.	Pitot tube Manometer Inches of water Left	Right	Micrometer Reading inches	Notes	Velocity fps
1*	-1.5	-1.5	0.340	No flow	0
2**	-1.30	-1.55	0.340	window.	1.16
3	-1.25	-1.60	0.454		1.37
4	-1.18	-1.72	0.565		1.70
5	-1.12	-1.80	0.666		1.91
6	-1.05	-1.90	0.833		2.13
7	-1.00	-1.95	1.042		2.26
8	-0.97	-1.95	1.209		2.29
9	-0.94	-2.00	1.429		2.38
10	-0.90	-2.05	1.615		2.48
11	-0.90	-2.03	1.843		2.43
12	-0.95	-2.00	2.006		2.37
13	-0.93	-2.03	2.237		2.43
14	-0.95	-2.02	2.452		2.39
15	-1.00	-1.97	2.634		2.28
16	-1.04	-1.93	2.861		2.18
17	-1.05	-1.93	2.955		2.17
18	-1.05	-1.93	3.046		2.17
19	-1.07	-1.90	3.165		2.11
20***	-1.10	-1.87	3.259	Max.	2.03

Water Temperature 71.5°F

* Point No. 1 above was made to ascertain the absence of air in the lines between the pitot tube and the inverted manometer.

** Point No. 2, labeled window, was made with the pitot tube against the glass. The point of measurement was 3/32" from the window.

*** Point No. 20 was 0.237" from the wall.

TABLE B-II

VELOCITY PROFILE DATA

Date: October 19, 1964

Orifice Manometer: 10.80 in. Hg (109 gpm)

Pitot Tube: Normal to longitudinal axis at midpoint, test section empty.

Point No.	Pitot tube Manometer Inches of water Left	Right	Micrometer Reading inches	Notes	Velocity fps
1	-0.55	-1.65	0.305	Window	2.43
2	-0.47	-1.75	0.391		2.62
3	-0.32	-1.87	0.472		2.89
4	-0.07	-2.15	0.567		3.34
5	0.36	-2.57	0.713		3.96
6	0.60	-2.77	0.867		4.25
7	0.68	-2.87	1.014		4.37
8	0.75	-2.95	1.208		4.45
9	0.85	-3.03	1.464		4.56
10	0.82	-3.00	1.355		4.52
11	0.97	-3.14	1.554		4.70
12	1.00	-3.17	1.675		4.75
13	0.95	-3.15	1.805		4.69
14	0.93	-3.13	1.883		4.66
15	0.90	-3.10	2.036		4.64
16	0.90	-3.10	2.169		4.64
17	0.90	-3.10	2.036	Midpoint	4.64
18	0.92	-3.15	2.314		4.66
19	0.83	-3.07	2.468		4.57
20	0.74	-3.00	2.630		4.48
21	0.58	-2.85	2.821		4.29
22	0.55	-2.83	3.001		4.26
23	0.47	-2.68	3.144		4.11
24	0.35	-2.67	3.252	Max.	4.03

Water Temperature 72°F

Maximum reading was 0.209" from the wall.

TABLE B-III

VELOCITY PROFILE DATA

Date: October 19, 1964

Orifice Manometer: 20.2 in. Hg (147 gpm)

Pitot Tube: Normal to longitudinal axis at midpoint, test section empty.

Point No.	Pitot tube Manometer Inches of water Left	Right	Micrometer Reading inches	Notes	Velocity fps
1	-3.57	2.05	3.252	Max.	5.32
2	-3.73	2.25	3.041		5.66
3	-3.95	2.47	2.804		5.86
4	-4.15	2.67	2.642		6.06
5	-4.25	2.90	2.453		6.19
6	-4.40	2.95	2.310		6.28
7	-4.37	2.90	2.165		6.25
8	-4.37	2.90	2.040	Midpoint	6.25
9	-4.45	2.97	1.910		6.31
10	-4.50	3.00	1.836		6.34
11	-4.57	3.10	1.653		6.41
12	-4.20	2.80	1.430		6.12
13	-3.95	2.35	1.204		5.81
14	-3.87	2.33	1.012		5.77
15	-3.85	2.33	0.852		5.76
16	-3.80	2.25	0.657		5.69
17	-2.80	1.20	0.490		4.64
18	-2.37	0.75	0.412		4.10
19	-2.05	0.40	0.316	Window	3.63
20	-2.15	0.50	0.373		3.77

Water Temperature 71°F

Maximum reading was 0.209" from the wall.

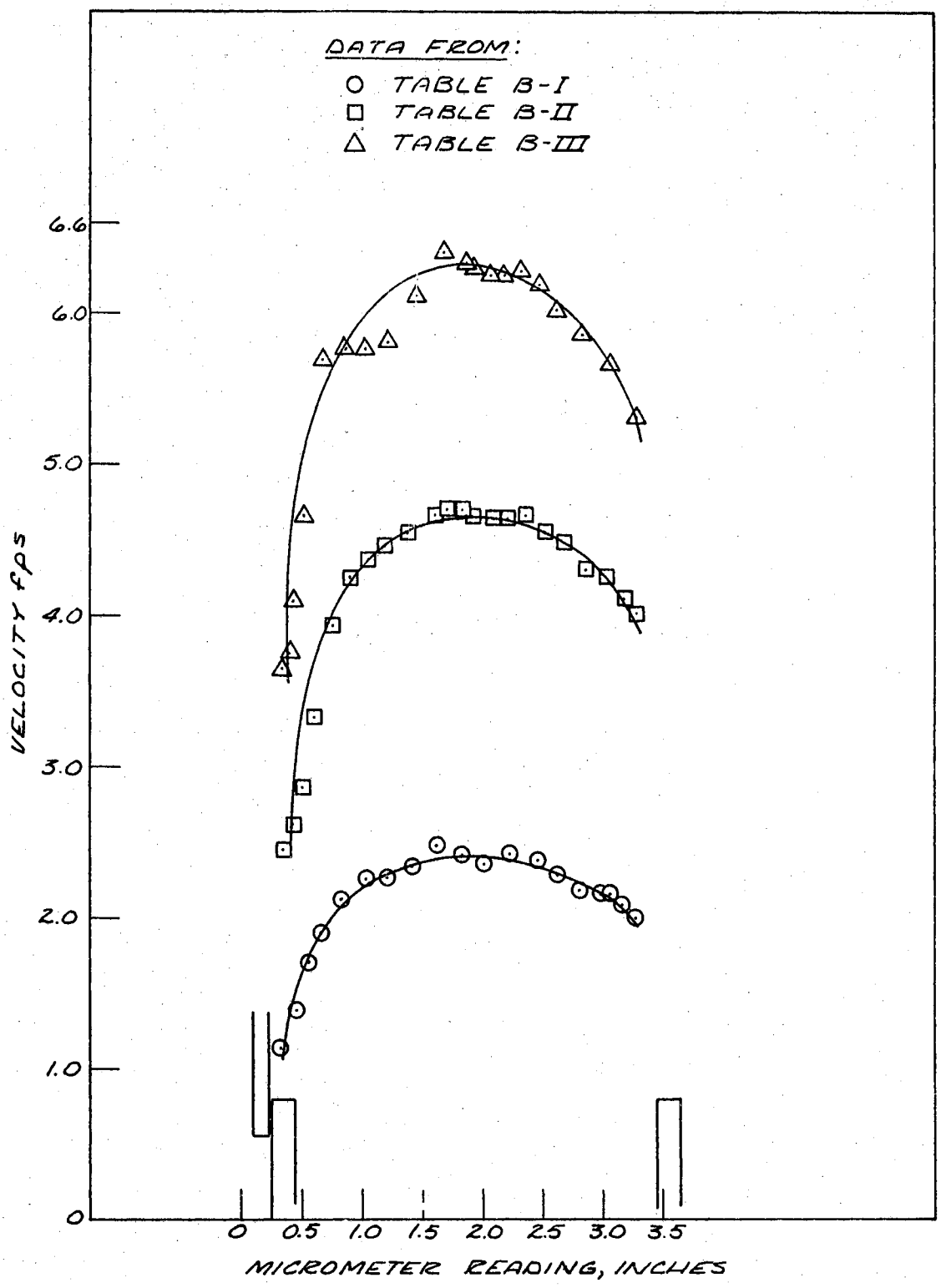

Figure B-1. Velocity Profile for Empty Channel

TABLE B-IV

VELOCITY PROFILE DATA

Date: October 20, 1964

Orifice Manometer: 10.9 in. Hg (110 gpm)

Pitot Tube: Normal to longitudinal axis at midpoint;
0.5" OD cylinder; 1.2" above centerline.

Point No.	Pitot tube Manometer Inches of water		Micrometer Reading inches	Notes	Velocity fps
	Left	Right			
1	-0.20	-3.10	3.266	Max.	3.94
2	-1.20	-3.18	3.116		4.05
3	-0.05	-3.25	3.005		4.15
4	0.05	-3.35	2.847		4.27
5	0.17	-3.47	2.723		4.41
6	0.20	-3.50	2.618		4.45
7	0.00	-3.30	2.509		4.21
8	-0.60	-2.75	2.423		3.40
9	-0.20	-3.13	2.464		3.96
10	-1.05	-2.30	2.384		2.59
11	-2.15	-1.35	2.303		-2.07
12	-2.95	-0.60	2.201		-3.56
13	-3.20	-0.35	2.106		-3.92
14	-3.15	-0.30	2.005		-3.92
15	-3.13	-0.35	1.905	Midpoint	-3.86
16	-3.15	-0.40	1.806		-3.84
17	-2.70	-0.80	1.707		-3.20
18	-1.60	-1.80	1.608		1.03
19	-0.35	-2.95	1.507		3.73
20	0.10	-3.40	1.406		4.33
21	0.10	-3.40	1.257		4.33
22	0.05	-3.30	1.103		4.24
23	-0.03	-3.23	0.936		4.15
24	-0.10	-3.15	0.749		4.04
25	-0.30	-3.00	0.607		3.81
26	-0.55	-2.65	0.451		3.36
27	-1.05	-2.30	0.314	Window	2.59

Water Temperature 73°F

Maximum reading was 0.204" from the wall.

TABLE B-V

VELOCITY PROFILE DATA

Date: June 22, 1965

Orifice Manometer: 10.9 in. Hg (112 gpm)

Pitot Tube: Normal to longitudinal axis at midpoint;
0.5" OD cylinder; 1.2" above centerline.

Point No.	Pitot tube Manometer Inches of water Left	Right	Micrometer Reading inches	Notes	Velocity fps
1	10.55	8.60	0.597	Window	3.24
2	11.05	8.10	0.782		3.98
3	11.30	7.80	1.000		4.34
4	11.35	7.80	1.208		4.36
5	11.90	7.80	1.417		4.69
6	11.45	7.78	1.635		4.44
7	10.80	8.55	1.809		2.59
8	9.45	10.10	1.989		-1.87
9	9.05	10.50	2.133		-2.79
10	9.00	10.65	2.217		-2.98
11	8.95	10.70	2.357		-3.06
12	9.45	10.20	2.524		-2.01
13	10.20	8.85	2.648		2.70
14	11.55	7.98	2.885		4.37
15	11.45	8.10	3.108		4.24
16	10.95	8.70	3.306		3.48
17	11.25	8.35	3.517		3.94
18	11.10	8.60	3.675	Max.	3.66

Water Temperature 70°F

Maximum reading was 0.078" from the wall.

TABLE B-VI

VELOCITY PROFILE DATA

Date: October 21, 1964

Orifice Manometer: 19.8 in. Hg (146 gpm)

Pitot Tube: Normal to longitudinal axis at midpoint; 0.5" OD cylinder; 1.2" above centerline.

Point No.	Pitot tube Manometer Inches of water Left	Right	Micrometer Reading inches	Notes	Velocity fps
1	0.0	-2.25	0.337	Window	3.47
2	0.30	-2.60	0.405		3.94
3	1.60	-3.90	0.706		5.43
4	1.95	-4.20	1.004		5.74
5	2.20	-4.45	1.202		5.97
6	1.20	-3.50	1.502		5.03
7	-1.55	-0.95	1.613		-1.80
8	-3.35	0.65	1.705		-4.62
9	-3.95	1.25	1.806		-5.29
10	-3.93	1.20	1.902		-5.22
11	-3.93	1.20	2.007		-5.25
12	-4.00	1.30	2.107		-5.32
13	-3.80	1.10	2.216		-5.12
14	-2.73	0.05	2.303		-3.86
15	-0.65	-1.85	2.402		2.54
16	1.20	-3.60	2.504		5.08
17	2.15	-4.48	2.708		5.96
18	1.90	-4.20	2.904		5.72
19	1.55	-3.85	3.115		5.37
20	1.40	-3.75	3.260		5.26
21	2.33	-4.60	3.355	Max.	6.10

Water Temperature 70°F

Maximum reading was 0.138" from the wall.

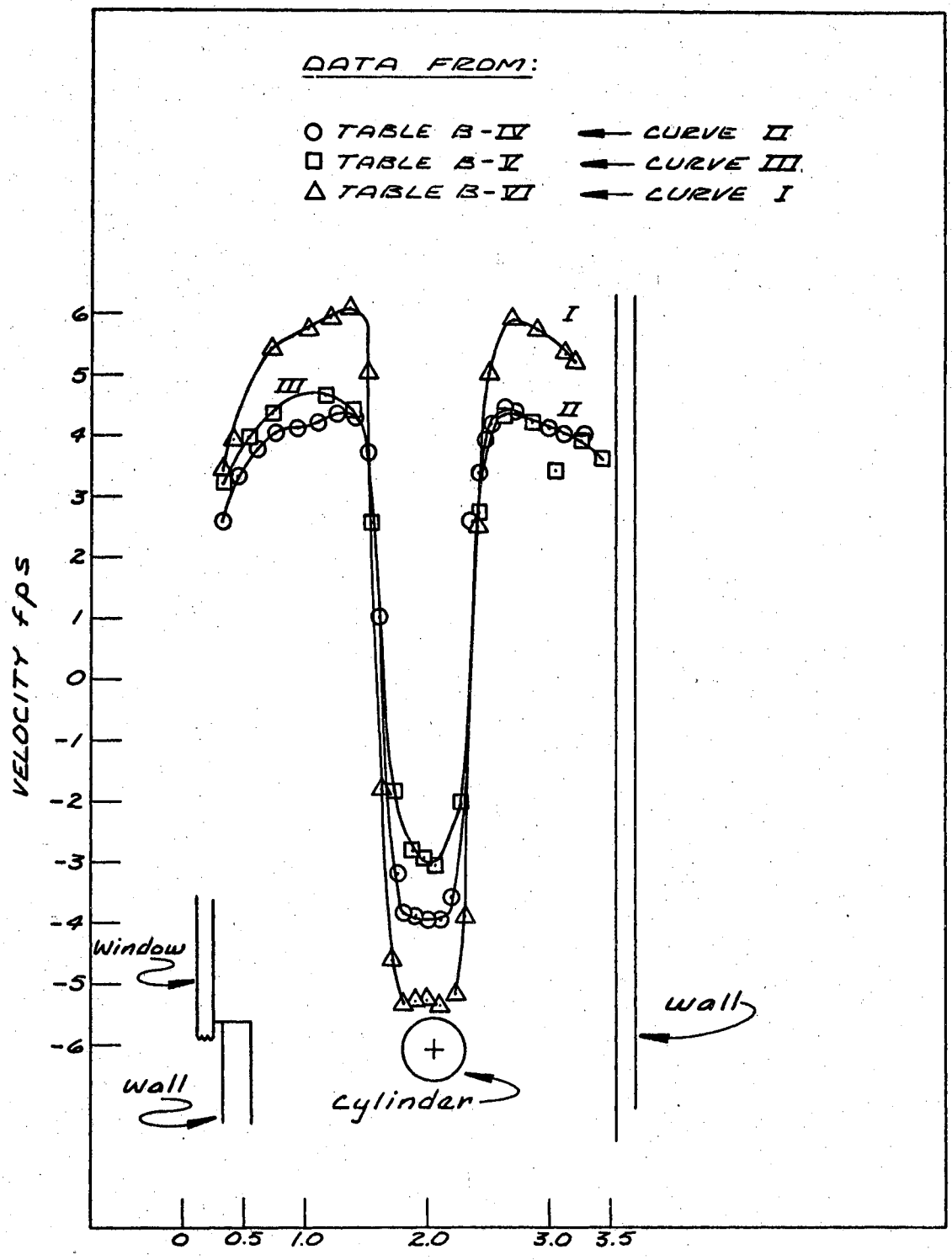

Figure B-2. Velocity Profile Normal to the Cylinder

TABLE B-VII

VELOCITY PROFILE DATA

Date: October 22, 1964

Orifice Manometer: 19.8 in. Hg (146 gpm)

Pitot Tube: Parallel to longitudinal axis;
0.5" OD cylinder; 1.2" above centerline.

Point No.	Pitot tube Manometer Inches of water Left	Right	Micrometer Reading inches	Notes	Velocity fps
1	0.50	-2.85	0.448	Window	4.24
2	0.90	-3.20	0.520		4.70
3	0.70	-3.05	0.653		4.49
4	-0.15	-2.20	0.799		3.32
5	-0.70	-1.70	0.949		2.32
6	-1.30	-1.15	1.102		-0.90
7	-1.80	-0.65	1.254		-2.48
8	-2.35	-0.20	1.402		-3.40
9	-2.80	0.25	1.552		-4.04
10	-3.45	0.80	1.703		-4.75
11	-3.55	0.90	1.851		-4.88
12	-3.50	0.85	2.043		-4.83
13	-3.60	0.95	2.253		-4.94
14	-3.50	0.85	2.455		-4.83
15	-3.50	0.85	2.651		-4.83
16	-3.50	0.85	2.854		-4.83
17	-3.50	0.85	3.053		-4.83
18	-3.30	0.80	3.278	Max.	-4.70

Water Temperature 71°F

Maximum reading was 0.326" from the wall.

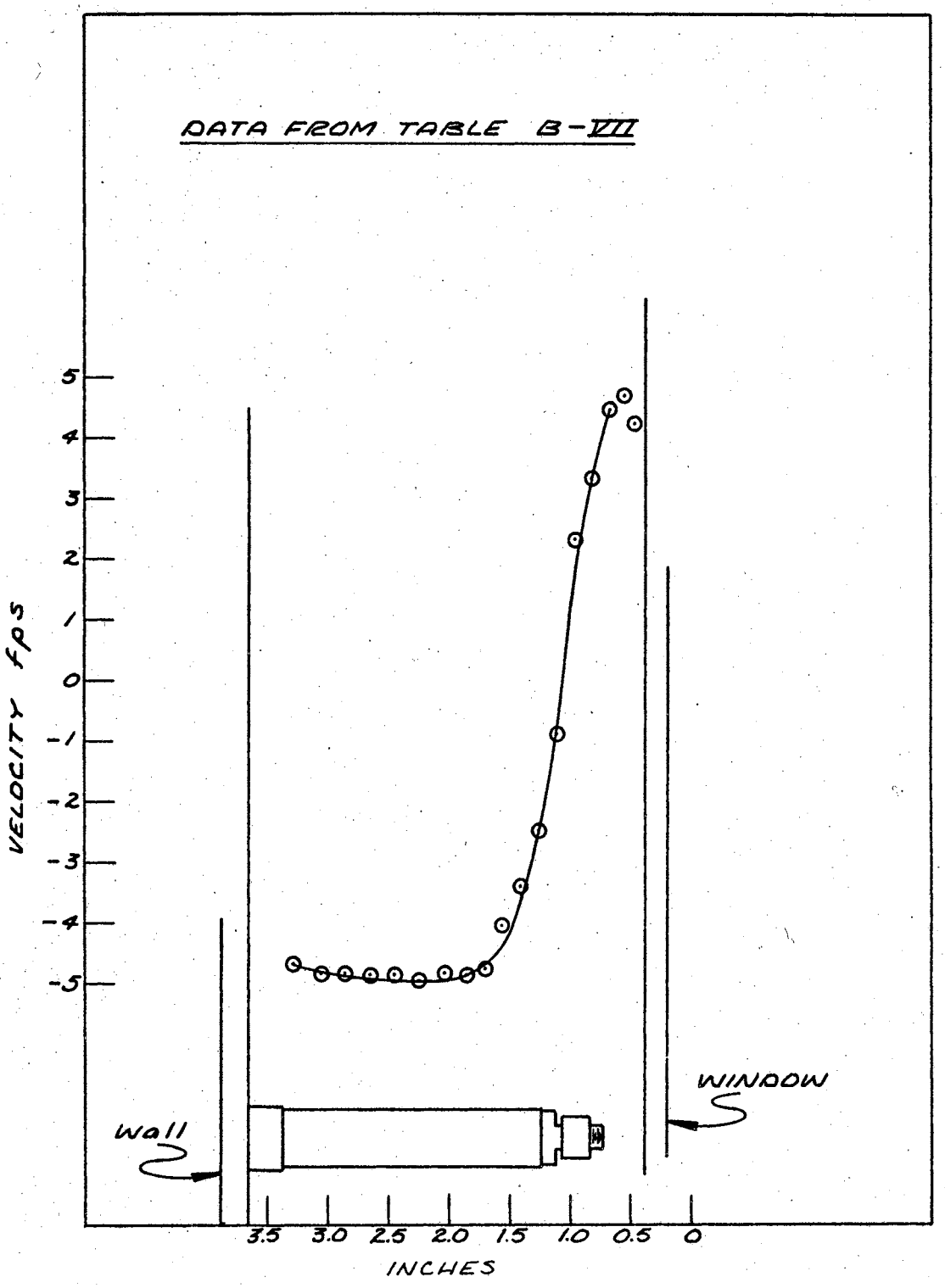

Figure B-3. Velocity Profile Parallel to the Cylinder

TABLE B-VIII

VELOCITY PROFILE DATA

Date: October 15, 1965

Orifice Manometer: 21.0 in. Hg (152 gpm)

Pitot Tube: Normal to longitudinal cylinder axis at midpoint; test section empty.

Point No.	Pitot tube Manometer Inches of water Left	Right	Micrometer Reading inches	Notes	Velocity fps
1	-5.95	-3.20	0.573	Window	3.84
2	6.90	2.20	0.816	T.C. No.8	5.03
3	7.95	1.10	1.026	1.437 mv	6.06
4	8.25	0.65	1.256		6.39
5	8.20	0.65	1.522		6.37
6	7.95	0.60	1.792		6.29
7	8.35	0.65	2.011		6.42
8	8.20	0.90	2.340		6.27
9	8.00	1.15	2.640		6.06
10	7.90	1.20	2.847		6.00
11	7.85	1.30	3.013		5.94
12	7.70	1.40	3.232	1.430 mv	5.82
13	1.55	1.60	3.433		5.65
14	6.85	2.45	3.641	Max.	4.86
Water Temperature 82.5°F Maximum reading was 0.088" from the wall.					
15	-5.30	-2.30	0.590	Window	3.34
16	-5.80	-1.85	0.734	T.C. No.8	4.70
17	6.85	1.00	0.912	5.182 mv	5.71
18	7.55	0.65	1.102		6.20
19	7.70	0.85	1.334		6.19
20	8.10	0.55	1.529		6.50
21	8.10	0.55	1.790		6.50
22	8.15	0.70	2.059		6.45
23	8.25	0.90	2.314		6.41
24	8.10	1.10	2.556	5.142 mv	6.25
25	8.10	1.30	2.753		6.16
26	8.15	1.35	2.942		6.16
27	8.20	1.40	3.117		6.16
28	8.30	1.50	3.298	5.137 mv	6.16
29	8.20	1.65	3.483		6.04
30	7.90	2.15	3.600		5.67
31	7.80	2.35	3.677	5.045 mv	5.51
Water Temperature 209.°F Maximum reading was 0.069" from the wall.					

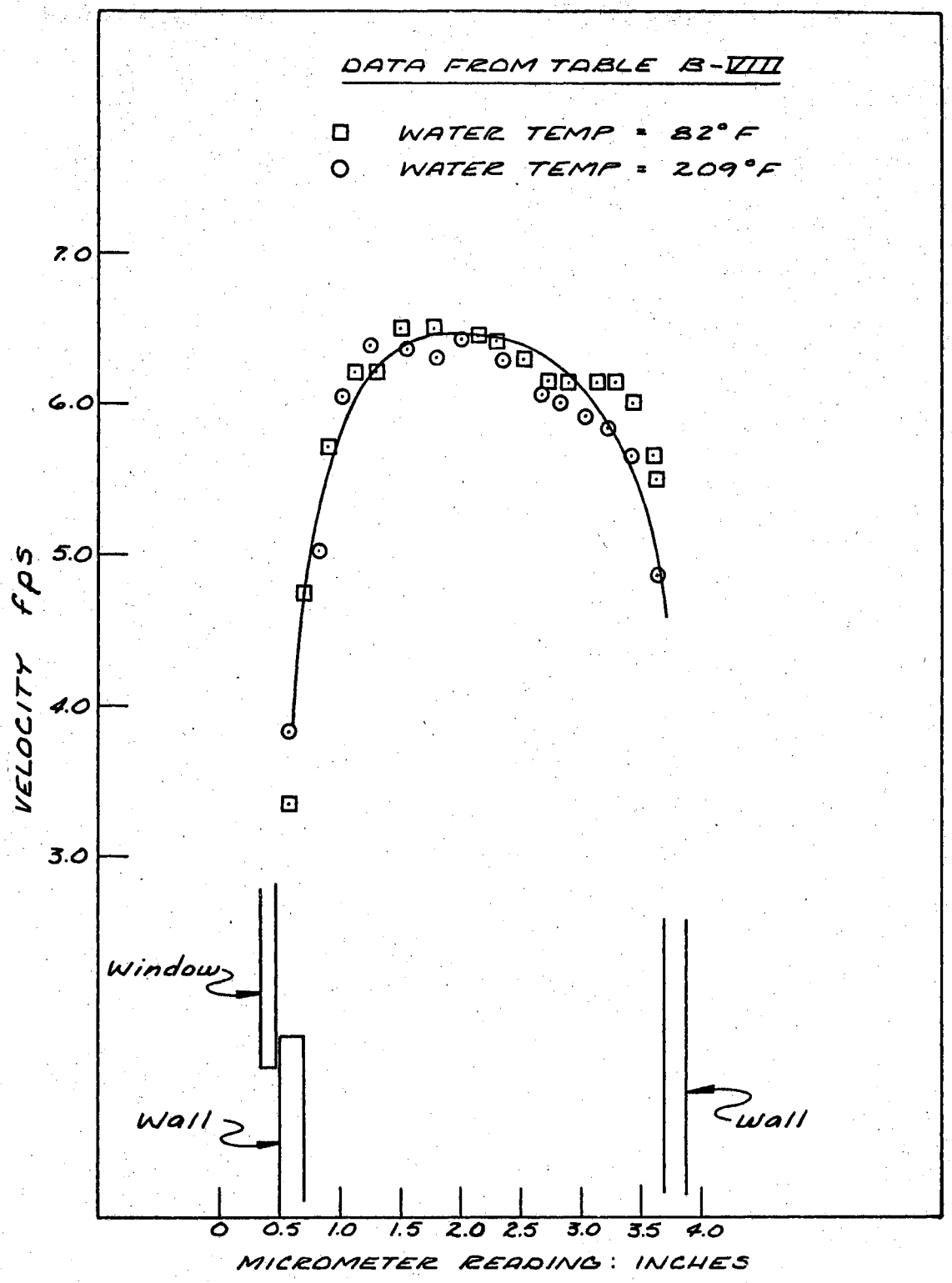

Figure B-4. Velocity Profile for Cold and Hot Water

APPENDIX C

BOILING HEAT TRANSFER DATA

INDEX

APPENDIX C

BOILING HEAT TRANSFER DATA

TABLE C - I

RUN NUMBER 43 DATE: MARCH 20, 1966

OUTSIDE DIAMETER	LENGTH	THICKNESS	FLOW RATE	THERMOCOUPLE POSITION
0.2497 in.	2.129 in.	0.0277 in.	00 gpm	NO.5 Cylinder Centerline

THERMOCOUPLE READING MV. NO.5	NO.7	POWER INPUT VOLTS	AMPS	TIME MIN.	OUTSIDE TEMPERATURE °F NO.5	BULK TEMP °F	FLUX
5.216	5.125	0.00	000	00	210	207	000
5.807	5.217	0.88	250	10	225	210	66,300
5.864	5.214	0.93	267	17	226	210	75,259
5.937	5.215	0.99	281	24	227	210	84,315
6.273	5.212	1.01	291	33	238	210	89,080
6.011	5.223	1.04	303	44	227	210	95,508
6.068	5.220	1.13	324	59	229	211	103,073
6.035	5.230	1.09	312	51	229	210	110,966
6.071	5.229	1.17	331	67	228	211	117,376
6.090	5.230	1.19	339	72	228	211	122,268
6.111	5.229	1.21	348	78	228	211	127,623
6.162	5.233	1.29	363	82	228	211	141,376
6.217	5.232	1.33	378	87	229	211	151,800

TABLE C - I (Continued)

THERMOCOUPLE READING MV. NO.5	NO.7	POWER VOLTS	INPUT AMPS	TIME MIN.	OUTSIDE TEMPERATURE °F NO.5	BULK TEMP °F	FLUX
6.273	5.236	1.41	398	92	229	211	169,482
6.357	5.241	1.47	417	98	230	211	185,789
6.737	5.241	1.53	438	106	241	211	202,446
6.808	5.242	1.59	451	111	241	211	217,340
6.964	5.242	1.65	467	119	244	211	233,543
6.979	5.249	1.71	488	124	243	211	253,658
7.084	5.241	1.78	508	129	244	211	274,062
7.180	5.243	1.84	524	133	245	211	291,429
7.465	5.241	1.90	540	136	252	211	310,148

Maximum on number one terminal: No burnout, off at 141 minutes.

Water purity at 80°F: Dissolved oxygen 3.0 ppm: Conductivity 109 micromhos/cm.

TABLE C - II

RUN NUMBER 44 DATE: MARCH 21, 1966

OUTSIDE DIAMETER	LENGTH	THICKNESS	FLOW RATE	THERMOCOUPLE POSITION
0.2497 in.	2.129 in.	0.0277 in.	00 gpm	No.5 Cylinder Centerline

THERMOCOUPLE READING MV. NO.5	NO.7	POWER INPUT VOLTS	AMPS	TIME MIN.	OUTSIDE TEMPERATURE °F NO.5	BULK TEMP °F	FLUX
5.221	5.130	0.00	000	00	210	207	000
6.557	5.235	1.205	348	22	243	211	127,096
6.694	5.264	1.315	380	37	245	212	151,452
6.790	5.269	1.390	399	45	246	212	168,094
6.850	5.271	1.480	421	54	246	212	188,847
6.985	5.254	1.560	451	66	247	211	213,239
7.129	5.250	1.660	480	74	249	211	241,500
7.285	5.252	1.710	502	82	252	211	260,175
7.411	5.248	1.780	524	90	254	211	282,700
7.581	5.255	1.883	550	96	256	211	313,900
7.720	5.252	1.960	572	101	257	211	339,800
Burnout		2.03	598	103			350,000

Water purity at 80°F: Dissolved oxygen 3.0 ppm: Conductivity 123 micromhos/cm.

TABLE C-III

RUN NUMBER 18 DATE: OCTOBER 20, 1965

OUTSIDE DIAMETER	LENGTH	THICKNESS	FLOW RATE	THERMOCOUPLE POSITION
.2490 in.	2.102 in.	.0277 in.	96.0 gpm	NO.5 Cylinder Centerline

THERMOCOUPLE READING MV. NO.5	NO.7	POWER INPUT VOLTS	AMPS	TIME MIN.	OUTSIDE TEMPERATURE °F NO.5	BULK TEMP °F	FLUX
5.070	5.051	0.00	000	00	205	205	000
6.196	5.150	1.09	279	9	233	208	90,502
6.320	5.186	1.16	300	11	236	209	103,564
6.642	5.212	1.29	332	16	244	210	127,455
6.809	5.252	1.39	359	19	247	211	148,504
6.939	5.286	1.45	372	23	250	212	160,524
7.112	5.323	1.51	394	29	253	214	177,053
7.330	5.365	1.64	425	35	257	215	207,426
7.510	5.366	1.72	450	39	261	215	230,341
7.637	5.534	1.81	475	47	262	221	255,860
7.975	5.323	1.95	510	52	268	214	295,961
8.119	5.322	2.02	533	58	270	214	320,411
7.864	5.340	1.96	511	61	265	214	298,062
8.165	5.320	2.01	532	66	272	214	318,227
8.460	5.295	2.23	584	70	274	213	387,567
8.622	5.272	2.32	612	73	275	212	422,541

TABLE C - III (Continued)

THERMOCOUPLE READING MV. NO.5	NO.7	POWER VOLTS	INPUT AMPS	TIME MIN.	OUTSIDE TEMPERATURE °F NO.5	BULK TEMP °F	FLUX
8.762	5.267	2.41	634	78	276	212	454,711
9.026	5.265	2.53	670	82	280	212	504,458
9.194	5.270	2.66	698	88	280	212	552,543
9.378	5.266	2.75	721	90	281	212	590,062
9.451	5.262	2.79	730	94	282	212	606,117
9.602	5.270	2.83	750	97	284	212	631,651
Burnout			770	98			673,000

Water purity at 80°F: Dissolved oxygen 2.6 ppm: Conductivity 98 micromhos/cm.

TABLE C - IV

RUN NUMBER 16 DATE: SEPTEMBER 14, 1965

OUTSIDE DIAMETER	LENGTH	THICKNESS	FLOW RATE	THERMOCOUPLE POSITION
.2490 in.	2.102 in.	.0277 in.	152.6 gpm	No.5 Cylinder Centerline

THERMOCOUPLE READING MV.		POWER INPUT		TIME	OUTSIDE TEMPERATURE °F	BULK $_{C}$TEMP	FLUX
NO.5	NO.7	VOLTS	AMPS	MIN.	NO.5	°F	
5.161	5.090	0.00	000	00	208	206	000
5.602	5.127	0.99	268	19	214	207	81,513
6.060	5.151	1.43	402	39	219	208	176,611
6.805	5.172	1.40	398	50	244	209	171,186
7.220	5.140	1.51	430	55	254	208	199,481
7.218	5.112	1.50	428	58	255	207	197,238
7.478	5.112	1.59	450	65	261	207	219,819
7.824	5.111	1.74	492	75	267	207	263,009
8.081	5.110	1.86	524	82	272	207	299,434
8.165	5.105	1.90	535	93	273	207	312,294
8.386	5.105	2.00	560	97	277	207	344,092
8.511	5.105	2.08	580	100	278	207	370,636
8.663	5.104	2.14	599	105	280	207	393,819
8.949	5.105	2.28	638	111	284	207	446,902
9.146	5.106	2.38	666	116	285	207	486,976
9.335	5.107	2.48	690	122	287	207	525,723

TABLE C - IV (Continued)

THERMOCOUPLE READING MV. NO.5	NO.7	POWER VOLTS	INPUT AMPS	TIME MIN.	OUTSIDE TEMPERATURE °F NO.5	BULK TEMP °F	FLUX
9.575	5.109	2.56	713	136	291	207	560,771
9.425	5.111	2.47	688	145	291	207	522,086
9.656	5.120	2.59	719	147	293	207	572,117
9.770	5.154	2.63	730	149	294	208	589,841
9.906	5.160	2.70	748	154	295	208	620,471
10.054	5.169	2.78	769	165	296	209	656,792

Water purity at 80°F: Dissolved oxygen 2.0 ppm: Conductivity 118 micromhos/cm.

Note: No burnout.

TABLE C - V

RUN NUMBER 17 DATE: SEPTEMBER 27, 1965

OUTSIDE DIAMETER	LENGTH	THICKNESS	FLOW RATE	THERMOCOUPLE POSITION
.2495 in.	2.170 in.	.0277 in.	152.6 gpm	No.5 Cylinder Centerline

THERMOCOUPLE READING MV. NO.5	NO.7	POWER INPUT VOLTS	AMPS	TIME MIN.	OUTSIDE TEMPERATURE °F NO.5	BULK TEMP °F	FLUX
5.130	5.127	0.00	000	00	207	207	000
8.555	5.107	2.09	593	11	279	207	368,833
8.696	5.107	2.12	598	16	283	207	377,282
9.118	5.397	2.33	659	20	288	216	456,952
9.326	5.098	2.45	685	24	290	206	499,443
9.739	5.099	2.64	739	26	294	206	580,601
9.962	5.099	2.75	758	28	297	206	620,342
10.309	5.100	2.91	809	31	300	206	700,601
10.460	5.105	2.99	823	33	301	207	732,319
10.651	5.112	3.07	842	37	303	207	769,272
10.887	5.115	3.17	870	40	305	207	820,744
11.082	5.117	3.28	890	43	306	207	868,747
11.300	5.120	3.35	912	45	309	207	909,220
Burnout			950	47			990,000

Water purity at 80°F: Dissolved oxygen 2.4 ppm: Conductivity 96 micromhos/cm.

TABLE C - VI

RUN NUMBER 36 DATE: MARCH 15, 1966

OUTSIDE DIAMETER	LENGTH	THICKNESS	FLOW RATE	THERMOCOUPLE POSITION FROM F.S.P.
.3370 in.	2.093 in.	.0155 in.	000 gpm	No.2 270°, No.3 0°, No.4 180°, No.5 90°

THERMOCOUPLE READING MV.					POWER INPUT		TIME	OUTSIDE TEMPERATURE °F				BULK TEMP °F	FLUX
NO.2	NO.3	NO.4	NO.5	NO.7	VOLTS	AMPS	MIN.	NO.2	NO.3	NO.4	NO.5		
5.231	5.195	5.228	5.235	5.248	0.00	000	00	211	210	211	211	211	000
6.159	6.094	6.163	6.162	5.257	1.07	250	10	237	237	237	237	212	61,106
6.284	6.176	6.196	6.231	5.260	1.19	279	18	240	239	237	238	212	75,842
6.364	6.252	6.351	6.291	5.259	1.28	300	26	242	240	241	239	212	87,719
6.479	6.296	6.423	6.357	5.255	1.35	322	32	245	241	243	241	212	99,300
6.534	6.346	6.388	6.410	5.252	1.42	340	40	246	242	241	242	211	110,288
6.620	6.401	6.431	6.465	5.254	1.51	363	47	248	243	241	243	211	125,211
6.675	6.460	6.515	6.527	5.250	1.60	380	54	249	244	243	244	211	138,888
6.709	6.552	6.605	6.611	5.247	1.70	408	61	249	246	245	245	211	158,442
6.896	6.657	6.751	6.720	5.249	1.80	433	68	253	248	248	248	211	178,041
6.868	6.754	6.895	6.731	5.270	1.83	450	77	252	250	252	247	212	188,115
6.956	6.875	7.009	6.852	5.280	1.88	460	85	254	254	256	251	212	197,550
7.092	7.040	7.110	7.010	5.287	2.00	503	92	256	257	257	254	213	229,804
Burnout					2.14	533	93						245,000

Water purity at 80°F: Dissolved Oxygen 1.9 ppm: Conductivity 126 micromhos/cm.

TABLE C - VII

RUN NUMBER 8 DATE: DECEMBER 22, 1964

OUTSIDE DIAMETER	LENGTH	THICKNESS	FLOW RATE	THERMOCOUPLE POSITION FROM F.S.P.
.3410 in.	2.100 in.	.0180 in.	96.5 gpm	No.2 270°, No.3 180°, No.4 90°, No.5 0°

THERMOCOUPLE READING MV.					POWER INPUT		TIME	OUTSIDE TEMPERATURE °F				BULK TEMP	FLUX
No.2	NO.3	NO.4	NO.5	NO.7	VOLTS	AMPS	MIN.	NO.2	NO.3	NO.4	NO.5	°F	
5.210	5.215	5.215	5.215	5.190	0.00	000	00	210	210	210	210	209	000
6.370	6.400	6.250	6.410	5.160	1.50	312	14	241	242	237	243	208	105,301
6.740	6.760	6.700	6.780	5.160	1.88	399	21	249	249	247	250	208	168,778
6.950	6.970	6.960	6.990	5.165	2.08	441	28	253	253	253	254	209	206,390
7.210	7.230	7.285	7.200	5.165	2.31	495	34	257	258	260	257	209	257,278
7.400	7.410	7.495	7.370	5.165	2.55	552	40	259	259	262	258	209	316,713
7.550	7.550	7.660	7.510	5.160	2.74	600	45	260	260	264	259	208	369,903
7.670	7.680	7.780	7.640	5.155	2.92	640	50	260	260	264	259	208	420,483
7.410	7.420	7.485	7.385	5.157	2.54	554	58	259	260	262	259	208	316,614
7.240	7.270	7.300	7.250	5.150	2.32	502	63	258	259	260	258	208	262,046
7.010	7.040	7.005	7.030	5.150	2.11	453	68	254	255	254	255	208	215,063
6.710	6.730	6.670	6.730	5.140	1.89	402	73	247	248	246	248	208	170,952
6.480	6.510	6.350	6.510	5.130	1.62	345	78	243	244	239	244	207	125,365
6.340	6.380	6.210	6.360	5.120	1.50	320	84	240	241	236	241	207	108,001

Water purity at 80°F: Dissolved oxygen NA ppm: Conductivity NA micromhos/cm.

TABLE C - VIII

RUN NUMBER 48 DATE: APRIL 2, 1966

OUTSIDE DIAMETER	LENGTH	THICKNESS	FLOW RATE	THERMOCOUPLE POSITION FROM F.S.P.
.3371 in.	2.075 in.	.0150 in.	96.5 gpm	No.2 270°, No.3 0°, No.4 180°, No.5 90°

THERMOCOUPLE READING MV.					POWER INPUT		TIME	OUTSIDE TEMPERATURE °F				BULK TEMP °F	FLUX
NO.2	NO.3	NO.4	NO.5	NO.7	VOLTS	AMPS	MIN.	NO.2	NO.3	NO.4	NO.5		
5.146	5.040	5.148	5.149	5.146	0.00	000	00	208	204	208	208	208	000
6.248	5.962	6.210	6.307	5.146	1.32	276	15	239	226	238	241	208	83,920
6.401	6.113	6.326	6.362	5.131	1.47	309	21	243	230	240	241	207	104,631
6.575	6.324	6.448	6.429	5.127	1.64	348	29	246	235	242	242	207	131,464
Burnout, red glow					1.90	381	30						166,500

Water purity at 80°F: Dissolved oxygen 2.8 ppm: Conductivity 110 micromhos/cm.

TABLE C - IX

RUN NUMBER 50 DATE: APRIL 6, 1966

OUTSIDE DIAMETER	LENGTH	THICKNESS	FLOW RATE	THERMOCOUPLE POSITION FROM F.S.P.
.3371 in.	2.075 in.	.0150 in.	96.5 gpm	No.2 0°, No.3 90°, No.4 270°, No.5 180°

THERMOCOUPLE READING MV.					POWER INPUT		TIME	OUTSIDE TEMPERATURE °F				BULK TEMP	FLUX
NO.2	NO.3	NO.4	NO.5	NO.7	VOLTS	AMPS	MIN.	NO.2	NO.3	NO.4	NO.5	°F	
5.146	5.040	5.148	5.149	5.146	0.00	000	00	208	204	208	208	208	000
5.966	6.274	6.375	6.160	5.171	1.22	280	24	230	237	243	236	209	78,687
6.165	6.362	6.507	6.326	5.222	1.37	311	34	235	238	247	241	210	98,144
6.413	6.470	6.725	6.547	5.230	1.53	351	44	242	240	252	246	211	123,703
6.544	6.592	6.819	6.692	5.237	1.63	371	52	245	243	254	250	211	139,298
6.683	6.700	6.949	6.768	5.235	1.78	393	62	248	245	257	251	211	161,137
6.865	6.800	7.066	6.842	5.220	1.90	420	69	253	247	259	252	210	183,817
6.973	6.983	7.227	6.919	5.225	2.07	450	78	254	251	263	253	211	214,568
7.059	7.000	7.263	6.973	5.223	2.15	471	87	256	251	263	253	210	233,261
7.102	7.049	7.313	7.032	5.225	2.25	492	92	256	251	263	254	211	254,994
7.176	7.110	7.431	7.092	5.224	2.34	518	98	257	251	265	254	210	279,208
7.216	7.131	7.476	7.130	5.220	2.39	529	105	257	251	266	255	210	291,230
Burnout					2.55	568	108						321,000

Water purity at 80°F: Dissolved oxygen 2.7 ppm: Conductivity 127 micromhos/cm.

TABLE C - X

RUN NUMBER 9 DATE: JANUARY 4, 1965

OUTSIDE DIAMETER	LENGTH	THICKNESS	FLOW RATE	THERMOCOUPLE POSITION FROM F.S.P.
.3410 in.	2.100 in.	.0180 in.	151.0 gpm	No.2 270°, No.3 180°, No.4 90°, No.5 0°

THERMOCOUPLE READING MV.					POWER INPUT		TIME	OUTSIDE TEMPERATURE °F				BULK TEMP	FLUX
NO.2	NO.3	NO.4	NO.5	NO.7	VOLTS	AMPS	MIN.	NO.2	NO.3	NO.4	NO.5	°F	
5.210	5.215	5.215	5.215	5.190	0.00	000	00	210	210	210	210	209	000
6.120	6.150	6.060	6.120	5.200	1.56	320	3	232	234	231	233	210	112,321
6.660	6.680	6.600	6.670	5.200	2.06	430	6	244	244	242	244	210	199,307
7.180	7.200	7.150	7.230	5.200	2.46	520	15	254	255	253	256	210	287,822
7.580	7.590	7.575	7.610	5.170	2.72	579	20	262	262	262	263	209	354,351
7.890	7.930	7.970	7.880	5.170	3.00	631	23	267	268	270	267	209	425,928
7.275	7.310	7.250	7.325	5.160	2.51	536	27	256	257	255	258	208	302,708
6.710	6.760	6.695	6.720	5.160	2.15	459	31	243	245	243	244	208	222,043
6.310	6.330	6.240	6.320	5.150	1.75	372	34	236	237	234	237	208	146,895
5.930	5.940	5.890	5.950	5.140	1.40	290	38	228	228	227	229	208	91,351

Water purity at 80°F: Dissolved oxygen NA ppm: Conductivity NA micromhos/cm.

TABLE C - XI

RUN NUMBER 54 DATE: APRIL 16, 1966

OUTSIDE DIAMETER	LENGTH	THICKNESS	FLOW RATE	THERMOCOUPLE POSITION FROM F.S.P.
.3380 in.	2.0850 in.	.01508 in.	152.6 gpm	No.2 180°, No.3 0°, No.4 90°, No.5 270°

THERMOCOUPLE READING MV.					POWER INPUT		TIME	OUTSIDE TEMPERATURE °F				BULK TEMP	FLUX
NO.2	NO.3	NO.4	NO.5	NO.7	VOLTS	AMPS	MIN.	NO.2	NO.3	NO.4	NO.5	°F	
5.047	5.040	5.040	5.048	5.036	0.00	000	00	205	204	204	205	205	000
5.935	5.842	5.946	6.057	5.197	1.16	291	13	229	226	229	237	210	76,844
6.092	5.994	6.144	6.240	5.222	1.25	318	20	234	230	235	242	210	90,881
6.173	6.132	6.193	6.317	5.223	1.38	350	26	235	233	235	243	210	110,829
6.571	6.330	6.404	6.549	5.225	1.52	382	33	247	239	241	249	211	132,753
6.810	6.570	6.618	6.787	5.230	1.68	421	40	253	245	246	255	211	162,188
6.936	6.773	6.773	6.975	5.231	1.82	455	46	255	250	250	260	211	188,810
7.003	6.917	6.873	7.080	5.231	1.90	476	51	256	253	252	262	211	206,775
7.096	7.100	6.992	7.229	5.233	2.00	503	57	258	258	254	265	211	230,579
7.183	7.305	7.119	7.409	5.231	2.12	532	64	259	263	256	270	211	257,860
7.270	7.528	7.247	7.577	5.233	2.24	559	70	260	268	259	273	211	286,284
7.361	7.724	7.367	7.732	5.235	2.34	583	76	261	273	261	277	211	311,904
7.098	7.075	7.030	7.327	5.235	2.00	500	86	258	257	255	269	211	228,632
7.287	7.514	7.276	7.648	5.239	2.22	554	94	261	268	260	276	211	281,823

TABLE C - XI (Continued)

THERMOCOUPLE READING MV.					POWER INPUT		TIME	OUTSIDE TEMPERATURE °F				BULK TEMP °F	FLUX
NO.2	NO.3	NO.4	NO.5	NO.7	VOLTS	AMPS	MIN.	NO.2	NO.3	NO.4	NO.5		
7.442	7.831	7.472	7.850	5.238	2.42	600	99	263	275	263	279	211	331,288
7.537	7.914	7.526	7.968	5.239	2.51	628	106	264	276	263	281	211	360,388
7.677	8.081	7.726	8.120	5.239	2.68	663	112	266	279	267	283	211	405,484
7.785	8.205	7.837	8.214	5.242	2.79	692	118	267	280	268	284	211	441,415
7.902	8.309	7.978	8.383	5.239	2.94	727	126	268	281	270	287	211	489,504
8.017	8.426	8.108	8.515	5.241	3.06	758	131	269	282	271	288	211	530,307
8.120	8.503	8.200	8.612	5.244	3.18	779	137	270	282	272	289	211	566,372
8.217	8.581	8.284	8.710	5.244	3.25	798	142	271	283	273	291	211	592,957
8.292	8.640	8.361	8.800	5.242	3.32	816	147	272	283	274	292	211	619,391
Burnout					3.51	852	149						664,000

Water purity at 80°F: Dissolved Oxygen 2.0 ppm: Conductivity 104 micromhos/cm.

TABLE C - XII

RUN NUMBER 37 DATE: MARCH 16, 1966

OUTSIDE DIAMETER	LENGTH	THICKNESS	FLOW RATE	THERMOCOUPLE POSITION FROM F.S.P.
.4570 in.	2.100 in.	.01203 in.	000 gpm	No.2 270°, No.3 90°, No.4 0°, No.5 180°

THERMOCOUPLE READING MV.					POWER INPUT		TIME	OUTSIDE TEMPERATURE °F				BULK TEMP	FLUX
NO.2	NO.3	NO.4	NO.5	NO.7	VOLTS	AMPS	MIN.	NO.2	NO.3	NO.4	NO.5	°F	
5.202	5.201	5.218	5.218	5.230	0.00	000	00	210	210	210	210	211	000
5.925	5.881	5.949	5.997	5.242	1.08	250	14	230	229	232	233	211	45,330
6.046	5.974	6.012	6.014	5.283	1.20	283	32	234	231	233	233	212	57,015
6.106	6.070	6.052	6.089	5.282	1.30	316	40	235	234	234	235	212	68,969
6.183	6.137	6.115	6.181	5.284	1.39	344	50	237	235	235	237	212	80,278
6.242	6.188	6.190	6.219	5.287	1.48	368	57	238	237	237	238	213	91,439
6.277	6.232	6.209	6.275	5.284	1.58	389	65	239	237	237	239	212	103,188
6.356	6.279	6.265	6.344	5.289	1.65	411	73	241	238	238	241	213	113,854
6.406	6.324	6.338	6.375	5.283	1.73	432	81	242	239	240	242	212	125,474
6.471	6.382	6.400	6.425	5.285	1.82	458	88	243	240	242	242	213	139,946
6.525	6.423	6.454	6.463	5.289	1.91	478	95	244	241	243	243	213	153,280
6.541	6.467	6.489	6.502	5.293	2.01	499	102	244	242	243	243	213	168,392
6.594	6.516	6.561	6.562	5.295	2.11	521	108	245	243	245	245	213	184,563
6.684	6.585	6.657	6.624	5.300	2.21	542	115	247	244	247	246	213	201,102
Burnout						560	116						219,000

Water purity at 80°F: Dissolved oxygen 1.8 ppm: Conductivity 114 micromhos/cm.

TABLE C - XIII

RUN NUMBER 30 DATE: FEBRUARY 11, 1966

OUTSIDE DIAMETER	LENGTH	THICKNESS	FLOW RATE	THERMOCOUPLE POSITION FROM F.S.P.
.4479 in.	2.200 in.	.00765 in.	96.0 gpm	No.2 270°, No.3 90°, No.4 180°, No.5 0°

THERMOCOUPLE READING MV.					POWER INPUT		TIME	OUTSIDE TEMPERATURE °F				BULK TEMP	FLUX
NO.2	NO.3	NO.4	NO.5	NO.7	VOLTS	AMPS	MIN.	NO.2	NO.3	NO.4	NO.5	°F	
4.991	4.994	4.989	5.101	4.987	0.00	000	00	206	206	206	206	206	000
6.330	6.245	6.364	6.158	5.114	2.19	304	16	244	241	245	238	207	108,861
6.580	6.490	6.552	6.434	5.140	2.52	352	26	251	248	250	246	208	145,044
6.695	6.624	6.632	6.580	5.139	2.71	382	38	254	251	251	250	208	169,273
Run terminated due to poor connection							39						

Water purity at 80°F: Dissolved oxygen 2.9 ppm: Conductivity 106 micromhos/cm.

TABLE C - XIV

RUN NUMBER 31 DATE: FEBRUARY 18, 1966

OUTSIDE DIAMETER	LENGTH	THICKNESS	FLOW RATE	THERMOCOUPLE POSITION FROM F.S.P.
.4550 in.	2.2125 in.	.01160 in.	96.0 gpm	No.2 270°, No.3 90°, No.4 180°, No.5 0°

THERMOCOUPLE READING MV.					POWER INPUT		TIME	OUTSIDE TEMPERATURE °F				BULK TEMP	FLUX
NO.2	NO.3	NO.4	NO.5	NO.7	VOLTS	AMPS	MIN.	NO.2	NO.3	NO.4	NO.5	°F	
5.148	5.143	5.144	5.149	5.140	0.00	000	00	208	208	208	208	208	000
6.151	6.030	6.154	5.932	5.130	1.50	314	13	238	233	238	230	207	75,385
6.291	6.182	6.300	6.064	5.140	1.62	340	22	242	238	242	234	208	88,157
6.428	6.324	6.442	6.232	5.152	1.79	378	32	245	241	245	239	208	108,295
6.544	6.430	6.539	6.403	5.153	1.90	408	40	248	244	248	243	208	124,073
6.649	6.530	6.617	6.547	5.158	2.02	433	49	251	247	250	247	208	139,992
6.732	6.601	6.676	6.701	5.161	2.16	461	59	252	248	250	251	208	159,375
7.344	7.038	7.205	7.231	5.145	2.28	489	66	272	261	267	268	208	178,838
Burnout at above power setting													178,838

Water purity at 80°F: Dissolved oxygen 2.3 ppm: Conductivity 125 micromhos/cm.

TABLE C - XV

RUN NUMBER 32 DATE: FEBRUARY 22, 1966

OUTSIDE DIAMETER	LENGTH	THICKNESS	FLOW RATE	THERMOCOUPLE POSITION FROM F.S.P.
.4500 in.	2.088 in.	.0088 in.	96.0 gpm	No.2 270°, No.3 90°, No.4 180°, No.5 0°

THERMOCOUPLE READING MV.					POWER INPUT		TIME	OUTSIDE TEMPERATURE °F				BULK TEMP	FLUX
NO.2	NO.3	NO.4	NO.5	NO.7	VOLTS	AMPS	MIN.	NO.2	NO.3	NO.4	NO.5	°F	
4.941	4.940	4.940	4.952	4.910	0.00	000	00	201	201	201	201	200	000
6.179	6.049	6.172	6.031	5.122	1.61	292	22	239	235	239	234	207	80,617
6.348	6.217	6.351	6.232	5.159	1.78	321	35	244	240	244	240	208	97,981
6.477	6.355	6.474	6.579	5.182	1.90	348	62	248	244	248	251	209	113,383
6.557	6.447	6.543	6.515	5.185	2.04	371	70	250	246	249	248	209	129,784
6.650	6.546	6.604	6.661	5.176	2.21	400	79	252	248	250	252	209	151,589
6.720	6.601	6.642	6.744	5.172	2.33	422	89	254	250	251	254	209	168,611
6.805	6.698	6.700	6.875	5.170	2.50	453	100	255	252	252	258	209	194,203
6.917	6.789	6.758	7.000	5.170	2.68	483	109	258	254	253	261	209	221,972
6.991	6.850	6.804	7.090	5.172	2.81	508	116	260	255	253	263	209	244,786
7.076	6.922	6.855	7.181	5.168	3.00	534	124	261	256	254	265	209	274,713
Burnout						562	126						294,000

Water purity at 80°F: Dissolved oxygen 3.0 ppm: Conductivity 129 micromhos/cm.

TABLE C - XVI

RUN NUMBER 15 DATE: JULY 26, 1965

OUTSIDE DIAMETER	LENGTH	THICKNESS	FLOW RATE	THERMOCOUPLE POSITION FROM F.S.P.
.4587 in.	2.130 in.	.01198 in.	152.6 gpm	No.2 0°, No.3 90°, No.4 270°, No.5 180°

THERMOCOUPLE READING MV.					POWER INPUT		TIME	OUTSIDE TEMPERATURE °F				BULK TEMP	FLUX
NO.2	NO.3	NO.4	NO.5	NO.7	VOLTS	AMPS	MIN.	NO.2	NO.3	NO.4	NO.5	°F	
5.212	5.207	5.224	5.242	5.174	0.00	000	00	210	210	210	211	209	000
6.661	6.826	6.704	6.706	5.188	2.01	442	58	250	255	252	253	209	146,511
7.228	7.249	7.183	7.403	5.194	2.35	529	67	265	266	264	272	209	205,010
7.638	7.515	7.504	7.715	5.193	2.58	590	71	276	272	272	279	209	251,029
8.020	7.794	7.776	7.801	5.192	2.81	648	83	285	278	278	279	209	300,284
8.334	8.320	8.005	7.844	5.191	3.04	708	90	292	292	282	277	209	354,943
7.978	7.767	7.773	7.654	5.190	2.81	648	98	284	277	278	274	209	300,284
7.714	7.597	7.586	7.495	5.195	2.62	602	105	278	274	274	272	210	260,105
7.084	7.274	7.096	7.060	5.200	2.25	510	115	261	267	262	262	210	189,236
7.394	7.480	7.392	7.334	5.202	2.46	550	131	270	272	270	269	210	223,125
8.089	7.897	7.952	7.580	5.203	2.83	650	138	287	281	283	272	210	303,355
8.496	8.191	8.226	8.026	5.204	3.08	710	145	297	287	289	283	210	360,629
8.731	8.390	8.467	8.217	5.206	3.28	757	150	302	291	294	286	210	409,469
8.879	8.634	8.593	8.376	5.207	3.51	809	155	303	295	294	288	210	468,281
Burnout						850							

Water purity at 80°F: Dissolved oxygen 2.0 ppm: Conductivity 112 micromhos/cm.

TABLE C - XVII

RUN NUMBER 38 DATE: MARCH 17, 1966

OUTSIDE DIAMETER .5535 in. LENGTH 2.0965 in. THICKNESS .01283 in. FLOW RATE 000 gpm THERMOCOUPLE POSITION FROM F.S.P. No.2 90°, No.3 270°, No.4 180°, No.5 0°

THERMOCOUPLE READING MV.					POWER INPUT		TIME	OUTSIDE TEMPERATURE °F				BULK TEMP °F	FLUX
NO.2	NO.3	NO.4	NO.5	NO.7	VOLTS	AMPS	MIN.	NO.2	NO.3	NO.4	NO.5		
5.201	5.273	5.194	5.180	5.223	0.00	000	00	210	212	209	209	210	000
5.745	5.769	5.746	5.688	5.234	0.80	252	12	225	227	225	223	211	27,992
5.815	5.833	5.825	5.756	5.205	0.90	288	19	227	229	227	225	210	35,990
5.897	5.919	5.910	5.864	5.232	1.02	331	26	229	231	230	211	211	46,879
5.990	5.972	5.966	5.950	5.228	1.11	358	34	232	232	231	230	211	55,176
6.037	6.020	6.017	6.021	5.229	1.18	381	41	233	233	232	232	211	62,424
6.107	6.072	6.081	6.104	5.223	1.28	413	49	235	234	234	234	210	73,689
6.163	6.113	6.129	6.164	5.252	1.34	431	58	236	235	235	236	211	80,192
6.201	6.169	6.184	6.220	5.231	1.44	461	66	237	236	236	237	211	92,495
6.227	6.200	6.208	6.261	5.300	1.74	482	73	236	236	235	237	213	116,652
Voltmeter lead broken, run terminated							74						

Water purity at 80°F: Dissolved oxygen 2.1 ppm: Conductivity 98 micromhos/cm.

TABLE C - XVIII

RUN NUMBER 39 DATE: MARCH 18, 1966

OUTSIDE DIAMETER	LENGTH	THICKNESS	FLOW RATE	THERMOCOUPLE POSITION FROM F.S.P.
.5535 in.	2.0965 in.	.01283 in.	000 gpm	No.2 90°, No.3 270°, No.4 180°, No.5 0°

THERMOCOUPLE READING MV.					POWER INPUT		TIME	OUTSIDE TEMPERATURE °F				BULK TEMP	FLUX
NO.2	NO.3	NO.4	NO.5	NO.7	VOLTS	AMPS	MIN.	NO.2	NO.3	NO.4	NO.5	°F	
5.201	5.273	5.194	5.180	5.223	0.00	000	00	210	212	209	209	210	000
6.051	6.051	6.132	5.939	5.286	1.07	346	19	234	235	237	230	213	51,400
6.119	6.107	6.185	5.995	5.361	1.18	373	30	236	236	238	231	215	61,114
6.184	6.286	6.187	6.061	5.386	1.28	408	36	238	241	237	233	216	72,513
6.225	6.336	6.235	6.112	5.366	1.35	434	44	238	243	238	234	215	81,352
6.260	6.411	6.265	6.150	5.399	1.38	458	51	239	245	239	235	216	88,077
6.301	6.455	6.318	6.202	5.391	1.48	485	58	240	246	240	236	216	99,667
6.350	6.534	6.360	6.250	5.373	1.54	511	64	241	248	241	237	215	109,267
6.384	6.676	6.361	6.297	5.374	1.64	540	70	241	252	240	238	215	122,966
6.422	6.667	6.432	6.336	5.361	1.72	564	76	242	251	242	238	215	134,696
6.470	6.779	6.467	6.417	5.300	1.80	592	82	243	254	242	240	213	147,959
6.508	6.827	6.459	6.453	5.366	1.88	620	87	243	254	241	241	215	161,844
6.537	6.857	6.514	6.500	5.360	1.91	639	93	244	255	243	242	215	169,909
Burnout					1.99	678	95						183,000

Water purity at 80°F: Dissolved oxygen 2.1 ppm: Conductivity 100 micromhos/cm.

TABLE C - XIX

RUN NUMBER 22 DATE: JANUARY 2, 1966

OUTSIDE DIAMETER	LENGTH	THICKNESS	FLOW RATE	THERMOCOUPLE POSITION FROM F.S.P.
.5560 in.	2.100 in.	.0130 in.	96.0 gpm	No.2 90°, No.3 270°, No.4 0°, No.5 180°

THERMOCOUPLE READING MV.					POWER INPUT		TIME	OUTSIDE TEMPERATURE °F				BULK TEMP	FLUX
NO.2	NO.3	NO.4	NO.5	NO.7	VOLTS	AMPS	MIN.	NO.2	NO.3	NO.4	NO.5	°F	
5.076	5.075	5.079	5.092	5.041	0.00	000	00	206	206	206	206	204	000
5.826	5.912	5.751	6.027	4.970	1.04	410	13	228	233	226	235	202	58,841
6.067	6.164	5.906	6.172	5.022	1.12	449	19	236	240	230	240	204	69,395
6.199	6.258	6.081	6.318	5.040	1.21	483	30	239	243	235	244	204	80,649
6.401	6.403	6.350	6.430	5.091	1.38	546	33	245	246	243	246	206	103,977
6.542	6.522	6.576	6.526	5.120	1.50	590	37	248	249	249	248	207	122,126
6.664	6.648	6.782	6.605	5.139	1.62	648	39	251	252	255	250	208	144,862
6.751	6.756	6.900	6.719	5.151	1.72	689	44	253	255	258	252	208	163,536
6.815	6.801	7.006	6.796	5.155	1.74	692	53	255	256	261	255	208	166,158
6.960	6.985	7.232	6.993	5.151	1.89	750	60	258	260	267	259	208	195,609
7.081	7.093	7.373	7.139	5.154	2.00	791	68	261	263	270	263	208	218,309
7.129	7.136	7.432	7.204	5.164	2.02	802	73	262	264	272	265	209	223,559
7.142	7.158	7.446	7.211	5.157	2.01	799	77	262	264	273	265	208	221,620

Maximum output above: No burnout

Water purity at 80°F: Dissolved oxygen 2.9 ppm: Conductivity 96 micromhos/cm.

TABLE C - XX

RUN NUMBER 23 DATE: JANUARY 14, 1966

OUTSIDE DIAMETER	LENGTH	THICKNESS	FLOW RATE	THERMOCOUPLE POSITION FROM F.S.P.
.5560 in.	2.100 in.	.0130 in.	96.0 gpm	No.2 90°, No.3 270°, No.4 0°, No.5 180°

THERMOCOUPLE READING MV.					POWER INPUT		TIME	OUTSIDE TEMPERATURE °F				BULK TEMP	FLUX
NO.2	NO.3	NO.4	NO.5	NO.7	VOLTS	AMPS	MIN.	NO.2	NO.3	NO.4	NO.5	°F	
5.076	5.075	5.079	5.092	5.041	0.00	000	00	206	206	206	206	204	000
6.596	6.662	6.313	6.598	5.138	1.39	545	19	251	255	242	252	208	104,539
6.739	6.844	6.604	6.751	5.167	1.52	602	27	254	260	250	255	209	126,272
6.830	7.011	6.840	6.867	5.193	1.64	650	37	256	264	257	258	209	147,103
7.000	7.120	7.070	6.980	5.214	1.79	702	46	260	266	263	260	210	173,403
7.176	7.264	7.304	7.134	5.214	1.99	772	67	264	269	268	263	210	212,000
7.358	7.471	7.357	7.242	5.213	2.13	824	76	268	274	268	265	210	242,199
7.466	7.580	7.432	7.324	5.215	2.25	852	88	271	276	270	266	210	264,538
7.596	7.729	7.552	7.439	5.212	2.39	905	97	273	279	272	268	210	298,478
Burnout 7.742						955	120						324,000

Water purity at 80°F: Dissolved oxygen 2.3 ppm: Conductivity 118 micromhos/cm.

TABLE C - XXI

RUN NUMBER 26 DATE: JANUARY 23, 1966

OUTSIDE DIAMETER	LENGTH	THICKNESS	FLOW RATE	THERMOCOUPLE POSITION FROM F.S.P.
.5550 in.	2.100 in.	.0130 in.	152.6 gpm	No.2 0°, No.3 180°, No.4 90°, No.5 270°

THERMOCOUPLE READING MV.					POWER INPUT		TIME	OUTSIDE TEMPERATURE °F				BULK TEMP	FLUX
NO.2	NO.3	NO.4	NO.5	NO.7	VOLTS	AMPS	MIN.	NO.2	NO.3	NO.4	NO.5	°F	
5.234	5.226	5.226	5.225	5.142	0.00	000	00	211	211	211	211	208	000
6.372	6.532	6.564	6.585	5.170	1.50	562	8	243	248	249	250	209	116,540
6.556	6.673	6.684	6.752	5.155	1.64	618	15	248	251	252	254	208	140,113
6.669	6.754	6.756	6.832	5.154	1.71	643	25	251	253	253	256	208	152,004
6.836	6.859	6.854	6.940	5.160	1.86	690	32	255	255	255	258	208	177,423
7.066	7.016	7.031	7.056	5.157	2.03	757	40	261	258	259	260	208	212,441
7.177	7.096	7.138	7.154	5.162	2.18	799	44	263	259	261	262	208	240,797
7.287	7.195	7.282	7.286	5.166	2.31	850	49	265	261	264	264	209	271,443
7.441	7.314	7.427	7.418	5.189	2.46	901	54	268	263	267	267	209	306,413
7.481	7.357	7.488	7.476	5.160	2.51	917	59	269	264	268	268	208	318,193
7.542	7.419	7.565	7.578	5.162	2.59	942	64	269	265	269	270	208	337,286
7.616	7.483	7.662	7.679	5.163	2.68	978	70	270	265	271	272	208	362,344
7.666	7.540	7.696	7.714	5.156	2.70	988	75	272	267	272	273	208	368,781
7.588	7.474	7.641	7.637	5.150	2.60	952	82	271	266	272	272	208	342,182

TABLE C - XXI (Continued)

THERMOCOUPLE READING MV.					POWER INPUT		TIME	OUTSIDE TEMPERATURE °F				BULK TEMP °F	FLUX
NO.2	NO.3	NO.4	NO.5	NO.7	VOLTS	AMPS	MIN.	NO.2	NO.3	NO.4	NO.5		
7.482	7.383	7.529	7.533	5.157	2.49	908	88	269	265	270	270	208	312,559
7.429	7.320	7.416	7.429	5.178	2.36	858	94	269	265	268	269	209	279,928
7.330	7.246	7.318	7.335	5.195	2.21	802	100	268	264	267	268	210	245,027
7.131	7.107	7.171	7.241	5.192	2.01	732	106	263	262	264	267	209	203,402
6.729	6.907	7.025	6.942	5.195	1.75	630	111	253	258	262	260	210	152,414
Power off; very slight boiling							111						

Water purity at 80°F: Dissolved oxygen 2.1 ppm: Conductivity 100 micromhos/cm.

TABLE C - XXII

RUN NUMBER 27 DATE: JANUARY 27, 1966

OUTSIDE DIAMETER	LENGTH	THICKNESS	FLOW RATE	THERMOCOUPLE POSITION FROM F.S.P.
.5550 in.	2.100 in.	.0130 in.	152.6 gpm	No.2 90°, No.3 270°, No.4 180°, No.5 0°

THERMOCOUPLE READING MV.					POWER INPUT		TIME	OUTSIDE TEMPERATURE °F				BULK TEMP	FLUX
NO.2	NO.3	NO.4	NO.5	NO.7	VOLTS	AMPS	MIN.	NO.2	NO.3	NO.4	NO.5	°F	
5.096	5.074	5.074	5.086	5.048	0.00	000	00	206	206	206	206	205	000
6.722	6.716	6.594	6.513	5.201	1.68	612	13	253	253	248	246	210	142,137
6.828	6.809	6.700	6.612	5.224	1.73	642	21	256	255	251	248	210	153,542
6.985	6.970	6.852	6.826	5.230	1.88	692	30	260	259	255	254	211	179,850
7.107	7.130	6.994	7.047	5.251	2.01	754	41	262	262	258	260	211	209,515
7.212	7.235	7.092	7.197	5.276	2.15	807	50	264	264	259	263	212	239,861
7.297	7.221	7.182	7.320	5.435	2.28	848	58	264	261	260	265	217	267,500
7.441	7.226	7.286	7.454	5.477	2.46	898	72	267	260	261	267	219	306,000
7.561	7.406	7.370	7.539	5.352	2.54	925	83	270	264	263	269	215	325,000
7.728	7.770	7.503	7.708	5.204	2.74	999	91	273	274	265	272	210	378,400
Burnout						1048	94						402,000

Water purity at 80°F: Dissolved oxygen 2.6 ppm: Conductivity 101 micromhos/cm.

TABLE C - XXIII

RUN NUMBER 40 DATE: MARCH 18, 1966

OUTSIDE DIAMETER	LENGTH	THICKNESS	FLOW RATE	THERMOCOUPLE POSITION FROM F.S.P.
.7034 in.	2.098 in.	.0091 in.	000 gpm	No.2 90°, No.3 270°, No.4 180°, No.5 0°

THERMOCOUPLE READING MV.					POWER INPUT		TIME	OUTSIDE TEMPERATURE °F				BULK TEMP	FLUX
NO.2	NO.3	NO.4	NO.5	NO.7	VOLTS	AMPS	MIN.	NO.2	NO.3	NO.4	NO.5	°F	
5.246	5.272	5.216	5.231	5.212	0.00	000	00	211	212	211	211	210	000
5.905	5.794	5.689	5.872	5.218	1.23	342	15	232	229	224	230	210	46,115
5.966	5.875	5.743	5.959	5.268	1.38	370	22	234	231	226	233	212	55,950
6.058	5.951	5.837	5.986	5.264	1.48	382	33	236	233	228	234	212	61,727
6.094	6.010	5.870	5.996	5.264	1.61	400	42	237	235	229	234	212	70,313
Voltmeter connection broken, run terminated							45						

Water purity at 80°F: Dissolved oxygen 2.1 ppm: Conductivity 109 micromhos/cm.

TABLE C - XXIV

RUN NUMBER 41 DATE: MARCH 19, 1966

OUTSIDE DIAMETER	LENGTH	THICKNESS	FLOW RATE	THERMOCOUPLE POSITION FROM F.S.P.
.7034 in.	2.098 in.	.0091 in.	000 gpm	No.2 90°, No.3 270°, No.4 180°, No.5 0°

THERMOCOUPLE READING MV.					POWER INPUT		TIME	OUTSIDE TEMPERATURE °F				BULK TEMP °F	FLUX
NO.2	NO.3	NO.4	NO.5	NO.7	VOLTS	AMPS	MIN.	NO.2	NO.3	NO.4	NO.5		
5.195	5.195	5.152	5.152	5.080	0.00	000	00	210	210	208	208	206	000
5.811	5.864	5.857	5.904	5.124	1.25	346	17	229	231	230	231	207	47,221
5.826	5.945	5.785	5.952	5.182	1.36	368	30	229	233	227	233	209	54,644
5.860	6.067	5.856	6.062	5.222	1.49	392	38	230	237	229	236	210	63,771
5.871	6.010	5.810	6.056	5.126	1.61	418	46	230	235	227	235	207	73,477
5.890	6.087	5.849	6.043	5.108	1.69	431	56	230	237	228	235	207	79,527
5.911	6.149	5.875	6.065	5.082	1.78	458	69	231	239	229	235	206	89,010
6.126	6.375	6.082	6.265	5.284	1.85	480	78	237	246	235	241	212	96,954
6.146	6.451	6.104	6.236	5.266	2.00	518	84	237	248	235	240	212	113,113
6.160	6.457	6.111	6.234	5.219	1.91	543	92	237	248	235	240	210	113,236
6.145	6.405	6.083	6.214	5.170	1.98	588	114	237	246	234	238	209	127,435
6.181	6.452	6.119	6.311	5.179	2.04	613	120	238	247	235	241	209	136,535
6.204	6.441	6.142	6.300	5.171	2.12	633	125	238	246	235	241	209	146,518
6.214	6.506	6.160	6.392	5.152	2.20	658	132	238	248	235	243	208	158,411

TABLE C - XXIV(Continued)

THERMOCOUPLE READING MV.					POWER INPUT		TIME	OUTSIDE TEMPERATURE °F				BULK TEMP °F	FLUX
NO.2	NO.3	NO.4	NO.5	NO.7	VOLTS	AMPS	MIN.	NO.2	NO.3	NO.4	NO.5		
6.230	6.545	6.153	6.380	5.157	2.26	670	145	238	249	235	242	208	165,324
6.035	6.370	6.146	6.341	5.237	2.24	670	157	232	243	235	241	211	163,861
6.304	6.588	6.326	6.507	5.280	2.34	700	163	240	250	240	246	212	179,223
6.409	6.701	6.357	6.590	5.278	2.42	723	170	243	253	240	248	212	191,032
6.444	6.774	6.437	6.631	5.270	2.52	760	177	243	254	242	249	212	209,106
6.442	6.733	6.404	6.638	5.252	2.55	770	187	243	253	241	249	211	214,379

Maximum power output with this circuit at above setting

Water purity at 80°F: Dissolved oxygen 2.2 ppm: Conductivity 114 micromhos/cm.

TABLE C - XXV

RUN NUMBER 42 DATE: MARCH 20, 1966

OUTSIDE DIAMETER	LENGTH	THICKNESS	FLOW RATE	THERMOCOUPLE POSITION FROM F.S.P.
.7034 in.	2.098 in.	.0091 in.	000 gpm	No.2 90°, No.3 270°, No.4 180°, No.5 0°

THERMOCOUPLE READING MV.					POWER INPUT		TIME	OUTSIDE TEMPERATURE °F				BULK TEMP °F	FLUX
NO.2	NO.3	NO.4	NO.5	NO.7	VOLTS	AMPS	MIN.	NO.2	NO.3	NO.4	NO.5		
5.255	5.246	5.241	5.240	5.233	0.00	000	00	212	211	211	211	211	000
6.255	6.495	6.285	6.364	5.334	1.95	592	12	240	249	241	243	214	126,040
6.358	6.515	6.401	6.489	5.334	2.12	641	19	243	248	244	247	214	148,370
6.426	6.669	6.480	6.600	5.335	2.25	678	26	244	253	245	250	214	166,557
6.516	6.726	6.573	6.674	5.336	2.33	712	32	247	254	248	252	214	181,518
6.571	6.843	6.616	6.771	5.331	2.45	742	38	248	257	249	254	214	198,482
6.623	6.880	6.695	6.810	5.327	2.52	770	45	249	258	251	255	214	212,277
6.651	6.951	6.661	6.851	5.363	2.62	798	58	249	260	249	255	215	228,709
6.694	7.000	6.694	6.869	5.367	2.75	831	65	250	260	249	255	215	249,962
6.726	7.111	6.790	6.957	5.366	2.83	858	72	250	263	252	258	215	265,110
6.756	7.136	6.857	6.922	5.356	2.91	882	79	251	264	253	256	215	280,711
6.832	7.180	6.854	7.020	5.357	3.03	916	86	252	264	252	258	215	303,033
Burnout						970	87						327,000

Water purity at 80°F: Dissolved oxygen 2.1 ppm: Conductivity 128 micromhos/cm.

TABLE C - XXVI

RUN NUMBER 45 DATE: MARCH 28, 1966

OUTSIDE DIAMETER .7028 in. LENGTH 2.158 in. THICKNESS .0093 in. FLOW RATE 000 gpm THERMOCOUPLE POSITION FROM F.S.P. No.2 0°, No.3 180°, No.4 90°, No.5 270°

THERMOCOUPLE READING MV.					POWER INPUT		TIME	OUTSIDE TEMPERATURE °F				BULK TEMP °F	FLUX
NO.2	NO.3	NO.4	NO.5	NO.7	VOLTS	AMPS	MIN.	NO.2	NO.3	NO.4	NO.5		
5.254	5.235	5.234	5.232	5.264	0.00	000	00	211	211	211	211	212	000
5.965	5.880	5.896	5.947	5.277	1.18	342	15	233	230	231	232	212	42,873
6.010	5.946	5.975	6.005	5.280	1.24	367	24	234	232	233	234	212	48,346
6.045	5.987	6.031	6.055	5.275	1.32	390	33	235	233	235	235	212	54,484
6.050	6.044	6.047	6.096	5.278	1.39	411	46	235	235	235	237	212	60,692
6.100	6.125	6.103	6.162	5.282	1.48	440	60	237	237	236	238	212	69,182
6.163	6.195	6.160	6.217	5.280	1.60	480	69	238	239	238	240	212	81,845
6.201	6.237	6.195	6.233	5.280	1.70	507	78	239	240	239	240	212	91,566
6.249	6.271	6.235	6.261	5.282	1.78	538	84	240	240	239	240	212	102,023
6.290	6.317	6.262	6.285	5.285	1.88	562	91	241	241	240	241	213	111,947
6.304	6.367	6.310	6.331	5.282	1.95	587	98	241	243	241	242	212	121,604
6.371	6.436	6.356	6.354	5.280	2.06	621	105	243	244	242	242	212	135,905
6.394	6.467	6.375	6.410	5.278	2.11	638	112	243	245	242	244	212	143,014
6.432	6.467	6.390	6.467	5.280	2.18	656	119	244	245	243	245	212	151,579

TABLE C - XXVI (Continued)

THERMOCOUPLE READING MV.					POWER INPUT		TIME	OUTSIDE TEMPERATURE °F				BULK TEMP °F	FLUX
NO.2	NO.3	NO.4	NO.5	NO.7	VOLTS	AMPS	MIN.	NO.2	NO.3	NO.4	NO.5		
6.449	6.499	6.424	6.495	5.278	2.22	671	125	244	246	243	246	212	158,253
6.309	6.375	6.294	6.374	5.284	1.97	590	134	241	243	240	243	212	123,479
6.386	6.505	6.392	6.479	5.276	2.20	662	141	242	246	242	245	212	154,724
6.491	6.500	6.466	6.543	5.277	2.31	699	148	245	245	244	247	212	171,540
6.537	6.531	6.513	6.576	5.280	2.40	728	156	246	246	245	247	212	186,004
6.526	6.576	6.520	6.580	5.290	2.49	751	164	245	246	245	247	213	198,662
6.526	6.640	6.519	6.570	5.280	2.58	769	171	245	248	244	246	212	211,185

Maximum output at above setting, surface deteriorating

Water purity at 80°F: Dissolved oxygen 1.8 ppm: Conductivity 110 micromhos/cm.

TABLE C - XXVII

RUN NUMBER 46 DATE: MARCH 29, 1966

OUTSIDE DIAMETER	LENGTH	THICKNESS	FLOW RATE	THERMOCOUPLE POSITION FROM F.S.P.
.7028 in.	2.158 in.	.0093 in.	000 gpm	No.2 0°, No.3 180°, No.4 90°, No.5 270°

THERMOCOUPLE READING MV.					POWER INPUT		TIME	OUTSIDE TEMPERATURE °F				BULK TEMP	FLUX
NO.2	NO.3	NO.4	NO.5	NO.7	VOLTS	AMPS	MIN.	NO.2	NO.3	NO.4	NO.5	°F	
5.251	5.237	5.244	5.246	5.252	0.00	000	00	211	211	211	211	211	000
6.417	6.360	6.342	6.389	5.270	2.00	589	12	245	242	242	244	212	125,147
6.540	6.496	6.465	6.520	5.264	2.21	651	20	248	246	245	247	212	152,844
6.606	6.552	6.517	6.570	5.261	2.31	682	28	249	247	246	248	212	167,368
6.555	6.619	6.580	6.630	5.267	2.40	710	36	247	249	248	249	212	181,405
6.664	6.686	6.648	6.714	5.269	2.52	751	44	250	250	249	251	212	201,455
Burnout					2.69	799	46						212,700

Water purity at 80°F: Dissolved oxygen 2.5 ppm: Conductivity 136 micromhos/cm.

TABLE C - XXVIII

RUN NUMBER 28 DATE: FEBRUARY 1, 1966

OUTSIDE DIAMETER	LENGTH	THICKNESS	FLOW RATE	THERMOCOUPLE POSITION FROM F.S.P.
.7070	2.100 in.	.0120 in.	96.0 gpm	No.2 270°, No.3 90°, No.4 0°, No.5 180°

THERMOCOUPLE READING MV.					POWER	INPUT	TIME	OUTSIDE TEMPERATURE °F				BULK TEMP	FLUX
NO.2	NO.3	NO.4	NO.5	NO.7	VOLTS	AMPS	MIN.	NO.2	NO.3	NO.4	NO.5	°F	
5.006	5.007	5.020	5.041	5.003	0.00	000	00	203	203	204	204	203	000
6.192	6.346	6.081	6.284	5.103	1.51	590	17	238	244	234	241	206	96,683
6.360	6.488	6.320	6.410	5.122	1.68	641	27	242	247	241	244	207	116,866
6.429	6.584	6.422	6.481	5.146	1.76	675	34	244	250	244	246	208	128,925
6.509	6.692	6.513	6.552	5.167	1.87	715	45	245	252	246	248	209	145,100
6.617	6.796	6.612	6.604	5.175	1.99	755	61	248	255	248	248	209	163,050
6.715	6.924	6.770	6.720	5.177	2.10	802	67	250	258	252	251	209	182,774
6.826	7.050	6.887	6.876	5.172	2.18	825	77	253	262	256	256	209	195,178
6.904	7.158	6.980	6.945	5.176	2.29	870	82	255	264	258	257	209	216,210
6.940	7.241	7.060	7.010	5.173	2.38	898	90	255	266	259	258	209	231,939
7.032	7.312	7.104	7.055	5.170	2.48	938	95	257	267	260	258	209	252,450
7.115	7.391	7.169	7.110	5.173	2.59	978	100	259	269	261	259	209	274,890
7.180	7.469	7.226	7.155	5.168		1015	108						
Burnout						1050	109						

Water purity at 80°F: Dissolved oxygen 2.4 ppm: Conductivity 105 micromhos/cm.

TABLE C - XXIX

RUN NUMBER 29 DATE: FEBRUARY 7, 1966

OUTSIDE DIAMETER	LENGTH	THICKNESS	FLOW RATE	THERMOCOUPLE POSITION FROM F.S.P.
.7080 in.	2.096 in.	.0130 in.	152.6 gpm	No.2 180°, No.3 0°, No.4 270°, No.5 90°

THERMOCOUPLE READING MV.					POWER INPUT		TIME	OUTSIDE TEMPERATURE °F				BULK TEMP	FLUX
NO.2	NO.3	NO.4	NO.5	NO.7	VOLTS	AMPS	MIN.	NO.2	NO.3	NO.4	NO.5	°F	
5.195	5.195	5.197	5.187	5.154	0.00	000	00	209	209	210	209	208	000
6.173	6.202	6.450	6.450	5.139	1.880	640	14	236	237	245	245	208	130,639
6.306	6.418	6.501	6.511	5.146	1.970	671	24	239	243	246	246	208	143,524
6.485	6.629	6.648	6.642	5.144	2.140	732	32	244	249	249	249	208	170,083
6.620	6.823	6.907	6.802	5.154	2.290	781	40	247	254	256	253	208	194,188
6.835	7.026	7.141	7.070	5.156	2.410	821	52	253	259	263	260	208	214,830
6.900	7.106	7.202	7.123	5.161	2.520	858	59	254	261	264	261	208	234,759
6.948	7.171	7.272	7.194	5.166	2.620	890	68	254	262	265	262	209	253,178
7.004	7.232	7.356	7.252	5.156	2.720	920	75	255	263	267	263	208	271,701
7.060					2.830	960	77						
Burnout at above setting							80						

Water purity at 80°F: Dissolved oxygen 2.2 ppm: Conductivity 106 micromhos/cm.

APPENDIX D

SAMPLE CALCULATIONS

Laboratory Data:

Potential difference across the cylinder; volts

Circuit current; amperes

Thermocouple (cylinder and bulk) potential; millivolts

Orifice manometer reading

Cylinder dimensions; O.D., wall thickness, length-inches

Primary data reduction:

Millivolt conversion for the 200-300°F range:

$$^{\circ}F = 212 + (\text{millivolts} - \text{correction} - 5.27)/0.0303 \qquad \text{(D-1)}$$

$$\text{Volts} = \text{voltmeter reading } (1.02) \qquad \text{(D-2)}$$

$$\text{Flux} = (\text{Volts})(\text{Amps})(3.4128)/\text{outside area in sq.ft.} \qquad \text{(D-3)}$$

$$\text{Resistivity: } R = (\text{volts})\,\frac{\pi}{4}\,[(OD)^2-(ID)^2]/(\text{Amps})(\text{Length}) \qquad \text{(D-4)}$$

Calculated Quantities:

Temperature drop through the cylinder wall based on a uniform flux on the cylinder surface.

Conduction Equation:

$$\frac{d^2T}{dr^2} + \frac{1}{r}\frac{dT}{dr} + \frac{q''}{k} = 0 \qquad \text{(D-5)}$$

where $q'' = \text{Btu}/(\text{hr})(\text{ft}^3)$

$k = \text{Btu}/(\text{hr})(\text{ft})(^{\circ}F)$

Boundary conditions:

Let R_O = outside radius

R_I = inside radius

Then:

$$\frac{dT}{dr} = 0 \quad ; \quad r = R_I \tag{D-6}$$

$$T = T_I \quad ; \quad r = R_I \tag{D-7}$$

Solution:

Let $$\frac{dT}{dr} = Z \tag{D-8}$$

Then:

$$\frac{dZ}{dr} + \frac{Z}{r} + \frac{q''}{k} = 0 \tag{D-9}$$

$$r\frac{dZ}{dr} + Z + \frac{q''}{k} r = 0 \tag{D-10}$$

Since

$$\frac{d(Zr)}{dr} = Z + r\frac{dZ}{dr}$$

Then (D-10) becomes:

$$\frac{d(Zr)}{dr} + \frac{q''r}{k} = 0 \tag{D-11}$$

Integrating (D-11)

$$rZ + \frac{q''}{2k} r^2 = C \tag{D-12}$$

Using (D-8)

$$r\frac{dT}{dr} + \frac{q''r^2}{2k} = C \tag{D-13}$$

or

$$\frac{dT}{dr} + \frac{q''r}{2k} = \frac{c}{r} \tag{D-14}$$

Integrating (D-14)

$$\int_{T_I}^{T_O} dT + \frac{q''}{2k}\int_{R_I}^{R_O} r\,dr = \int_{R_I}^{R_O} \frac{C}{r}\,dr \qquad \text{(D-15)}$$

which gives:

$$T_O - T_I + \frac{q}{4k}\left[R_O^2 - R_I^2\right] - C\left[\ln \frac{R_O}{R_I}\right] = 0 \qquad \text{(D-16)}$$

combining (D-6) and (D-12)

$$C = \frac{q''R_I}{2k} \qquad \text{(D-17)}$$

and (D-16) becomes:

$$T_O - T_I + \frac{q''}{4k}\left[R_O^2 - R_I^2 - 2R_I^2\left(\ln \frac{R_O}{R_I}\right)\right] = 0 \qquad \text{(D-18)}$$

or

$$T_O - T_I = \frac{q''R_I^2}{4k}\left[-\frac{R_O^2}{R_I^2} + 1 + \ln \frac{R_O^2}{R_I^2}\right] \qquad \text{(D-19)}$$

which was written for the computer as:

$$T_O - T_I = \frac{q\,R_I^2}{4k\ (\text{wall thickness})}\left[1 + 2\ln\frac{R_O}{R_I} - \left(\frac{R_O}{R_I}\right)^2\right] \qquad \text{(D-20)}$$

The inside temperature was determined from (D-1).

Local outside temperature = Inside temperature + (D-20) (D-21)

Local ΔT_b = Local outside temperature - Bulk temperature (D-22)

Local coefficient = $8/\Delta T_b$ (D-23)

Bulk viscosity = 0.698

Wall viscosity = 241.9/2.1482 91.565 + $(T_{OA}$ - 212)/1.8 + [8078

+ 91.565 + $(T_{OA}$ - 212)/1.8]^2 $^{0.5}$ - 120

(D-24)

Mass velocity = (gpm)(60 min/hr)(59.97 lb/ft^3)/(7.48 gal/ft^3)

(9/144 ft^2)

= gpm (7,680) lb mass/hr ft^2

Reynolds Number = Re = Mass velocity (OD)/ bulk viscosity

Liquid coefficient

$$Nu = Pr^{0.4}\left(\frac{\mu_b}{\mu_w}\right)^{0.25} [0.31\ (Re)^{0.5} + 0.11\ (Re)^{0.67}] \qquad (D\text{-}25)$$

or $$h_L = 0.393\ (1.24)\ 12/(OD)\ \left[\frac{0.698}{\mu_w}\right]^{0.25} [0.31\ (Re)^{0.5} + 0.11(Re)^{0.67}] \qquad (D\text{-}26)$$

Calculations for figures:

Figs. 21-25 Forced convection lines:

$$a = h_L\ (T_w - T_b)$$

Figs. 14-18

$$T_s = 223.7$$

$$\Delta T_s = T_w - T_s = T_{OA} - 223.7$$

which is plotted against the flux corresponding to T_{OA}.

The method of averages for Figure 10 is illustrated in Table D-I.

TABLE D-I

METHOD OF AVERAGES

q	ΔT_s	Log q	Log ΔT_s	2.5446 LogΔT_s	Log q	q	Δq	Dev. %
61,106	25.28	4.78537	1.40106	3.56521	4.79810	62,820	1714	2.80
75,842	26.75	4.87991	1.42732	3.63203	4.86492	73,270	-2572	3.39
87,719	29.05	4.94310	1.46315	3.72319	4.95608	90,380	2660	3.02
99,300	30.87	4.99695	1.48954	3.79036	5.02325	105,500	6200	6.27
110,288	31.25	5.04254	1.49488	3.80395	5.03684	109,100	-1188	1.08
125,211	32.16	5.09764	1.50732	3.83560	5.06849	117,080	-8131	6.50
138,888	33.53	5.14270	1.52543	3.88168	5.11457	130,200	-8688	6.23
158,442	34.80	5.19980	1.54158	3.92278	5.15567	143,100	-15342	9.71
178,041	37.90	5.25043	1.57910	4.01826	5.25115	178,300	259	0.145
188,115	38.43	5.27440	1.58467	4.03243	5.26532	184,200	-3915	2.08
197,550	41.14	5.29568	1.61426	4.10773	5.34062	219,100	21550	10.9
229,804	43.38	5.36135	1.63729	4.16633	5.39922	250,700	20900	9.1
							Average	5.1%

Method of averages (continued)

From the sum of the first six entries in D-I:

$$29.74551 = 8.78327a + 6 \text{ Log } b$$

From the sum of the second six entries in D-I:

$$31.52436 = 9.48233a + 6 \text{ Log } b$$

which gives $a = 2.54465$

$$\text{Log } b = 1.23289 \qquad b = 17.10$$

The equation is:

$$\text{Log } q = 2.5446 \text{ Log } \Delta T_s + 1.23289$$

or

$$q = 17.10\ \Delta T_s^{2.54} \qquad \text{(D-27)}$$

Figures 39-48 Superposition Method

Figure 41

Pool boiling curve $q = 17.10\ \Delta T_s^{2.54}$

$T_w - T_s$	q	T_s	T_w	T_b	$T_w - T_b$
20	34,960	223.7	243.7	210.4	33.3
30	98,100	223.7	253.7	210.4	43.3
40	204,000	223.7	263.7	210.4	53.3

Forced convection curve $q = h_L \Delta T_b$

$T_w - T_b$	h_L	q
27.85	3084	85,900
39.6	3139	124,200
47.0	3165	148,800

Forced convection boiling curve - from Fig. 19

$T_w - T_b$	q
30	96,500
35	125,000
40	162,500
45	230,000
47	272,000

Incipient boiling point: Average $\Delta T_b = 27.8^{\circ}F$

Following the method of Forster and Greif (72) we have q_0 as the intersection of the liquid phase forced convection line with the pool boiling line. The forced convection boiling curve then goes through the point $q_1 = 1.4q_0$. The point q_1 represents the flux at which the well established boiling contribution dominates the forced convection contribution.

OD/velocity	q_0	q_1
0.2495/3.42	112,000	157,000
0.2495/5.44	266,000	372,000
0.337/3.42	87,000	122,000
0.338/5.44	220,000	308,000
0.450/3.42	120,000	168,000
0.4587/5.44	171,000	239,000
0.556/3.42	108,000	151,000
0.555/5.44	157,000	220,000
0.707/3.42	113,000	158,000
0.708/5.44	173,000	242,000

The resulting curves are shown as dashed lines on Figs. 39-48.

Film studies results:

cylinder dimensions: 0.457" O.D.

2.070" long

water velocity: 3.42 fps

flux = (2.09)(531)(3.4128)/(0.0207) = 187,000

outside average T_w = 261°F

average bubble diameter: $0.0588 \left(\frac{0.457}{0.640}\right) = 0.0420"$

where

0.0588" is the average of 31 measurements

0.640" is the O.D. of the cylinder on the the microfilm reader screen.

bubble velocity: $5.7 \text{ fps } \left(\frac{0.457}{0.640}\right) = 4.07 \text{ fps}$

Average 3.8 - 5.2 fps

Individual 1.1 - 8.3 fps

water velocity: 5.44 fps

flux = (2.31)(590)(3.4128)/0.0207 = 224,000

outside average wall temperature = 259°F

water bulk temperature = 204°F

average bubble diameter

$0.0437 \left(\frac{0.457}{0.640}\right) = 0.0312"$

where

0.0437 is the average of 37 measurements

bubble velocity: $9.1 \left(\frac{0.457}{0.640}\right) = 6.5 \text{ fps}$

Average 5.4 - 8.6 fps

Individual 2.0 - 14.0 fps

Data Presentation: Equation 6-7, Figs. 49, 50.

$$q_B = \rho_v L \pi D^3 f n \qquad \text{(D-28)}$$

$\rho_v = 0.0466, \quad L = 962.8$

f = bubble velocity/diameter for a continuous stream of distinct spherical bubbles.

$$n = ae^{-\frac{b}{T_w^3}}$$

f is evaluated from film data above, and n is evaluated at the temperature where the forced convection boiling curve slope approaches the pool boiling curve slope. This was $\Delta T_s = 37^{\circ}F$ for 3.42 fps data, and $\Delta T_s = 47^{\circ}F$ for 5.44 fps data. The number of sites at these temperatures in the forward region was the surface area divided by the average bubble diameter squared, and in the wake region the number of sites was the projected area of the cylinder divided by the bubble diameter squared.

This gave: $$q_B = 2.84 \times 10^9 e^{-\frac{3.28 \times 10^9}{T_w^3}} \qquad \text{(D-29)}$$

Next

$$q_{tot} = q_B \frac{A_B}{A_{tot}} + q_{fc} \frac{A_{fc}}{A_{tot}} \qquad \text{(D-30)}$$

$$A_{tot} = A_B + A_{fc} \qquad \text{(D-31)}$$

$$q_{tot} = q_{fc} + \frac{A_B}{A_{tot}} (q_B - q_{fc}) \qquad \text{(D-32)}$$

This was compared to the experimental data and $\frac{A_B}{A_{tot}}$ was found to be a semilogarithmic function of ΔT_s so that

$$\frac{A_B}{A_T} = e^{0.0848\Delta T_s - 5.38} \qquad \text{(D-33)}$$

APPENDIX E

ERROR ANALYSIS

The sources of errors and their influence on the reported results will be considered here.

The random fluctuations in the pressure drop across the orifice plate were removed by adjusting the needle valves on the pressure tap connections. The maximum variation in the flow rate was less than 2 gpm, which was indicated by a 0.1 in. Hg change on the orifice manometer. The stability of the flow rate over extended periods of time was excellent. The error in the reported velocity is between 1 and 2%.

The flux is a function of the potential drop across the cylinder, the circuit current, and the outside surface area. The accuracy of the ammeter was guaranteed to be within 1% of full scale. The voltmeter was calibrated with a volt potentiometer, which in essence meant calibration against a standard cell. The resulting error in the voltmeter reading was less than 1% of full scale. The outside diameter was measured to 0.001 in., and the length to 0.01 in. The largest contributing factor in the flux error is the ammeter error which is responsible for about one-half the total error. At fluxes of 70,000 to 80,000, which is the region of incipient boiling, the error in the calculated flux may

be as large as 3%. In the boiling regime the error will decrease to 1.5% at a flux of 300,000 and for fluxes of 600,000 or greater, the error becomes 1%.

The thermocouple calibration with the NBS thermometer afforded the bulk temperature to be correct to $1^{\circ}F$. This allows the reported inside cylinder temperature to differ from the actual temperature by no more than $2^{\circ}F$, since the difference between the inside wall temperature and the bulk water temperature is correct to less than $1^{\circ}F$.

The calculated temperature drop through the cylinder wall is a function of the flux, outside cylinder radius, and the wall thickness. The outside cylinder radius measurement errors contribute almost nothing to the temperature drop error through the wall. For the extreme case of 0.2495 in O.D. cylinder at a flux of 1×10^{6}, this error was $0.02^{\circ}F$. The wall thickness variation contributed from $0.1^{\circ}F$ to $1.1^{\circ}F$ and the errors in the measured flux contributed between 0.2 and $0.8^{\circ}F$ at fluxes of 10^{5} and 10^{6}, respectively. This means that the maximum error in the wall temperature drop will be $2^{\circ}F$. When this error is combined with the calibration error, the maximum resulting error will be 8% of the bulk temperature difference. The largest percentage error will exist in the pool boiling data, since the maximum temperature difference encountered was of the order of 30 to $40^{\circ}F$.

NOMENCLATURE

A	area	sq ft
a	constant	dimensionless
a'	cylinder radius	ft
b	constant	dimensionless
c_p	heat capacity	Btu/lb^{o}F
D	cylinder outside diameter	ft
$\overline{F}$	angle averaged fraction of heat flux transferred directly to vapor when the bubble is on the surface	
g	acceleration of gravity	ft/hr^2
g_c	conversion constant 4.17×10^8	ft lb mass/lb force hr^2
h	local heat transfer coefficient	Btu/hr sq ft^{o}F
k	thermal conductivity	Btu/hr ft^{o}F
L	latent heat of vaporization	Btu/lb
Nu	Nusselt Number	hD/k, dimensionless
n	number of active sites	1/sq ft
OD	outside of diameter	ft
Pr	Prandtl number	$c_p\mu/k$, dimensionless
q	flux	Btu/hr sq ft
r	cylindrical space coordinate	ft
Re	Reynolds number	$DU\rho/\mu$, dimensionless
T	temperature	^{o}R or ^{o}F
T_l	Free stream temperature at boundary layer	^{o}F

ΔT_{sat}	temperature excess of heater above saturation	^{o}F
ΔT_{b}	temperature excess of heater surface above bulk	^{o}F
t	time	sec
U	liquid velocity b ased on empty channel	ft/sec
x,y,z	rectangular space coordinates	ft

Greek symbols

α	thermal diffusivity	sq ft/sec
δ	velocity boundary layer thickness	ft
Δ	thermal boundary layer thickness	ft
θ	angle from forward stagnation point	radians
λ	pressure gradient parameter	dimensionless
μ	dynamic viscosity	lb/ft sec
ν	kinematic viscosity	sq ft/sec
ξ	arbitrary function	
ρ	density	lb/cu ft
σ	surface tension	lb/ft
τ	shear stress	lb/ft sec^2
ϕ_c	burnout flux	Btu/hr sq ft

Subscripts

B	boiling
Bu	bubble
b	bulk
c	critical
f.c.	forced convection
I	inside
L	liquid phase

nb	non-boiling
O	outside
OH	outside average
pb	pool boiling
s	saturation
tot.	total
v	vapor
w	wall

VITA

Hugh Richard McKee

Candidate for the Degree of

Doctor of Philosophy

Thesis: FORCED CONVECTION BOILING FROM A CYLINDER NORMAL TO THE FLOW

Major Field: Chemical Engineering

Biographical:

Personal Data: Born in Rochester, New York on January 22, 1935

Education: Attended Benjamin Franklin High School in Rochester, New York, graduated in June, 1953; received the Bachelor of Science Degree in Chemical Engineering from Tri-State College, Angola, Indiana in August, 1956; the Master of Science Degree was awarded in May, 1959, from the University of Tulsa, with a major in Petroleum Refining; completed the requirements for the Doctor of Philosophy Degree in May, 1967.

Professional Experience: Employed as a Chemical Engineer with the Petrolite Corporation, Bareco Wax Division, Kilgore, Texas, 1958-1959; appointed to the Faculty of the University of Tulsa in September, 1959 and served until June, 1962 as an Instructor in Chemical Engineering.